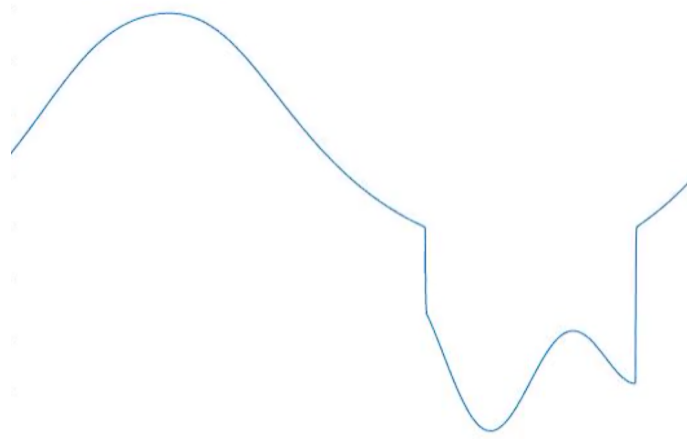


Institut  
Camille  
Jordan

Laboratoire de recherche en mathématiques Lyon/Saint-Étienne

# Phase separation and boundary effects in out-of-equilibrium lattice gases

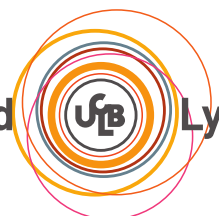


**Clément Erignoux**

Manuscrit d'Habilitation a Diriger la Recherche

*Inria*

Université Claude Bernard



Lyon 1



Université Claude Bernard Lyon 1  
École doctorale InfoMath, ED 512  
Spécialité : **Mathématiques**

**Phase separation and boundary effects  
in out-of-equilibrium lattice gases**

**Manuscrit d'Habilitation à Diriger la Recherche**

Soutenue publiquement le 7 mai 2025 par

**Clément Erignoux**

devant le Jury composé de:

M. Paul Chleboun	Warwick University	
M. Christophe Garban	Université Lyon 1	
M. Cyril Labbé	Université Paris Cité	
M. Jean-Christophe Mourrat	CNRS & ENS Lyon	
Mme Ellen Saada	CNRS & Université Paris-Cité	Rapporteur
M. Fabio Toninelli	Technical University of Vienna	Rapporteur



# TABLE OF CONTENTS

<b>LIST OF PUBLICATIONS AND PREPRINTS</b>	<b>3</b>
<b>INTRODUCTION</b>	<b>9</b>
<b>1 Macroscopic behavior of lattice gases</b>	<b>9</b>
1.1 A general exclusion process	9
1.2 Characterization of macroscopic behavior.	10
1.3 Sketch of the entropy method	11
1.4 Fluctuating hydrodynamics and large deviations	13
<b>2 Influence of kinetic constraints</b>	<b>16</b>
2.1 The Facilitated Exclusion Process	16
2.2 Hydrodynamic limit and transience time for the symmetric FEP	16
2.3 Hydrodynamic limit for the asymmetric FEP	18
2.4 Stationary CLT fluctuations for the FEP	19
2.5 SWT and cutoff for the transience time	20
2.6 Critical behavior for a 2-dimensional FEP	21
<b>3 Boundary-driven models</b>	<b>21</b>
3.1 SSEP with general boundary dynamics	21
3.2 Non-reversible boundary dynamics	22
3.3 Static large deviations for the SSEP in weak contact with equilibrium reservoirs	23
3.4 Zero-range process with destruction at the origin	24
3.5 Macroscopic behavior of the boundary-driven FEP	25
<b>4 Active matter, phase separation, and nematic phase transition</b>	<b>26</b>
4.1 My PhD work : Hydrodynamic limit for a active exclusion process	26
4.2 Exact phase diagrams for simple active matter models	27
4.3 Phase separation for the non-gradient active lattice gas	29
4.4 First order nematic transition for a liquid crystal model	31
<b>I MACROSCOPIC BEHAVIOR OF THE FACILITATED EXCLUSION PROCESS</b>	<b>33</b>
<b>5 Transience time and cutoff phenomenon</b>	<b>34</b>
5.1 Transient, ergodic, and frozen configurations	35
5.2 Transience time starting from a Bernoulli product measure	36
5.3 Mapping with an attractive zero-range process	37
5.4 Strategy of the proof in the supercritical case : Theorem 5.1	40

5.5	Microscopic front creation : Theorem 5.2 . . . . .	42
5.6	Sharp uniform estimate of the transience time and cutoff . . . . .	44
<b>6</b>	<b>Hydrodynamic limit in the symmetric case . . . . .</b>	<b>48</b>
6.1	Grand canonical and canonical states for the FEP . . . . .	48
6.2	Hydrodynamic limit for the supercritical symmetric FEP . . . . .	49
6.3	Stephan problem for the symmetric FEP . . . . .	50
6.4	Critical behavior in two dimensions . . . . .	52
<b>7</b>	<b>Hydrodynamics and fluctuations for the asymmetric FEP . . . . .</b>	<b>54</b>
7.1	Hydrodynamic limit for the AFEP . . . . .	54
7.2	Sketch of the proof . . . . .	55
7.3	CLT stationary fluctuations for the FEP . . . . .	56
	<b>Conclusion and perspectives . . . . .</b>	<b>59</b>
<b>II</b>	<b>MACROSCOPIC BEHAVIOR OF BOUNDARY-DRIVEN LATTICE GASES . . . . .</b>	<b>63</b>
<b>8</b>	<b>Hydrostat. and hydrodyn. limit for non-rev. boundary dynamics . . . . .</b>	<b>64</b>
8.1	Hydrostatics for a linear boundary dynamics . . . . .	65
8.2	sketch of the proof of Theorems 8.1 . . . . .	66
8.3	Hydrodynamic limit . . . . .	69
8.4	Small perturbation of equilibrium reservoirs . . . . .	71
8.5	Stronger boundary dynamics . . . . .	72
8.6	Weaker boundary dynamics . . . . .	73
<b>9</b>	<b>Static large deviations for SSEP with weak boundary interactions . . . . .</b>	<b>75</b>
9.1	Static large deviations functional for the non-equilibrium SSEP . . . . .	75
9.2	Dynamical large deviations and weakly asymmetric dynamics . . . . .	76
9.3	DLS equation and static characterization . . . . .	77
9.4	Sketch of the proof of Theorem 9.1 . . . . .	78
<b>10</b>	<b>Destruction at the origin for the asymmetric ZRP . . . . .</b>	<b>79</b>
10.1	Asymmetric zero-range process with destruction at the origin . . . . .	80
10.2	Stationary states . . . . .	80
10.3	Hydrodynamic limit . . . . .	81
<b>11</b>	<b>Hydrodynamic behavior for the boundary-driven FEP . . . . .</b>	<b>83</b>
11.1	Kinetically constrained reservoirs and dynamics . . . . .	83
11.2	Hydrodynamic limit for weak and strong reservoir interactions . . . . .	84
	<b>Conclusion and perspectives . . . . .</b>	<b>85</b>

# LIST OF PUBLICATIONS AND PREPRINTS

## Publications

- [BEL23] A. Bouley, C. Erignoux, and C. Landim. Steady state large deviations for one-dimensional, symmetric exclusion processes in weak contact with reservoirs. *Annales de l'Institut Henri Poincaré (B) Probabilités et Statistiques*, (In Press), 2023.
- [BES21] O. Blondel, C. Erignoux, and M. Simon. Stefan problem for a nonergodic facilitated exclusion process. *Probability and Mathematical Physics*, 2(1):127–178, 2021.
- [BESS20] O. Blondel, C. Erignoux, M. Sasada, and M. Simon. Hydrodynamic limit for a facilitated exclusion process. *Annales de l'Institut Henri Poincaré (B), Probabilités et Statistiques*, 56(1):667–714, 2020.
- [EG20] C. Erignoux and A. Giuliani. Nematic first order phase transition for liquid crystals in the van der Waals - Kac limit. *Journal of Mathematical Physics*, 61, 2020.
- [EGN20a] C. Erignoux, P. Gonçalves, and G. Nahum. Hydrodynamics for SSEP with non-reversible slow boundary dynamics: Part I, the critical regime and beyond. *Journal of Statistical Physics*, 181:1433–1469, 2020.
- [EGN20b] C. Erignoux, P. Gonçalves, and G. Nahum. Hydrodynamics for SSEP with non-reversible slow boundary dynamics: Part II, below the critical regime. *ALEA*, 17:791–823, 2020.
- [ELX18] C. Erignoux, C. Landim, and T. Xu. Stationary states of boundary driven exclusion processes with nonreversible boundary dynamics. *Journal of Statistical Physics*, 171:599–631, 2018.
- [Eri18] C. Erignoux. Hydrodynamic limit of boundary driven exclusion processes with nonreversible boundary dynamics. *Journal of Statistical Physics*, 172:1327–1357, 2018.
- [Eri21] C. Erignoux. Hydrodynamic limit for an active exclusion process. *Mémoires de la SMF*, 169, 2021.
- [Eri24] C. Erignoux. On the hydrodynamics of active matter models on a lattice. *Markov Processes and Related Fields - IRS proceedings*, 30:57–80, 2024.
- [ERSS24] C. Erignoux, A. Roget, A. Shapira, and M. Simon. Hydrodynamic behavior near dynamical criticality of a facilitated conservative lattice gas. *Phys. Rev. E*, 110:L032101, Sep 2024.

- [ESZ23a] C. Erignoux, M. Simon, and L. Zhao. Asymmetric attractive zero-range processes with particle destruction at the origin. *Stochastic Processes and their Applications*, 159:1–33, 2023.
- [ESZ23b] C. Erignoux, M. Simon, and L. Zhao. Mapping hydrodynamics for the facilitated exclusion and zero-range processes. *To appear in Annals of Applied Probability*, 34(1B):1524–1570, 2023.
- [EZ24] C. Erignoux and L. Zhao. Stationary fluctuations for the facilitated exclusion process. *Electronic Journal of Probability*, 29(152):1–41, 2024.
- [KEBT18] M. Kourbane-Houssene, C. Erignoux, T. Bodineau, and J. Tailleur. Exact hydrodynamic description of active lattice gases. *Physical Review Letter*, 120, 2018.
- [MEJB23] J. Mason, C. Erignoux, R.L. Jack, and M. Bruna. Exact hydrodynamics and onset of phase separation for an active exclusion process. *Proceedings of the Royal Society A*, 479, 2023.

## Preprints

- [DCES24] H. Da Cunha, C. Erignoux, and M. Simon. Hydrodynamic limit for an open facilitated exclusion process with slow and fast boundaries. *Arxiv preprint 2401.16535*, 2024.
- [EM24] C. Erignoux and B. Massoulié. Cutoff for the transience and mixing time of a ssep with traps and consequences on the fep. *Arxiv preprint 2403.20010*, 2024.

## REMERCIEMENTS – ACKNOWLEDGMENTS

First and foremost, I would like to warmly thank Alessandra Faggionato, Ellen Saada, and Fabio Toninelli, who refereed this manuscript, and together with Paul Chleboun, Christophe Garban, Cyril Labbé and Jean-Christophe Mourrat, agreed to participate in my HDR jury. Un grand merci aussi à Brune et Hugo, pour m'avoir fait confiance pour encadrer votre thèse, et pour l'enthousiasme dont vous faites preuve au quotidien pour la recherche, qui est pour moi une source sans cesse renouvelée de motivation, ainsi qu'à Cristina et Marielle pour avoir accepté d'être mes co-encadrantes.

Comme ce manuscrit en atteste, mon travail de recherche depuis la fin de ma thèse a été porté et inspiré par de nombreuses collaborations, en France et à l'étranger. Merci tout d'abord à Thierry, qui, bien qu'il ne figure pas de manière prééminente dans ce manuscrit, est celui qui m'a appris à faire de la recherche, à prendre du recul pour comprendre la physique derrière les problèmes de calculs. Je voudrais également remercier Marielle et Oriane, qui ont toutes les deux été des moteurs de nombreux aspects de ma vie professionnelle, et avec qui j'ai toujours un immense plaisir à travailler. Bien que partant toutes deux vers de nouveaux horizons cette année, je ne doute pas que nous aurons de nombreuses occasions de continuer à travailler ensemble.

Avec le recul sur ma carrière que m'a fait prendre ce manuscrit, je me dois également de remercier Claudio de m'avoir proposé de faire un post doc à l'IMPA, il y a de cela maintenant presque 10 ans : scientifiquement, j'ai énormément appris à son contact et à celui de mes collègues de l'Institut, et personnellement, ça a été un des plus belles expériences de ma vie de passer ces deux années au Brésil. Plus généralement, merci à tous ceux avec qui j'ai eu le plaisir de travailler ces dix dernières années, qu'ils soient en France où ailleurs, chercheurs, doctorants, post-doctorants, ou stagiaires. Il va sans dire que ce manuscrit n'aurait pas vu le jour sans vous.

Mon début de carrière à INRIA s'est fait à Lille dans l'équipe PARADYSE, et je souhaite remercier toute l'équipe pour avoir soutenu ma candidature, et surtout Guillaume et Karine, grâce auxquels mes premières années d'ISFP ont bénéficié d'un environnement professionnel idéal. Je voudrais également remercier toute l'équipe DRACULA/MUSICS, et en particulier Thomas et Mostafa, pour m'avoir accueilli à Lyon dans ce nouveau chapitre de ma vie professionnelle et personnelle. Par ailleurs, la recherche et l'enseignement supérieur en mathématique n'iraient pas bien loin sans toutes les fonctions support des laboratoires, départements, et équipes de recherche, et je voudrais donc profiter de cette occasion pour remercier toutes celles et ceux qui nous aident au quotidien à naviguer les contraintes administratives et imprévus divers et variés, pour nous permettre d'exercer notre métier dans les meilleures conditions.

Merci aussi à ma famille, mon frère et mes parents, pour leur soutien indéfectible. Enfin, merci à Mylène dont la passion des maths n'a d'égal que l'amour de Gabriel pour les cailloux, et qui me supporte de jour en jour, ce qui n'est pas, soyons honnêtes, une mince affaire. Ce n'est jamais une mauvaise chose qu'ils me rappellent au quotidien qu'il n'y a pas que les maths dans la vie.



# FOREWORD

*The purpose of this manuscript is to put in perspective, in a coherent framework, the various topics I have worked on since the end of my PhD, in May 2016. My work in statistical physics has so far focused on the large scale behavior of lattice gases, particularly in out-of-equilibrium and non-equilibrium situations where non-trivial physical behavior can occur. The topic of scaling limits of interacting lattice gases can involve significant technical difficulties, and I wanted this manuscript to be, as much as possible, readable both by the mathematics and the physics community. For this reason I chose, in the introduction in particular, to present the various results obtained with my collaborators in a slightly less rigorous and exact way, in order to make them more easily accessible. When needed, I will refer to the exact result and/or comment on the differences between the results presented here and the ones stated in the corresponding original article. Furthermore, in order to present a uniform manuscript based on various articles, in some instances the notations introduced here may differ from those of the original article. Hopefully, this will not be an issue to the reader, and I tried whenever possible to keep notations as close as possible to the original. To ease reading through the manuscript, I also chose to put *in color* the new notations introduced inside of paragraphs that are relevant at several other points of the manuscript.*



# INTRODUCTION

## 1 Macroscopic behavior of lattice gases

We start by briefly reviewing a few classical tools to characterize the macroscopic behavior of lattice gases that will be referred to repeatedly throughout this manuscript, in the context of a generic exclusion process. This section contains no original results, but it will allow us to introduce our general setup, as well as many notations that will be exploited throughout this manuscript. More details on the technical and physical aspects of scaling limits of lattice gases can respectively be found in [48, 70].

### 1.1 A general exclusion process

In the context of lattice gases, the theory of hydrodynamic limits is a set of tools that allow to characterize the macroscopic behavior of a microscopic stochastic model by a set of PDE satisfied by its locally conserved quantities. Let us briefly present it in the context of a symmetric exclusion process on a one-dimensional ring  $\mathbb{T}_N = \{1, \dots, N\}$ , meaning a Markov process on the set of configurations

$$\Omega_N := \{0, 1\}^{\mathbb{T}_N}, \quad (1)$$

with Markov generator given by

$$\mathcal{L}_N f(\eta) := \sum_{x \in \mathbb{T}_N} c_{x,x+1}(\eta) \{f(\eta^{x,x+1}) - f(\eta)\}. \quad (2)$$

Above,  $\eta^{x,x+1}$  is the configuration where the values at sites  $x$  and  $x+1$  have been exchanged, namely

$$\eta_y^{x,x+1} = \begin{cases} \eta_x & \text{for } y = x+1 \\ \eta_{x+1} & \text{for } y = x \\ \eta_y & \text{for } y \neq x, x+1. \end{cases} \quad (3)$$

Define  $\tau_x$  the translation by  $x$ , meaning

$$(\tau_x \eta)_y = \eta_{y+x} \quad \text{and} \quad \tau_x g(\eta) = g(\tau_x \eta), \quad (4)$$

for any function  $g$  of the configuration. Throughout, we call *local function* a function that depends only on a finite set which does not depend on the size  $N$  of the lattice. We assume in this introductory example that

(H1) the jump rates  $c_{x,x+1}(\eta) = \tau_x(c_{1,2}(\eta))$  are translation-invariant local functions of the configuration and bounded away from 0, meaning that for some positive constant  $c$ , and any  $\eta \in \Omega_N$ ,

$$c_{1,2}(\eta) \geq c. \quad (5)$$

(H2) For any  $\rho \in [0, 1]$  the generator  $\mathcal{L}_N$  is reversible w.r.t. Bernoulli product measures on  $\Omega_N$

$$\mu_\rho(\eta) := \prod_{x \in \mathbb{T}_N} \{\eta_x \rho + (1 - \eta_x)(1 - \rho)\}. \quad (6)$$

Note that this is in particular the case if  $c_{x,x+1}(\eta)$  does not depend on  $\eta_x$ , and  $\eta_{x+1}$ . These distributions are referred to as *grand-canonical measures* for the process, and we denote by  $\mathbb{E}_\rho$  the corresponding expectation.

(H3) The model is *gradient*, meaning that there exists a local function  $h(\eta)$  such that the instantaneous current  $j_{x,x+1}(\eta)$  along any edge is the discrete gradient of  $h$ ,

$$j_{x,x+1} := c_{x,x+1}(\eta_x - \eta_{x+1}) = \tau_x h - \tau_{x+1} h. \quad (7)$$

## 1.2 Characterization of macroscopic behavior.

Consider the continuous (periodic) ring  $\mathbb{T} := [0, 1]$ , we now define the notion of a configuration distribution fitting a macroscopic profile.

**Definition 1.1 (Measure fitting a macroscopic profile)** *We will say that a sequence of measures  $\mu^N$  on  $\Omega_N$  fits a macroscopic profile  $\rho : \mathbb{T} \rightarrow [0, 1]$  if for any smooth test function  $H$  on  $\mathbb{T}$  and any  $\delta > 0$ ,*

$$\lim_{N \rightarrow \infty} \mu^N \left( \left| \frac{1}{N} \sum_{x \in \mathbb{T}_N} \eta_x H(x/N) - \int_{\mathbb{T}} \rho(u) H(u) du \right| > \delta \right) = 0 \quad (8)$$

*As a particular case of the latter, we say that  $\mu^N$  is a product measure fitting  $\rho$  is*

$$\mu^N(\eta) = \prod_{x \in \mathbb{T}_N} \{\eta_x \rho(x/N) + (1 - \eta_x)(1 - \rho(x/N))\}, \quad (9)$$

*meaning each site  $x$  is independently filled by a particle with probability  $\rho(x/N)$ .*

This definition readily applies to the case of a non periodic or infinite lattice, like  $\mathbb{Z}$ , in which case (8) needs to hold for any test function on  $\mathbb{R}$  with compact support.

We now consider a continuous time Markov Process  $\{\eta(t), t \geq 0\}$  driven by the generator  $N^2 \mathcal{L}_N$  defined by (2) with a diffusive time scaling (time being accelerated by a factor  $N^2$ ), and we denote by  $\mathbb{P}_{\mu^N}$  its distribution starting from an initial distribution  $\mu^N$ , and by  $\mathbb{E}_{\mu^N}$  the corresponding expectation. We can now characterize the macroscopic behavior of our generic exclusion process.

**Theorem 1.1 (Hydrodynamic limit for  $\eta$ )** *Assume for simplicity that the initial distribution  $\mu^N$  is a product state associated in the sense of (9) with an initial profile  $\rho_0 : \mathbb{T} \rightarrow [0, 1]$ . Then, for any time  $t > 0$ , the distributions  $\mu_t^N := \mathbb{P}_{\mu^N}(\eta(t) = \cdot)$  of  $\eta(t)$  is associated with  $\rho(t, \cdot)$ , where the function  $\rho(t, u) : [0, +\infty) \times \mathbb{T} \rightarrow [0, 1]$  is the unique weak solution to the hydrodynamic equation*

$$\begin{cases} \partial_t \rho = \partial_u^2 \mathcal{H}(\rho) \\ \rho(0, \cdot) = \rho_0, \end{cases} \quad (10)$$

*where  $\mathcal{H}(\rho)$  is the expectation under  $\mu_\rho$  of the function  $h$  introduced in (7).*

$$\mathcal{H}(\rho) := \mathbb{E}_\rho(h).$$

To keep things short, we will not systematically define weak solutions to hydrodynamic equations. We simply define them in the generic case considered here, that will be straightforwardly adapted to the various setups considered throughout this manuscript. The following definition is obtained by integrating by parts against a smooth test function the solution to the hydrodynamic limit, with the significant upside that defining weak solutions requires much less regularity than strong ones. Furthermore, in all cases considered in this manuscript, we retain uniqueness of such solutions.

**Definition 1.2 (Weak solution to the hydrodynamic equation (10))** *We call any measurable trajectory  $\rho : [0, +\infty) \times \mathbb{T} \rightarrow [0, 1]$  a weak solution to (10) if for any smooth test function  $H$ , and any  $t > 0$*

$$\langle \rho(t, \cdot), H \rangle = \langle \rho_0, H \rangle + \int_0^t \langle \rho(s, \cdot), \partial_u^2 H \rangle ds,$$

where  $\langle \cdot, \cdot \rangle$  is the  $L^2(\mathbb{T})$  inner product.

In order not to have, each time, to give the full statement of the hydrodynamic limit, we adopt the following convention.

**Definition 1.3 (Hydrodynamic limit)** *Throughout, we will say that “the process  $\{\eta(t), t \geq 0\}$  has for hydrodynamic limit the weak solution  $\rho$  to a given PDE” – in this case, (10) for example –, if for any time  $t > 0$ , the distribution  $\mu_t^N$  of  $\eta(t)$  is associated with the profile  $\rho(t, \cdot)$  in the sense of Definition 1.1, where  $\rho$  is the unique weak solution to the hydrodynamic equation (10).*

Once again, analogous results can be derived in the cases where the lattice is infinite, or when boundary dynamics are added to the bulk dynamics, in which case (10) needs to be supplemented by macroscopic boundary conditions. Depending on the specificities of the microscopic dynamics considered (symmetric or not, gradient or not, reversible or not, etc.) a broad range of techniques can be used to prove this type of results, many of them are detailed in [48]. We sketch here one of the most classical techniques, namely Guo Papanicolaou and Varadhan’s *entropy method* [42], whose estimates will be referenced in several places throughout this manuscript.

### 1.3 Sketch of the entropy method

By Dynkin’s formula, shortening for any function  $h$  of the configuration  $h(s) := h(\eta(s))$ , we can write for any  $t$  and any test function  $H$

$$\frac{1}{N} \sum_{x \in \mathbb{T}_N} \eta_x(t) H(x/N) = \frac{1}{N} \sum_{x \in \mathbb{T}_N} \eta_x(0) H(x/N) + N^2 \int_0^t \frac{1}{N} \sum_{x \in \mathbb{T}_N} H(x/N) \mathcal{L}_N \eta_x(s) ds + M_t^{H,N}. \quad (11)$$

In the identity above,  $M^{H,N}$  is a martingale encompassing the CLT fluctuations around the hydrodynamic limit. Its quadratic variation can be explicitly computed (see [48, Appendix 1.5, Lemma 5.1]) and is of order  $O(t/N)$  and therefore vanishes in the limit  $N \rightarrow \infty$ . Regarding the time integral, thanks to the gradient condition (H3) above, we can write using (7)

$$\mathcal{L}_N \eta_x = j_{x-1,x} - j_{x,x+1} = \tau_{x+1} h + \tau_{x-1} h - 2\tau_x h$$

as a discrete Laplacian. Defining  $\partial_{u,N}^2$  as the discretization of  $\partial_u^2$ ,

$$\partial_{u,N}^2 H(u) = N^2 \{H(u + 1/N) + H(u - 1/N) - 2H(u)\} = \partial_u^2 H(u) + O(1/N),$$

summing by parts in (11), we obtain

$$\frac{1}{N} \sum_{x \in \mathbb{T}_N} \eta_x(t) H(x/N) = \frac{1}{N} \sum_{x \in \mathbb{T}_N} \eta_x(0) H(x/N) + \int_0^t \frac{1}{N} \sum_{x \in \mathbb{T}_N} \partial_u^2 H(x/N) \tau_x h(s) ds + \varepsilon_N, \quad (12)$$

where the error term  $\varepsilon_N$  vanishes in  $L^2$ . Note in particular that the factor  $N^2$  coming from the diffusive timescale has been absorbed in the test function's Laplacian.

At this point, we would like to express the identity above as a function of the *empirical measure*  $\pi_t^N$  of the process, namely

$$\pi_t^N := \frac{1}{N} \sum_{x \in \mathbb{T}_N} \eta_x \delta_{x/N}, \quad (13)$$

where  $\delta_u$  represents a Dirac measure at  $u$ . The upside of the empirical measure is that it is defined on the space  $\mathcal{M}$  of non-negative measures on  $\mathbb{T}$ , so that its limit as  $N \rightarrow \infty$  belongs to the same space. Given a measure  $\pi$  and a test function  $H$  on  $\mathbb{T}$ , we also denote by  $\langle \pi, H \rangle = \int_{\mathbb{T}} H(u) \pi(du)$  their inner product. With these notations, we can rewrite (14) as

$$\langle \pi_t^N, H \rangle = \langle \pi_0^N, H \rangle + \int_0^t \frac{1}{N} \sum_{x \in \mathbb{T}_N} \partial_u^2 H(x/N) \tau_x h(s) ds + \varepsilon_N. \quad (14)$$

Define a sequence of probability measures  $\mathbb{Q}_N := \mathbb{P}_{\mu^N} \circ \pi^{-1}$ , on the set  $D([0, T], \mathcal{M})$  of càdlàg trajectories on  $\mathcal{M}$ , as the pushforward of  $\mathbb{P}_{\mu^N}$  through the mapping

$$\pi : \{\eta(t), t \in [0, T]\} \mapsto \{\pi_t^N, t \in [0, T]\}.$$

One can show using classical tools that the sequence  $(\mathbb{Q}_N)_N$  is relatively compact, and that any of its limit points  $\mathbb{Q}^*$  is concentrated on trajectories which are, at any time  $t$ , absolutely continuous w.r.t. the Lebesgue measure,

$$\mathbb{Q}^*(\pi_t(du) = \rho(t, u) du) = 1.$$

In order for (14) to be expressed under any limit point  $\mathbb{Q}^*$  of  $(\mathbb{Q}_N)_N$ , we need to replace the microscopic observable  $\tau_x h$  by a function of the empirical measure. More precisely, define the mesoscopic density

$$\rho_x^{\varepsilon N}(t) := \frac{1}{2\varepsilon N + 1} \sum_{|y-x| \leq \varepsilon N} \eta_y(t) = \langle \pi_t^N, \iota_{x/N}^\varepsilon \rangle + O(1/N), \quad (15)$$

where  $\iota_u^\varepsilon = \mathbf{1}_{[u-\varepsilon, u+\varepsilon]}$ . The last identity shows that, as  $N \rightarrow \infty$   $\rho_x^{\varepsilon N}(t)$  is closely approximated, by a function of the empirical measure. Such a replacement of  $\tau_x h$  by a function  $\mathcal{H}(\rho_x^{\varepsilon N})$  typically holds in the limit where  $\varepsilon \rightarrow 0$  *after* letting  $N \rightarrow \infty$ , and is stated as a *replacement Lemma* as follows.

**Lemma 1.2 (Replacement Lemma)** *For any test function  $H$ , any local function  $g$  of the configuration, and any positive  $\delta, t$ ,*

$$\limsup_{\varepsilon \rightarrow 0} \limsup_{N \rightarrow \infty} \mathbb{P}_{\mu^N} \left( \left| \int_0^t ds \frac{1}{N} \sum_{x \in \mathbb{T}_N} H(x/N) \{ \tau_x g(s) - \mathbb{E}_{\rho_x^{\varepsilon N}(s)}(g) \} \right| > \delta \right) = 0, \quad (16)$$

where  $\mathbb{E}_\rho$  is the expectation w.r.t. the grand-canonical state  $\mu_\rho$  defined in (6).

This replacement Lemma together with (14) yields that as  $N \rightarrow \infty$ , any limit point  $\mathbb{Q}^*$  of  $(\mathbb{Q}^N)$  satisfies

$$\limsup_{\varepsilon \rightarrow 0} \mathbb{Q}^* \left( \left| \langle \pi_t, H \rangle - \langle \pi_0, H \rangle - \int_0^t \langle \mathcal{H}(\langle \pi_s, \ell^\varepsilon \rangle), \partial_u^2 H \rangle ds \right| > \delta \right) = 0.$$

Since  $\mathbb{Q}^*$ -a.s.,  $\pi_t(du) = \rho(t, u)du$ , we obtain letting  $\varepsilon$  to 0 that  $\mathbb{Q}^*$ -a.s.

$$\langle \rho_t, H \rangle = \langle \rho_0, H \rangle + \int_0^t \langle \mathcal{H}(\rho_s), \partial_u^2 H \rangle ds, \quad (17)$$

which proves the hydrodynamic limit stated in Theorem 1.1 since there is a unique weak solution  $\rho$  to (17). This strategy to prove the Replacement Lemma is called the *entropy method* because it strongly relies on estimating the local relative entropy  $H(\mu_t^N | \mu_\rho)$  between the distribution of the process  $\mu_t^N$  and its grand canonical distributions  $\mu_\rho$ , where the relative entropy is given by

$$H(\mu | \nu) := \sum_{\eta} d\mu(\eta) \log \frac{d\mu(\eta)}{d\nu(\eta)} = \mathbb{E}_\nu \left( \frac{d\mu}{d\nu} \log \frac{d\mu}{d\nu} \right). \quad (18)$$

As is the case with several models in this manuscript, entropy techniques can fail for processes where the actual distribution of the process is not well approximated by a well behaved reference distribution, either because boundary effects distort it (Chapter II), or in the presence of different microscopic phases (Chapter I).

## 1.4 Fluctuating hydrodynamics and large deviations

As the key argument to prove the hydrodynamic limit of diffusive lattice gases is the Replacement Lemma 1.2, Hydrodynamic limits play the role of a law of large numbers for interacting particle systems. In many cases, the hydrodynamic limit, as an idealized deterministic limit, does not contain all the information needed to characterize phenomena like phase transitions and phase separation. A natural question once the hydrodynamic limit is derived is therefore to obtain results on the fluctuations of the microscopic system around it, through

- Fluctuating hydrodynamics, analogous to the CLT for interacting particle systems. This is a mathematically very challenging topic, and although general techniques allow to characterize the fluctuation process in the stationary state, the general case of the fluctuating hydrodynamics starting from any density profile remains in large parts an open problem, despite significant recent progress [45, 46].
- Dynamical large deviations principles for the density and the current profiles in the hydrodynamic regime, for which the strategy, at least in finite volume, has been well established for decades [49, 24].

For a diffusive model like the Exclusion Process introduced in Section 1.1, which is reversible w.r.t. Bernoulli Product measure, both of these fluctuation regimes (stationary CLT and dynamical large deviations principle) can be characterized. Obviously, its static large deviations can be characterized as well, since the stationary state is explicit and given by (6). For non-equilibrium models, for example driven by boundary dynamics, the stationary state is typically not known explicitly, and obtaining its static large deviations regime becomes

much more challenging [23, 9, 12]. Fix once and for all a density  $\rho \in (0, 1)$ , macroscopic stationary fluctuations for our exclusion process can be characterized by the distribution  $\mathcal{Y}_t^N$  acting on test functions  $H : \mathbb{T} \rightarrow \mathbb{R}$  as

$$\mathcal{Y}_t^N(H) = \frac{1}{\sqrt{N}} \sum_{x \in \mathbb{T}_N} H(x/N)(\eta_x(t) - \rho). \quad (19)$$

Once again, we want to derive the limiting field  $(Y_t)$  as  $N \rightarrow \infty$ .

To do so, define our processe's *diffusion coefficient*

$$D(\rho) := \mathcal{H}'(\rho) = \frac{d}{d\rho} \mathbb{E}_\rho(h), \quad (20)$$

its *conductivity*

$$\sigma(\rho) = \mathbb{E}_\rho(c_{1,2}). \quad (21)$$

The CLT fluctuations for our generic exclusion process can now be characterized thusly.

**Theorem 1.3** *The fluctuation field  $\mathcal{Y}_t^N$  converges as  $N \rightarrow \infty$  to a stationary solution  $Y_t$  to the stochastic heat equation*

$$\partial_t Y_t = D(\rho) \partial_u^2 Y_t + \sqrt{2\sigma(\rho)} \partial_u \dot{\mathcal{W}}_t, \quad (22)$$

where  $\partial_u \dot{\mathcal{W}}_t$  is a space-time white noise.

Note that in order to avoid introducing burdensome notations, we do not specify here the proper topological setup for the convergence above, and refer the reader to e.g. [48, Chapter 11] for more details.

To go beyond this equilibrium CLT, one can try and understand the large deviations regime for the density field  $\rho$ . In other words, given a smooth enough function  $\rho : [0, T] \times \mathbb{T} \rightarrow [0, 1]$  (which is not a solution to the hydrodynamic equation (10)), can we estimate as a function of  $N$  the decaying probability  $\mathbb{P}_{\mu^N}(\pi_t^N \simeq \rho(t, u) du)$ ? In what follows, according to the terminology defined in the Macroscopic Fluctuations Theory [10], we will call such deviations *fluctuations*, but the reader should bear in mind that these fluctuations are not the fluctuations, of order  $1/\sqrt{N}$  which are typical under the CLT, but rather very unlikely fluctuations of order 1 that can occur for fixed but large  $N$ , that are encompassed in the regime of large deviations. According to large deviations theory, to do so one needs first to understand *how* such a deviation would occur. In this regime, two types of fluctuations coexist to create a deviation  $\rho$  from the hydrodynamic limit, that correspond to the two types of randomness in the process  $\{\eta(t), t \geq 0\}$ :

- *static large deviations* come from the randomness of the initial configuration, and occur if the initial distribution has produced a configuration which is close to an unlikely initial profile  $\rho(t, 0)$ .
- *dynamical large deviations* come from the randomness of the dynamics, and translate the fact that an anomalous number of jumps, producing an anomalous particle current, can occur throughout the evolution of the Markov process, resulting in an unlikely macroscopic profile.

Consider now the latter : because our exclusion process locally conserves mass, we know that under any trajectory of the process, we must have a relation between variation of the

density in a local region, and the current going through this region. More precisely, even for a very unlikely realization of the process, at the macroscopic level the local particle current  $j(t, u) = j[\rho]$  must satisfy

$$\partial_t \rho = \partial_u j. \quad (23)$$

In particular, knowing the initial density profile  $\rho(0, \cdot)$  and the current  $j$  fully characterizes  $\rho$ , and it is much more convenient to work with  $j$  because dynamical large deviations come from deviations in the microscopic current  $j_{x, x+1}$ , that can be readily translated in terms of macroscopic current  $j$  (see Section 9.2 for more on the topic). More precisely, we have the following formal result.

**Theorem 1.4** *Fix an initial profile  $\rho_0 : \mathbb{T} \rightarrow [0, 1]$ , and consider the process  $\eta(t)$  with initial product distribution fitting  $\rho_0$ , given by (9) and driven by  $N^2 \mathcal{L}_N$ . For any (smooth enough) function  $\rho : [0, T] \times \mathbb{T} \rightarrow [0, 1]$ , letting  $j = j[\rho]$  be the associated current defined through (23), we have*

$$\mathbb{P}(\pi_t^N \simeq \rho(t, u) du, \forall t \in [0, T], u \in \mathbb{T}) \asymp \exp(-N\{S_0[\rho(0, \cdot)] + I_{[0, T]}[\rho, j]\}), \quad (24)$$

where the statical large deviations functional  $S_0$  is the classical relative entropy w.r.t.  $\rho_0$

$$S_0[\gamma] := \int_{\mathbb{T}} du \left\{ \gamma \log \frac{\gamma}{\rho_0} + (1 - \gamma) \log \frac{1 - \gamma}{1 - \rho_0} \right\}$$

and the dynamical large deviations functional  $I_{[0, T]}$  is given by

$$I_{[0, T]}[\rho, j] = \frac{1}{2} \int_0^T \int_{\mathbb{T}} \frac{1}{\sigma(\rho)} (j - D(\rho) \partial_u \rho)^2 du ds,$$

where the conductivity  $\sigma$  was defined in (21). Note that as expected, both  $S_0[\rho(0, \cdot)]$  and  $I_{[0, T]}[\rho]$  vanish if  $\rho$  is solution to the hydrodynamic equation (10) with the correct initial data  $\rho_0$ , because in this case  $j[\rho] \equiv D(\rho) \partial_u \rho$ .

Now that the main notions and notations have been briefly introduced, we present, chapter by chapter, the various results presented in this manuscript. In order to avoid introducing straight away burdensome notations, and to keep things (relatively) short, many of the results presented in this introduction will not be stated in a mathematically rigorous way. The precise statements will be given in the chapter themselves, together with sketches of the salient points of the proofs.

## 2 Influence of kinetic constraints

The first part of this manuscript concerns kinetically constrained models [83], in particular the so-called Facilitated Exclusion Process (FEP) introduced by physicists in [65].

### 2.1 The Facilitated Exclusion Process

The FEP is a toy model for phase separation defined by supplementing the classical SSEP with a hard kinetic constraint. More precisely, in the one-dimensional FEP, particles can jump to an empty neighboring site iff their other neighbor is occupied by a particle. In other words, only *active* particles can jump, meaning particles with at least one occupied neighbor. In the symmetric case, the jump rates in its Markov generator (2), at which sites  $x$  and  $x + 1$  are exchanged, encompass this kinetic constraint, and are given by

$$c_{x,x+1}(\eta) = \eta_{x-1}\eta_x(1 - \eta_{x+1}) + \eta_{x+2}\eta_{x+1}(1 - \eta_x). \quad (25)$$

Since they vanish when the kinetic constraint is not satisfied, those jump rates are not bounded away from 0, and it is easy to check that they are not reversible w.r.t. Bernoulli product measures, so that assumptions (H1) and (H2) in Section 1.1 are not satisfied by the FEP. However, it is *gradient*, since the gradient condition (7) is satisfied by the function

$$\tau_x h(\eta) = \eta_{x-1}\eta_x + \eta_x\eta_{x+1} - \eta_{x-1}\eta_x\eta_{x+1}.$$

Note that the function  $\tau_x h$  is the indicator function that  $x$  and at least one of its neighbors are occupied, or in other words the indicator function that there is an *active particle* at site  $x$ .

Because of the kinetic constraint, the facilitated exclusion process has two phases, depending on the local density  $\rho$ : in the supercritical phase ( $\rho > 1/2$ ), after a transience time, all empty sites become isolated, which defines an *ergodic component*

$$\mathcal{E} := \{\eta, \eta_x + \eta_{x+1} \geq 1 \ \forall x\} \quad (26)$$

for the process. Indeed, pairs of neighboring empty sites can only be split up by the process, because a particle surrounded by empty sites cannot jump out. In the subcritical phase ( $\rho < 1/2$ ), instead, after a transience time, particles become isolated and the process eventually reaches a frozen state  $\eta \in \mathcal{F}$ , where

$$\mathcal{F} := \{\eta, \eta_x + \eta_{x+1} \leq 1 \ \forall x\} \quad (27)$$

because there are no active particles left. The critical phase  $\rho = 1/2$  concentrates on alternated configurations  $\cdots \circ \bullet \circ \bullet \cdots$ , where  $\bullet$  represents particles and  $\circ$  represents empty sites.

### 2.2 Hydrodynamic limit and transience time for the symmetric FEP

In order to derive the macroscopic behavior of the FEP, one could hope to straightforwardly apply the *entropy method* sketched in Section 1.3 to derive a result analogous to Theorem 1.1 for the FEP. As mentioned previously, however, the *entropy method* relies on estimating the relative entropy of the distribution of the microscopic process w.r.t. its grand canonical states  $\pi_\rho$ . The latter are defined in the supercritical phase  $\rho \geq 1/2$  and are supported on the

ergodic component  $\mathcal{E}$ , since in the subcritical phase any frozen configuration is a stationary state. To derive in the supercritical phase the FEP's hydrodynamic limit using the entropy method, one therefore needs first to show that the ergodic component is reached after a subdiffusive transience time  $t_N \ll N^2$ , and then apply the *entropy method* from this point, where the entropy will be well defined and finite. For this purpose, we have proved [BESS20, Theorem 2.4] that given a supercritical profile  $\rho_0 \geq 1/2$  on  $\mathbb{T}$ , and the associated product measure  $\mu^N$  in the sense of (9), the FEP  $\{\eta(t), t \geq 0\}$  with jump rates (1.2) and started from  $\mu^N$  reaches the ergodic component w.h.p. at a subdiffusive time

$$t_N := (\log N)^{32} \ll N^2.$$

We then exploited this estimate to adapt the *entropy method* to the FEP, and proved in [BESS20, Theorem 2.2] that the hydrodynamic limit for the *supercritical* FEP, started from a product state  $\mu^N$ , is given by the parabolic equation

$$\partial_t \rho = \partial_u^2 \left\{ \frac{2\rho - 1}{\rho} \right\}. \quad (28)$$

In reality, once the ergodic component is reached, the behavior of the FEP is not too different from that of the SSEP, so that deriving its macroscopic behavior is fairly straightforward.

Once the supercritical behavior has been characterized, it is natural to consider what happens when the initial profile charges both the supercritical and the subcritical phase. This is much more challenging, because entropy based-techniques usually require a well defined set of reference measures to which one locally compares the process, but in the presence of phase separation like for the FEP, the distributions of the local states in the two phases have disjoint support, so that no unique set of reference distributions exist. For that reason, we exploited instead a scheme of proof due to Funaki [31] to derive in [BES21, Theorem 2.4] the phase separated hydrodynamic limit in the general case, which translates as a Stefan (also called free boundary) problem

$$\partial_t \rho = \partial_u^2 \left\{ \frac{2\rho - 1}{\rho} \mathbf{1}_{\{\rho \geq 1/2\}} \right\}, \quad (29)$$

whose behavior is represented in Figure 1. Of course, the function in the Laplacian above is not smooth at the interfaces, so that this equation is to be taken either in a weak sense, integrated against test functions, or in a strong sense, where the diffusion equation inside the supercritical region is supplemented by evolution equation for the critical interfaces (with trajectories  $u_1(t)$  and  $u_2(t)$  for example, in the case where there is one supercritical and one subcritical region).

In the latter, we further showed that at the microscopic level, phase separation occurs in a subdiffusive timescale as well. More precisely, consider for example an initial density profile  $\rho_0$  like the one represented in figure 1, with one supercritical region and one subcritical region, separated by interfaces  $u_1(t=0)$ ,  $u_2(t=0)$  where the gradient of  $\rho_0$  is non-zero. Then, as stated in [BES21, Theorem 2.6], microscopic phase separation occurs before a subdiffusive time  $t_N := N^{7/4} \ll N^2$ , meaning that w.h.p. there exists a partition of  $\mathbb{T}_N = E \sqcup F$  into two segments  $E$ ,  $F$  such that

$$\eta(t_N)|_E \in \mathcal{E} \quad \text{and} \quad \eta(t_N)|_F \in \mathcal{F},$$

where  $\mathcal{E}$  and  $\mathcal{F}$  are the ergodic and frozen sets defined in (26) and (27). Finally, we proved that in the two phased regime, the microscopic and macroscopic interfaces match, in the sense that their (macroscopic) distance vanishes as  $N \rightarrow \infty$ .

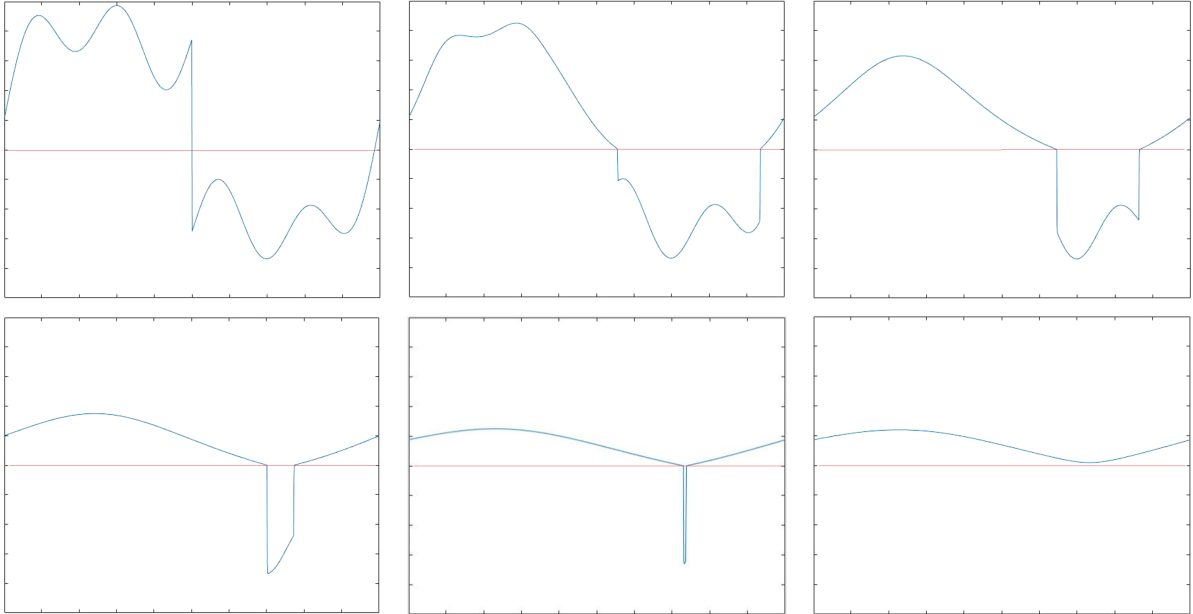


**Figure 1:** Snapshots of the evolution of the solution (blue curve) to the Stefan problem (29). The red line marks the critical density.

### 2.3 Hydrodynamic limit for the asymmetric FEP

There are several rather robust tools to derive the hydrodynamic limit of diffusive or weakly asymmetric (for asymmetries of order  $1/N$ ) systems e.g. Guo, Papanicolaou and Varadhan’s *entropy method* [42], Yau’s *relative entropy method* [78] or Varadhan’s *non-gradient method* [73, 61]. Asymmetric systems are typically much more challenging, and the only case where their hydrodynamic limit can be reliably characterized is when the underlying microscopic dynamics is *attractive* [64], [48, Chapter 8], in which case powerful coupling arguments allow to locally compare the evolution of the system to its equilibrium counterparts. For *non-attractive* systems, the best options are the *relative entropy method* [78], which only characterizes the hydrodynamic limit up until the first shock of the hydrodynamic equation, or Fritz’s *compensated compactness arguments* [29], which are extremely technical and require adding some symmetric stirring rates to mix the configuration in the spirit of the vanishing viscosity limit for PDEs.

The FEP, unfortunately, is not attractive. However, as already exploited in [8], it can be mapped to a degenerate zero-range (ZR) process  $\omega$ , in which any site with at least two particles makes one of them jump away at rate 1. In fact, this mapping was already instrumental in the estimations of the transience times started from a product distribution obtained in [BESS20, BES21]. Because the ZR jump rate  $g(\omega_y) = \mathbf{1}_{\{\omega_x \geq 2\}}$  is non decreasing, this non-ergodic zero-range process *is* attractive, and its hydrodynamic limit  $\alpha(t, v)$  can be derived by adapting [64]. As proved in [ESZ23b, Theorem 2.6], it is given in the symmetric case by the diffusive Stefan problem

$$\partial_t \alpha = \partial_v^2 \left\{ \frac{\alpha - 1}{\alpha} \mathbf{1}_{\{\alpha \geq 1\}} \right\}, \quad (30)$$

and in the asymmetric case by the unique entropy solution to the hyperbolic Stefan problem

$$\partial_t \alpha = -(2p - 1) \partial_v \left\{ \frac{\alpha - 1}{\alpha} \mathbf{1}_{\{\alpha \geq 1\}} \right\}, \quad (31)$$

where  $p \in (1/2, 1]$  is a parameter that tunes the asymmetry of the zero-range particle's motion. Hyperbolic equations develop shocks, and because of that solutions to hyperbolic equations are not unique. Here, *entropy solution* means choosing the unique physically relevant solution to the PDE, which can be seen as the limiting vanishing viscosity solution (where a small diffusive term is added to smooth everything out, and vanishes in the limit) to (31) (see e.g. [26, Chapter 11]). Note that it is not true in general that the functions characterizing the hyperbolic and parabolic equations are the same as in (30) and (31), this is a specific feature of zero-range processes.

Thanks to these two results, we were then in a position to map back and forth the hydrodynamic limit. This is by no means immediate, since mapping at the macroscopic level requires smoothness of the mapping, which is not the case here both because of the shocks due to the hyperbolic equation, and the shocks due to the Stefan problem. Nevertheless, by smoothing everything out, we were able to recover the diffusive hydrodynamic limit already obtained in [BES21], as well as to derive the hydrodynamic limit of the asymmetric FEP, which takes the form of a hyperbolic Stefan problem as well:

$$\partial_t \rho = -(2p - 1) \partial_u \left\{ \frac{(1 - \rho)(2\rho - 1)}{\rho} \mathbf{1}_{\{\rho \geq 1/2\}} \right\}. \quad (32)$$

Once again, making sense in a unique way of the solution to this equation requires singling out its entropy solution.

## 2.4 Stationary CLT fluctuations for the FEP

In order to derive the stationary CLT for the FEP, in an analogous sense to Theorem 1.3, in both symmetric and asymmetric cases, we exploit the same mapping and use the zero-range process's attractiveness in [EZ24]. The symmetric case can in reality be derived directly on the FEP, whose equilibrium states are explicit, by deriving refined equivalence of ensembles estimates (see [EZ24, Proposition 5.5]) w.r.t. those necessary to prove the hydrodynamic limit (28). This strategy, however, no longer works in the asymmetric case. In the latter, we get back to the mapping with the facilitated zero-range process. Exploiting its attractiveness, its stationary fluctuations in the weakly asymmetric and totally asymmetric cases were derived respectively in [40] and [38].

Applying those results through the mapping is not immediate either however, for two reasons. First, the explicit definition of the stationary states  $\pi_\rho$  for the FEP is not easily exploitable, in the sense that nice properties like correlation decay are not immediate. It is therefore more convenient to use a Markovian construction for those stationary states, however this Markovian construction breaks the natural translation invariance of  $\pi_\rho$ , which raises a separate set of issues. For this reason, much of the work [EZ24] revolves around obtaining explicit estimates and constructions for the mapping and the stationary states for both processes.

Second, as described in details in Section 5.3-B), the dynamical mapping involves a tagged empty site, whose position both at the microscopic and macroscopic level needs to be kept track of in order map back and forth the fluctuations process. Once this is achieved, as one could expect, the macroscopic fluctuations field for the weakly asymmetric FEP (symmetric jumps at rate  $N^2$ , asymmetric jumps at rate  $N^\gamma$ ) travels at constant speed  $vN^{\gamma-1}$ , where  $v$  depends on the chosen  $\rho$ . Mapping back and forth with the zero-range process, we can then show [EZ24, Theorem 2.2] that in the weakly asymmetric case, the traveling fluctuation field  $\tau_{-vN^{\gamma-1}} \mathcal{Y}_t^N$  converges to

- the solution of the stochastic heat equation (I.50) for  $\gamma < 3/2$ , and
- to the stochastic Burgers equation

$$\partial_t Y_t = D(\rho) \partial_u^2 Y_t + \frac{1}{2} D'(\rho) \partial_u Y_t^2 + \sqrt{2\sigma(\rho)} \partial_u \dot{W}_t, \quad (33)$$

for  $\gamma = 3/2$ .

In the totally asymmetric case where symmetric jumps are suppressed, so that as expected  $\tau_{-vN^{\gamma-1}} \mathcal{Y}_t^N$  converges instead the solution of  $\partial_t Y_t = \sqrt{2\sigma(\rho)} \partial_u \dot{W}_t$  [EZ24, Theorem 2.3].

## 2.5 SWT and cutoff for the transience time

In [BESS20, BES21], we characterized the transience time for the FEP started from a product measure with smoothly varying initial density in the context of the FEP's hydrodynamic limit. In [EM24], we develop a more detailed approach in order to estimate the transience time started from any given deterministic configuration. To compare the transience time starting from different configurations, however, is not straightforward in the absence of monotonicity arguments. For this reason, mapping the FEP to attractive processes like the zero-range process mentioned in the previous sections seems a natural option. This was, however, not the mapping we used, because our goal was to obtain sharp estimates on the transience time, and in the zero-range process the typical jump times of particles can only roughly be estimated.

Instead, we found a mapping of the FEP to a new process that we called SSEP with traps, in which particles behave as in the SSEP, except when they encounter traps in which they get stuck forever. Each trap can only contain a given number of particles, and then behaves as a typical SSEP empty site. This mapping, restricted to the ergodic component, maps the FEP to the classical SSEP, and was already exploited in recent results [3] on the FEP's mixing time under suitable assumptions on the initial state. This SSEP with traps is also attractive, and allowed us to prove

- that the longest transience time is for the FEP and the SSEP with traps is achieved for critical configurations.
- That the worst transience time for the SSEP with trap's critical configurations on  $\mathbb{T}_K$  undergoes cutoff at time  $t_K^* := \frac{1}{\pi^2} K^2 \log K$ . In other words, starting from the worst possible configuration, the probability for large  $K$  to still be in a transient state at time  $t$  goes from 1 to 0 at  $t_K^*$  in a time window of size  $\delta t \ll t_K^*$ .
- That the same is true for the FEP on  $\mathbb{T}_N$ , with cutoff occurring at time  $\frac{1}{4\pi^2} N^2 \log N$ .

The sharp estimate on the transience time yields in turn a sharp estimate on the mixing time for the SSEP with traps. This, however, does not translate straightforwardly to a general estimate on the FEP's mixing time that would drop the assumption on the initial configuration made in [3]: contrary to the transience time, which is translated trajectory per trajectory from one process to the other, the mixing time concerns the full distribution of the configuration at time  $t$ . To let such information go through our mapping, one needs refined characterization on the joint law of the configuration and that of a tracer particle in the system, which fell beyond the scope of our article and was studied separately in [58].

## 2.6 Critical behavior for a 2-dimensional FEP

Because of their reliance on mapping arguments, and on the explicit shape of the FEP's stationary states, hardly any of our one-dimensional results translate to higher dimension FEP-like models. In [25], we consider a two dimensional kinetically constrained exclusion process, where particles jump at rate 1 to empty neighbors provided they had an occupied neighbor before the jump. We study the macroscopic behavior near criticality of this process –that we call CLG in accord with the physics literature [65]– meaning near the transition between frozen and diffusive behavior over *diffusive timescales*. Notably, contrary to the one-dimensional case, this transition occurs at a density  $\rho_c < 1/2$ , meaning that in the density range ( $\rho_c < \rho < 1/2$ ), frozen configurations do exist, and are ultimately reached by the process, but starting from a typical (e.g. product-measured) configuration, frozen states are not reached over diffusive timescales.

We numerically derive in [25] the critical exponents for this two-dimensional CLG. In particular, our simulations confirm the existence of two separate correlation length scales near criticality, conjectured in [44] : one related to the decay of 2-points correlations, and the other pertaining to the typical size of active clusters. Some critical exponents are fairly challenging to directly estimate numerically, so that we also derive a number of relations between critical exponents.

## 3 Boundary-driven models

*The second part of this manuscript is concerned with boundary-driven dynamics, which have come under significant scrutiny in recent years, because they provide simple examples of non-equilibrium models. Throughout this section, we consider the one-dimensional lattice*

$$\Lambda_N := \{1, \dots, N\}$$

*with non-periodic boundary conditions.*

### 3.1 SSEP with general boundary dynamics

The SSEP is characterized by its Markov generator

$$\mathcal{L}_{\text{bulk}} f(\eta) := \sum_{x=1}^{N-1} \{f(\eta^{x,x+1}) - f(\eta)\}. \quad (34)$$

where the configuration  $\eta^{x,x+1}$  was defined in (3). Note that the rate at which two sites are exchanged is 1, so that, all particles being identical, this process simply makes particle jumps on neighboring empty sites at rate 1. This *stirring dynamics* will be referred to in what follows as *bulk dynamics*. The latter stands in opposition to the *boundary dynamics*, driven by the left and right generators that can typically be written as

$$\mathcal{L}_{\text{left}} f(\eta) := c_{\text{left}}(\eta) \{f(\eta^1) - f(\eta)\}, \quad (35)$$

$$\mathcal{L}_{\text{right}} f(\eta) := c_{\text{right}}(\eta) \{f(\eta^N) - f(\eta)\}. \quad (36)$$

In these definitions,  $\eta^x$  represents the configuration where the value of the configuration at site  $x$  has been changed, namely

$$\eta_y^x := \begin{cases} \eta_y & \text{if } x \neq y \\ 1 - \eta_y & \text{if } x = y \end{cases}. \quad (37)$$

We denote by

$$\mathcal{L}_N = N^\theta (\mathcal{L}_{\text{left}} + \mathcal{L}_{\text{right}}) + N^2 \mathcal{L}_{\text{bulk}} \quad (38)$$

the total generator of the dynamics. In what follows, the constant  $\theta$  will allow us to tune the strength of the boundary dynamics w.r.t. the bulk dynamics.

The classical choice of boundary jump rates is  $c_{\text{left}} = \kappa_\alpha(\eta_1)$  and  $c_{\text{right}} = \kappa_\beta(\eta_N)$  where for  $r \in [0, 1]$ ,  $\sigma \in \{0, 1\}$  we defined

$$\kappa_r(\sigma) = r(1 - \sigma) + (1 - r)\sigma. \quad (39)$$

For simplicity, we will refer to those rates as *constant rate dynamics*, or *equilibrium reservoirs*. Physically speaking, these jump rates put the left (resp. right) boundary of the SSEP in contact with an infinite equilibrium reservoir at density  $\alpha$  (resp.  $\beta$ ), meaning that at rate 1, the occupation value  $\eta_1$  at site  $x = 1$  is replaced by an independent *Bernoulli*( $\alpha$ ) variable, and at site  $x = N$  by a *Bernoulli*( $\beta$ ) variable. This choice of reservoirs is natural for the SSEP, because they locally preserve the SSEP's stationary states. In particular, in the case where  $\alpha = \beta$  it is easy to check that the dynamics is reversible w.r.t. the product distribution  $\mu_\alpha := \otimes_{x \in \Lambda_N} \text{Bernoulli}(\alpha)$ . As soon as  $\alpha \neq \beta$  however, non-trivial correlations arise, and the boundary-driven SSEP's stationary state are no longer explicit [21]. It is not hard to check, using entropy-based techniques for example (see e.g. [5]), that if  $\theta > 1$  (strong interaction with reservoirs), this boundary-driven SSEP's hydrodynamic limit  $\rho$  is then given by the heat equation supplemented by Dirichlet boundary conditions

$$\rho(t, 0) = \alpha, \quad \rho(t, 1) = \beta \quad \text{for } t > 0.$$

### 3.2 Non-reversible boundary dynamics

Instead of those equilibrium reservoirs, we consider in several setups the case of boundary dynamics which are not reversible w.r.t. Bernoulli product measures, in which case at the two boundaries, a competition arise between boundary and bulk dynamics to impose their own stationary state. This competition prevents the use of classical entropy techniques, since those only work when the process's stationary state is well approximated by explicit distributions. For this reason, our work on these models is based on duality estimates. Throughout this paragraph, we consider boundary local jump rates, depending on a box of fixed size  $p$  independent of  $N$ , meaning that  $c_{\text{left}}$  (resp.  $c_{\text{right}}$ ) depends on  $\eta$  only through  $\eta_1, \dots, \eta_p$  (resp through  $\eta_{N+1-p}, \dots, \eta_N$ ), and we consider *strong* boundary interactions, meaning that  $\theta = 2$  is chosen in (38): the boundary dynamics and the bulk dynamics occur at same-order rates.

In [ELX18], we consider three distinct cases with non-reversible (w.r.t. Bernoulli product measures) boundary dynamics, and in each, derive the hydrostatic limit, i.e. the macroscopic stationary state, for the boundary-driven SSEP. The first case concerns boundary dynamics which are, in some sense, linear: this means that for  $1 \leq j, k \leq p$ , at constant rate  $c_{j,k}$ , site  $j$  *copies*, i.e. takes the same value as, site  $k$ . Also at constant rates  $a_{j,k}$ , site  $j$  *anti-copies*, i.e. takes the opposite value of, site  $k$ . Finally, each of the boundary sites  $1 \leq j \leq p$  is put in contact with an equilibrium reservoir analogous to (39). Analogous rates are defined at the other boundary  $\{N+1-p, \dots, N\}$ . What makes these three mechanisms special is that, in some sense, they are the only possible boundary dynamics that break down correlations at the boundary. More details will be given in Section 8.1.

The second case considered in [ELX18] is that of a perturbation of constant rates dynamics. In other words, we then assume that particles are created/annihilated at sites 1

and  $N$ , but at rates that do not depend “too much” on the state of the configuration near the boundary, i.e. on the sub-configurations  $(\eta_2, \dots, \eta_p)$  or  $(\eta_{N+1-p}, \dots, \eta_{N-1})$  respectively. More specifically, we assume that there exists a small enough constant  $c(p)$  (independent of  $N$ ) such that for two boundary states  $\eta_2, \dots, \eta_p$  and  $\sigma_2, \dots, \sigma_p$ ,

$$|c_{\text{left}}(\cdot, \eta_2, \dots, \eta_p) - c_{\text{left}}(\cdot, \sigma_2, \dots, \sigma_p)| \leq c(p), \quad (40)$$

and that the same is true at the other boundary. Because the boundary dynamics depends on the local state at the boundary, correlations do arise in the system, but those correlations only exist locally near the boundary, and do not propagate throughout the system. Because of that, a law of large numbers does hold at the boundary and allows to derive the Dirichlet boundary conditions in the hydrodynamic limit.

For the third case studied in [ELX18], the boundary dynamics is accelerated further by a factor  $\ell_N$  going to infinity as  $N \rightarrow \infty$ , meaning that the boundary dynamics occurs at a total rate  $N^2 \ell_N$  rather than  $N^2$ . In this case, the boundary dynamics thermalizes faster than the bulk dynamics, and we can drop assumption (40) on the boundary dynamics.

The duality estimates introduced to obtain in [ELX18] the *hydrostatic* limit of the non-reversible boundary-driven SSEP in the three cases above, on their own, were not sufficient to derive the *hydrodynamic* limit in the same three cases. Instead, this was done in [Eri18], by obtaining refined estimates. The main difficulty in the latter w.r.t. [ELX18] is that boundary-driven models can create sharp density gradients, in the case where the Dirichlet boundary condition was not satisfied by the initial profile, and needs to be enforced immediately at the boundary. These sharp density gradients, in turn, create strong spatial correlations locally at the boundary close to the initial time, and those spatial correlations need to be tightly controlled to derive the hydrodynamic limit. However, as explained in more details in Section 8.1, duality estimates are still essential to our approach, since they allow to completely bypass the lack of agreement between the bulk and boundary dynamics’s stationary states resulting in poor entropy estimates at the boundary. In particular, our work allows to derive the hydrodynamic limit in the case where several sites at the same boundary are put in contact with equilibrium reservoirs with different densities, which would be by no means trivial to achieve with entropy-based tools.

In subsequent works [EGN20a, EGN20b], we exploit both duality estimates and entropy estimates to derive both hydrostatic and hydrodynamic limit, and extend analogous results to the intermediary regime  $1 < \theta < 2$ , as well as in the subcritical regime  $\theta \leq 1$  for such a non-reversible boundary dynamics.

### 3.3 Static large deviations for the SSEP in weak contact with equilibrium reservoirs

We now get back to the SSEP put in contact at both extremities with equilibrium reservoirs with densities  $r = \alpha$  and  $r = \beta$  with rates defined by (39). As mentioned previously, when  $\alpha = \beta$  the dynamics is reversible w.r.t. Bernoulli product measures with density  $\alpha$ , regardless of the value of  $\theta$ . In the non-equilibrium case  $\alpha \neq \beta$ , the stationary state is no longer explicit. For strong boundary interactions  $1 < \theta < 2$ , it is well enough approximated by a product distribution

$$\tilde{\mu} := \bigotimes_{x=1}^N \text{Bernoulli} \left( \alpha + \frac{x}{N} (\beta - \alpha) \right)$$

to be able to derive hydrostatic and hydrodynamic limit. However, in the large deviations regime, lower order correlations intervene and the picture becomes much less clear. Let us denote by  $\bar{\mu} = \bar{\mu}(\alpha, \beta)$  the SSEP with reservoir's stationary state. Analogously to the dynamical setting (41), we want to obtain a static large deviations principle for the density, which can be formally written

$$\bar{\mu}(\pi^N \simeq \rho(u)du) \asymp \exp -NV[\rho], \quad (41)$$

where the functional  $V$  is referred to as the *quasi-potential* and can be defined through a variational principle for the *dynamical* large deviations functional  $I_{[0,T]}[\rho, J]$  introduced in Theorem 1.4.

In [23], Derrida et al.'s *Matrix Ansatz* [21] was used to show that for *strong* boundary interactions ( $\theta = 2$ ), the quasi-potential  $V = V_s[\rho]$  could be expressed as

$$V_s[\rho] := \begin{cases} \int_0^1 \rho(u) \log \frac{\rho(u)}{F(u)} + (1 - \rho(u)) \log \frac{1-\rho(u)}{1-F(u)} + \log \frac{F'}{\beta-\alpha} du & \text{if } \rho(0) = \alpha \quad \rho(1) = \beta, \\ \infty & \text{otherwise,} \end{cases} \quad (42)$$

where the function  $F = F[\rho]$  is solution to a non-linear differential equation, the Derrida–Lebowitz–Speer (DLS) equation

$$F'' = (\rho - F) \frac{(F')^2}{F(1 - F)} \quad (43)$$

with Dirichlet boundary conditions  $F(0) = \alpha$ ,  $F(1) = \beta$ . This representation was then extended, still using the Matrix ansatz, in [22] to the case of *weak* interactions ( $\theta = 1$ ) with the boundary in which case the boundary densities are no longer fixed, and the quasi-potential  $V = V_w[\rho]$  includes extra boundary terms

$$V_w[\rho] := V_s[\rho] + \log \frac{F(0) - \alpha}{\beta - \alpha} + \log \frac{\beta - F(1)}{\beta - \alpha}, \quad (44)$$

where  $F$  is still solution to the DLS equation, but this time with the same Robin boundary conditions that appear in the hydrodynamic limit, namely

$$\begin{cases} F'(0) = F(0) - \alpha \\ F'(1) = \beta - F(1) \end{cases} . \quad (45)$$

In [BEL23], we recover Derrida et al.'s formulation (44) for the quasi-potential of the SSEP in weak interactions with reservoirs. Using the same strategy as in [9] for the case of strong boundary interactions, we express the quasi-potential as a function of the dynamical large deviations functional derived in [28], and identify the optimal trajectory producing a stationary fluctuation.

### 3.4 Zero-range process with destruction at the origin

We consider in [ESZ23a] the influence of boundary dynamics on the attractive asymmetric zero-range process on  $\mathbb{Z}$ . The boundary dynamics intervenes at the origin, where particles are removed according to the same jump rates as in the bulk dynamics. This boundary dynamics is driven by the generator

$$\alpha N^\theta g(\omega_0) \{f(\omega - \mathbf{1}_0) - f(\omega)\}, \quad (46)$$

where  $\omega - \mathbf{1}_0$  represents the configuration obtained after removing a particle at the origin in  $\omega$ , and  $\alpha, \theta > 0$  tunes the boundary dynamics. As explained for the FEP in Section 2.3, attractiveness is a crucial tool in order to derive the hydrodynamic limit of asymmetric models, so that we assume the rate function  $g$  to be non-decreasing on the set of positive integers  $\{1, 2, \dots\}$ , making our zero-range process *attractive*. By convention, we assume  $g(0) = 0$ , and that it is the same rate as the bulk dynamics jump rate.

In [ESZ23a], we derive the hydrodynamic for this asymmetric zero-range process, for boundary dynamics scaling as  $N^\theta$ . We show that for  $\theta < 0$ , the boundary dynamics is very slow, and does not affect the hydrodynamic limit, which is then given by the unique entropy solution  $\rho^*$  on  $\mathbb{R}$  to the hyperbolic equation

$$\partial_t \rho + (2p - 1) \partial_u \Phi(\rho) = 0, \quad (47)$$

where the function  $\Phi$  depends explicitly on the rate function  $g$ , as detailed in Section 10.2 and  $p > 1/2$  is the asymmetry parameter for the bulk dynamics (see (II.50)).

For  $\theta = 0$ , the destruction dynamics intervenes at a macroscopic level on equal footing with the bulk dynamics. For this reason, the hydrodynamic limit in this case is given, on  $(-\infty, 0)$ , by the same function  $\rho_{\text{left}} := \rho^*_{|(-\infty, 0)}$  as in the previous case, whereas on  $[0, +\infty)$ , it is given by the solution  $\rho_{\text{right}}$  to (47) with source term  $\rho_{\text{right}}(t, 0) := f(t)$  at the origin, where the source term is given by

$$f(t) := \Phi^{-1} \left( \frac{2p - 1}{2p - 1 + \alpha} \Phi(\rho^*(t, 0)) \right). \quad (48)$$

Finally, for  $\theta > 0$ , the dynamics destroys particles so fast at the origin that no macroscopic density can cross the origin, meaning that in this case the hydrodynamic limit  $\rho$  is given on  $(-\infty, 0)$  by  $\rho_{\text{left}} := \rho^*_{|(-\infty, 0)}$ , and on  $[0, +\infty)$  by the solution  $\rho_{\text{right}}$  to (47) with null source term  $\rho_{\text{right}}(t, 0) \equiv 0$ .

### 3.5 Macroscopic behavior of the boundary-driven FEP

Given the amount of interest and progress made on boundary-driven lattice gases in recent years, it is natural to investigate the interaction of the FEP introduced in Section 2.1 with equilibrium reservoirs at its boundaries. We do so in [DCES24], both for strong and weak interactions. In what follows, the notations have been slightly modified with respect to [DCES24] in order to be coherent with the rest of the manuscript. The reservoirs are not typical SSEP ones, and instead mimic the contact with an infinite FEP with given densities  $\bar{\rho}(\alpha), \bar{\rho}(\beta) \in (1/2, 1]$ , where  $\alpha, \beta \in (0, 1)$  are two parameters representing the *active* densities of the reservoirs. More precisely, we enforce the following dynamics at the left boundary (and similarly at the right boundary, with  $\beta$  replacing  $\alpha$ ):

- If it is empty, a particle is injected at site 1 at a rate  $\alpha N^\theta$
- If site  $x = 1$  and  $x = 2$  are both occupied, the particle at site 1 jumps away (is removed) from the system at rate  $(1 - \alpha) N^\theta$
- Particles jump from site 1 to site 2 at rate  $\alpha N^2$  instead of  $N^2$ , to represent the fact that they are not always active but rather that they are active at any given time w.p.  $\alpha$ .

Aside from the last point, the FEP's bulk dynamics occurs at rate  $N^2$ . Strikingly, because of the kinetic constraint making the phase  $\rho < 1/2$  frozen, equilibrium reservoirs for the FEP, regardless of their exact microscopic definition, are not able to enforce subcritical densities at the boundaries of the FEP. Our choice of boundary dynamics is physically consistent with the notion of equilibrium FEP reservoir, and in particular preserves the ergodic component in the bulk.

Although we fully expect that our main result in [DCES24] holds starting from any reasonable initial state (in particular any smooth product Bernoulli state), for technical reasons, we assume that the initial state is already ergodic, in local equilibrium, and fits a given macroscopic profile  $\rho_0$ . Then, adapting the *entropy method*, we show in [DCES24] that the boundary-driven FEP is ruled by its standard hydrodynamic limit (29), supplemented by the boundary conditions

$$\begin{cases} \rho(\cdot, 0) = \bar{\rho}(\alpha), & \rho(\cdot, 1) = \bar{\rho}(\beta) & \text{for } \theta > 1 & (\text{Dirichlet}) \\ \partial_u \rho(\cdot, 0) = a(\rho(\cdot, 0)) - \alpha, & \partial_u \rho(\cdot, 1) = a(\rho(\cdot, 1)) - \alpha & \text{for } \theta = 1 & (\text{Robin}) \\ \partial_u \rho(\cdot, 0) = \partial_u \rho(\cdot, 1) = 0 & & \text{for } \theta > 1 & (\text{Neumann}) \end{cases}$$

where  $a(\rho) = (2\rho - 1)/\rho$  is the active density appearing in the hydrodynamic limit. Although we make use of the classical entropy method, its application is not straightforward : on the one hand, we need to be very careful in our construction of the reference measure in the non-equilibrium case  $\alpha \neq \beta$ , and additionally we need to adapt the classical one and two-blocks estimate to a non-translation invariant, locally correlated state.

## 4 Active matter, phase separation, and nematic phase transition

*This last section of the introduction is dedicated to my works on active matter and nematic phase transitions. Since my main mathematical achievement in this area is my PhD article [Eri24], I do not dedicate to this topic a chapter of this memoir, and instead briefly present here, in the introduction, my physics-oriented collaborations related to active matter which thematically followed from my PhD work.*

### 4.1 My PhD work : Hydrodynamic limit for a active exclusion process

As it is strongly related to the subsequent works presented in this section, I briefly present here my PhD work [Eri24], without expanding on the mathematical challenges involved. The model I considered was a two-dimensional exclusion process on the periodic lattice  $\mathbb{T}_N^2$ , in which each site  $x$  is either empty ( $\eta_x = 0$ ) or occupied by a particle with angle  $\theta$  ( $\eta_x = 1$ ,  $\theta_x = \theta$ ). The initial configuration is chosen according to a product state fitting a macroscopic profile  $\rho_0(u, \theta)$ , where site  $x$  is initially in a state  $(1, \theta)$  w.p.  $\rho_0(x/N, \theta)d\theta$ , and left empty w.p.  $1 - \int \rho_0(x/N, \theta)d\theta$ .

The dynamics is composed of three distinct parts.

- i) (Symmetric jumps with exclusion) For any  $x, y$  such that  $|x - y| = 1$ , at rate  $DN^2$ , a particle a site  $x$  jumps to  $y$  provided site  $y$  is empty.

- ii) (Asymmetric jumps with exclusion in direction  $\theta$ ) For any  $x, y$  such that  $|x - y| = 1$ , at rate  $\lambda N \begin{bmatrix} \cos(\theta) \\ \sin(\theta) \end{bmatrix} \cdot (y - x)$ , a particle at site  $x$  jumps to  $y$  provided site  $y$  is empty.
- iii) (Glauber alignment dynamics) A particle at site  $x$  changes its angle to  $\theta$  at a rate that depends on the neighboring particle's angles  $c(\{\theta_y, y \sim x\})d\theta$ . This part of the dynamics does not scale with  $N$ .

The weak asymmetry means that a particle with angle  $\theta$  will be on average driven in direction  $\theta$ . Because of it, this lattice gas model can be considered *active*, meaning that each individual particle is self driven in a specific direction, and this direction can change according to its surroundings.

Because of the different scalings in  $N$ , the three contributions contribute to the hydrodynamic limit, and we prove in [Eri24] the hydrodynamic limit for this model, which is given by the non-linear equation

$$\partial_t \rho = \nabla \cdot [\mathfrak{d}(\rho, r) \nabla r + d_s(r) \nabla \rho] - 2\lambda \nabla \cdot \left[ s(\rho, r) + \rho d_s(r) \begin{bmatrix} \cos(\theta) \\ \sin(\theta) \end{bmatrix} \right] + \Gamma(\rho) \quad (49)$$

where  $r(t, u) := \int \rho(t, u, \theta) d\theta$  represent the local (angle-blind) density. The vector  $s$  and the diffusion coefficient  $\mathfrak{d}$  both depend on the so-called self-diffusion coefficient  $d_s$ . The latter is not an explicit function of  $r$ , and is defined through a variational formula derived by Spohn [69], and was then shown to be smooth [53, 74]. The proof of this hydrodynamic limit involves considerable mathematical difficulty, mainly because of the non-gradient nature of the model [48], but also because of the complicated topological setup as well as the lack of mixing of the model at high densities.

## 4.2 Exact phase diagrams for simple active matter models

We initially hoped that the active exclusion process studied in [Eri24] would serve as toy microscopic model for the rich phenomenology of active matter, going from Viczek-type alignment phase transition [75, 76] to, more recently, the spontaneous condensation phenomenon known as Motility Induced Phase Separation (MIPS, [18]). However, because of its non-gradient nature, and its non-explicit diffusive and ballistic coefficients, its numerical study was not straightforward. For this reason, we chose to study instead in [KEBT18] two simpler microscopic models for MIPS and alignment phase transition, each only containing two types of particles  $\pm$ ,  $+$  particles ( $\theta = 0$ ) having a rightwards drift, and  $-$  particles ( $\theta = \pi$ ) having a leftwards drift.

The MIPS model was designed by, first, relaxing the symmetric dynamics i) above, in order to allow swaps of neighboring particles, instead of simply forbidding jumps to occupied sites. The Glauber dynamics iii) was enforced by just letting particles change type at constant rate  $\gamma > 0$ . For this model, and because of the relaxed symmetric dynamics, the hydrodynamic limit is straightforward to derive using the classical entropy method. It is expressed as a pair of coupled equations between the densities  $\rho^\pm$  of particles of type  $\pm$ , but is more easy to write for the magnetization ( $m = \rho^+ - \rho^-$ ) and density ( $\rho = \rho^+ + \rho^-$ ) fields, namely

$$\begin{cases} \partial_t \rho = D \Delta \rho - \lambda \partial_u [m(1 - \rho)] \\ \partial_t m = D \Delta m - \lambda \partial_u [\rho(1 - \rho)] - \gamma m \end{cases} \quad (50)$$

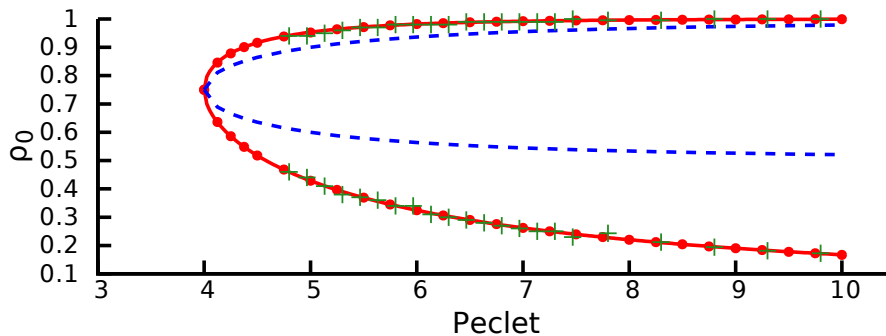


**Figure 2:** [KEBT18, Fig.3] Exact phase diagram for the stability of the homogeneous, zero-magnetization state for (50). Inside the spinodal curve (dashed blue), the homogeneous phase is unstable, and spontaneously separates into liquid and gas phases with respective densities given by the top and bottom binodal curves (red dots). The green crosses are simulations of the phase separated densities on the microscopic system, which show perfect agreement with their analytical counterparts.

Equipped with this hydrodynamic limit, the exact phase diagram for the stability of the homogeneous state with density  $\rho$  and no magnetization ( $m = 0$ ) can then be derived as a function of the *Peclet number*  $Pe := \lambda/\sqrt{D\gamma}$ , see Fig. 2. The latter show that that in the spinodal region, the homogeneous profile is unstable, which leads to spontaneous separation between a liquid and a gas phase.

For the alignment model considered in [KEBT18], we drop the exclusion rule, and consider instead independent, weakly asymmetric (the direction of the weak asymmetry still depends on the particle's type) random walkers in one dimension, however this time with an alignment Glauber dynamics, meaning that the rate at which a  $\pm$  particle at site  $x$  flips to  $\mp$  is given by

$$c^\pm(\eta_x^+, \eta_x^-) := \exp(\mp\beta(\eta_x^+ - \eta_x^-)),$$

where  $\eta_x^\pm$  represents the number of  $\pm$  particles at site  $x$  and  $\beta$  is the inverse temperature. Because of the Glauber dynamics, the system locally magnetizes, leading for high temperature to a global magnetization  $m \neq 0$  permeating throughout the system. Because of the relaxed symmetric dynamics, the hydrodynamic limit for this model can also be derived, and is given by

$$\begin{cases} \partial_t \rho = D\Delta\rho - \lambda\partial_u m \\ \partial_t m = D\Delta m - \lambda\partial_u \rho - F_\beta(\rho, m) \end{cases} \quad (51)$$

For an explicit reaction term  $F_\beta$ . Once again, the hydrodynamic limit allows for an explicit phase diagram (Fig. 3) for the stability of the homogeneous profile, which shows that at intermediary temperature, only parts of the system spontaneously magnetize to form traveling bands going through a non-magnetized gas phase. Our work illustrates the extent to which the mathematical theory of hydrodynamic limits can be used to successfully derive exact information on phase transitions directly from microscopic models, rather than mean-field types PDE ones, which in some occasion fail to capture the behavior of the corresponding microscopic model [68].

Based on the work done in [KEBT18, Eri24], I present in [Eri21], some key elements of hydrodynamic limit theory in the specific context of modeling active matter. The purpose of this note was to give people in the physics community some key elements to understand

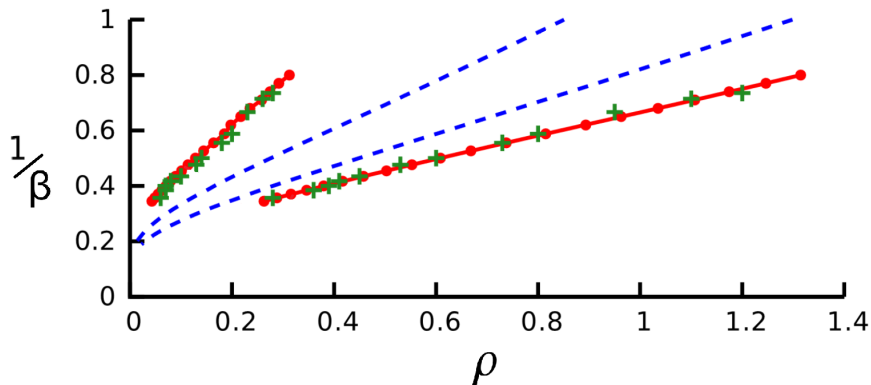


**Figure 3:** [KEBT18, Fig.5] Exact phase diagram for the stability of the homogeneous, zero-magnetization state for (51). Above the upper spinodal (blue dashed), temperature is high and the homogeneous disordered phase ( $m = 0$ ) is stable. Below the lower spinodal, temperature is low, and the homogeneous ordered phase ( $m \neq 0$ ) is stable. Between these two regions, the system spontaneously separate into a gas disordered phase and a liquid magnetized phase traveling through the system.

the derivation of macroscopic evolution equations from microscopic interactions. Indeed, the mean-field assumption which forms the basis for many arguments in the physics literature can typically fail for key models like zero-range type-processes, leading to an incorrect derivation of the macroscopic evolution PDE.

### 4.3 Phase separation for the non-gradient active lattice gas

In [MEJB23], we tackle the emergence of MIPS in a variant of the non-gradient lattice gas whose hydrodynamic limit was derived in [Eri24]. We chose however to replace the Glauber dynamics by angular diffusion, whose macroscopic effect is to replace, in the hydrodynamic limit (49), the contribution  $\Gamma(\rho)$  by the angular diffusion  $\partial_\theta^2 \rho$ . Once again, we are able to perform a linear stability analysis of the limiting hydrodynamic equation around the homogeneous profile  $\rho(u, \theta) = \phi/2\pi$  depending on the occupied volume fraction  $\phi$ , and the Peclet number ruling the level of asymmetry in the system.

To solve the problem of the non-explicit self diffusion coefficient  $d_s(\rho)$ , we exploited the approximation

$$d_s(\rho) \simeq (1 - \rho) \left( 1 - \alpha\rho + \alpha \frac{(2\alpha - 1)}{2\alpha + 1} \rho^2 \right), \quad (52)$$

derived through the so-called *matched asymptotics* technique in [57], where the constant  $\alpha := \pi/2 - 1$ . Figure 5 shows that our analytical linear instability closely matches, for the most part, the actual numerical instability of the discretized PDE. For large densities ( $\phi \rightarrow 1$ ) however, this is no longer the case, as can be expected because at high densities the active exclusion process loses its mixing properties due to the exclusion rule, resulting in complex phase separated behavior. As represented in Figure 5, we numerically show using the discretized PDE that MIPS occurs in the linearly unstable region for the non-gradient active exclusion process. Although it was numerically convenient to consider for this work active Brownian particles, we strongly expect that for a run-and-tumble type dynamics with discrete angular reorientations, the behavior of the limiting PDE would be qualitatively identical [17].

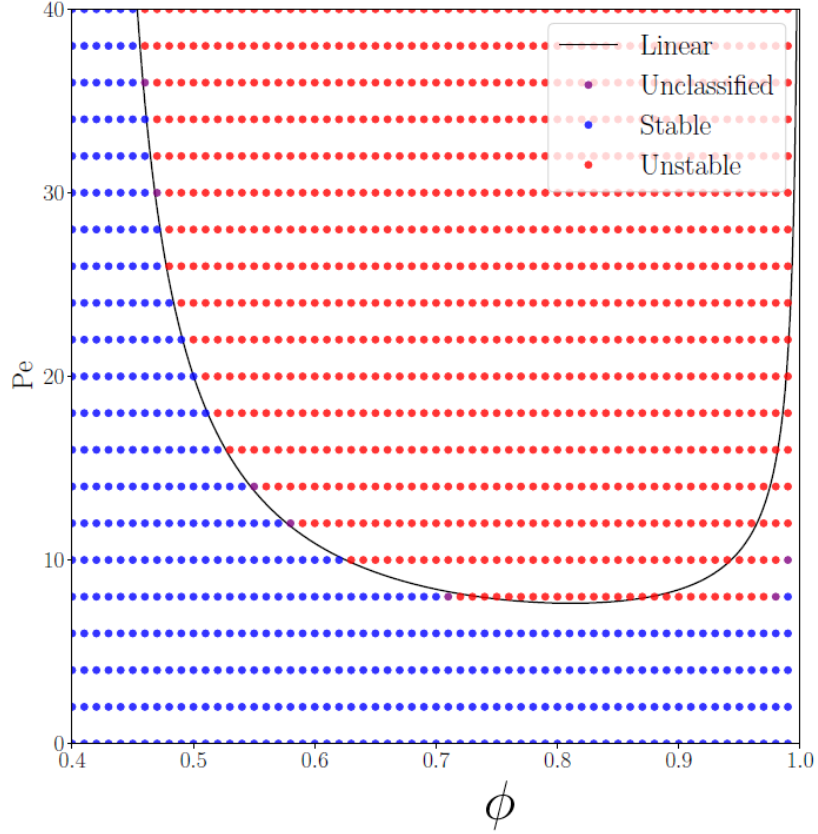


**Figure 4:** [MEJB23, Fig.1] Exact phase diagram for the linear stability of the homogeneous, zero-magnetization state for the non-gradient active lattice gas. The dots represent numerical stability under a discretized PDE scheme.

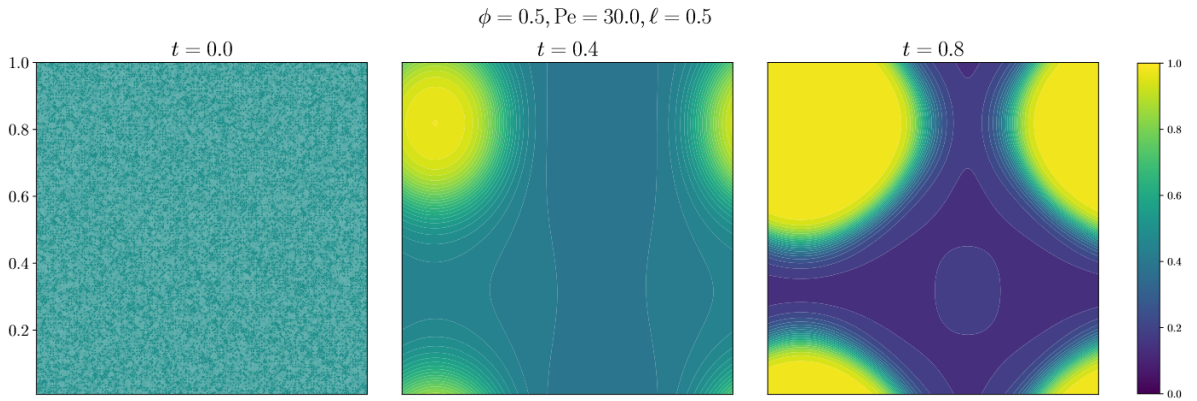


**Figure 5:** [MEJB23, Fig.3] Emergence of spontaneous phase separation for the non-gradient active exclusion process in the linearly unstable region.

## 4.4 First order nematic transition for a liquid crystal model

The nematic phase transition for liquid crystals was first uncovered in a seminal paper by Onsager [60], where he proved that the free energy

$$\mathcal{F}_\beta(\rho, f) := \frac{\rho}{\beta} \int_{\mathbb{S}^2} f(\Omega) \log f(\Omega) d\Omega + \frac{\rho^2}{2} \iint_{\mathbb{S}^2 \times \mathbb{S}^2} f(\Omega) f(\Omega') \varphi(\Omega \cdot \Omega') d\Omega d\Omega' \quad (53)$$

for a liquid crystal with orientations  $\Omega \in \mathbb{S}^2$  and orientation distribution  $f$  goes through a transition from isotropic to anisotropic at least for reasonable choices of the interaction potential  $\varphi$ . However, tying this free energy to a particle system with finite interaction range is still to this day an open question except in specific reflection positive cases [2, 1], which are very susceptible to small changes in the considered Hamiltonian. In [EG20], we revisit this question, and introduce a model of anisotropic molecules, interacting over long but finite range  $\gamma^{-1}$ . Using a criterium put forward by Lebowitz and Penrose [55] we show that the free energy functional's critical points are homogeneous to obtain an expression similar to (53) for its minimal value. We then analyze the behavior of the resulting effective free energy functional, and prove that the nematic phase transition is first order.

The microscopic model we consider is composed of  $N$  rods in  $\Lambda_L := [0, L]^d$  with respective positions and orientations  $\bar{x} := (x_1, \dots, x_N) \in \Lambda_L^N$  and orientations  $\bar{\Omega} := (\Omega_1, \dots, \Omega_N) \in (\mathbb{S}^2)^N$ . These particles interact over ranges  $\gamma^{-1}$ , through the potential

$$V_\gamma(\bar{x}, \bar{\Omega}) = \infty \mathbf{1}_{\{\exists i, j, |x_i - x_j| \leq r_0\}} + \gamma^d \sum_{1 \leq i \leq j \leq N} \varphi(\gamma(x_i - x_j), \Omega_i \cdot \Omega_j).$$

The first term translates the hard-core interaction with radius  $r_0$  between particles, and we will later on assume that  $\varphi$  is even in its second variable to translate a nematic rather than polar interaction : given an orientation, flipping the rod does not change the interaction potential. We then define the partition function at inverse temperature  $\beta$

$$Z_\beta(N, L, \gamma) := \int_{\Lambda_L^N \times (\mathbb{S}^2)^N} \frac{d\bar{x} d\bar{\Omega}}{N!} e^{-\beta V_\gamma(\bar{x}, \bar{\Omega})},$$

and the associated free energy

$$\mathcal{F}_\beta(\rho) := \lim_{\gamma \rightarrow 0} \lim_{L \rightarrow \infty} \frac{-1}{\beta L^d} \log Z_\beta(\lfloor \rho L^d \rfloor, L, \gamma).$$

We prove in [EG20] that, denoting by  $\hat{\varphi}$  the space integral of  $\varphi$ , the free energy  $\mathcal{F}_\beta(\rho)$  can be expressed as

$$\mathcal{F}_\beta(\rho) = C(\rho) + \mathcal{F}_\beta(\rho, f),$$

where the second term is Onsager's free energy (53). We then give a sufficient condition for the free energy functional to exhibit a first order phase transition.



# Chapter I

---

## MACROSCOPIC BEHAVIOR OF THE FACILITATED EXCLUSION PROCESS

### Contents

---

<b>5</b>	<b>Transience time and cutoff phenomenon</b> . . . . .	<b>34</b>
5.1	Transient, ergodic, and frozen configurations . . . . .	35
5.2	Transience time starting from a Bernoulli product measure . . . . .	36
5.3	Mapping with an attractive zero-range process . . . . .	37
5.4	Strategy of the proof in the supercritical case : Theorem 5.1 . . . . .	40
5.5	Microscopic front creation : Theorem 5.2 . . . . .	42
5.6	Sharp uniform estimate of the transience time and cutoff . . . . .	44
<b>6</b>	<b>Hydrodynamic limit in the symmetric case</b> . . . . .	<b>48</b>
6.1	Grand canonical and canonical states for the FEP . . . . .	48
6.2	Hydrodynamic limit for the supercritical symmetric FEP . . . . .	49
6.3	Stephan problem for the symmetric FEP . . . . .	50
6.4	Critical behavior in two dimensions . . . . .	52
<b>7</b>	<b>Hydrodynamics and fluctuations for the asymmetric FEP</b> . . . . .	<b>54</b>
7.1	Hydrodynamic limit for the AFEP . . . . .	54
7.2	Sketch of the proof . . . . .	55
7.3	CLT stationary fluctuations for the FEP . . . . .	56
	<b>Conclusion and perspectives</b> . . . . .	<b>59</b>

---

*This chapter focuses on the Facilitated Exclusion Process, a kinetically constrained lattice gas put forward by the physics community to model liquid-solid type phase transitions. Informally, the FEP can be described as a SSEP, in which however particles need an occupied neighbor to jump. This process is remarkable and deserves study for multiple reasons:*

- *it is non-reversible w.r.t. product measures but has explicit infinite volume stationary states.*

- It displays a phase separated behavior, both in its dynamics and its stationary states.
- It is a kinetically constrained model with an absorbing phase, but is conservative, and thus belongs to a separate universality class than the directed percolation one, which is the most well-known active/absorbing universality class.
- It is cooperative, meaning it does not have mobile clusters to locally mix the configuration, but gradient, making the exact derivation of its critical exponents achievable.
- The FEP has rich mapping features with various attractive processes, making it possible to understand in detail its microscopic and macroscopic behavior, despite its hard kinetic constraint and lack of local ergodicity.

Let us start by properly defining the (1-dimensional) FEP, which will be considered in two different setups, either the discrete ring  $\mathbb{T}_N$  or the full line  $\mathbb{Z}$ . For convenience, to define our process in a general way, we will denote by  $\mathbb{L}_N = \mathbb{T}_N$  or  $\mathbb{Z}$  the relevant lattice. Note that in the case of the full line, the lattice itself does not depend on the scaling parameters, but since our generator will, we keep the dependency apparent in any case. We can now define the FEP as a continuous-time Markov process on the space of configurations  $\Omega_N = \{0, 1\}^{\mathbb{L}_N}$ , with generator acting on local functions  $f : \Omega_N \rightarrow \mathbb{R}$  of the configuration as

$$\mathcal{L}_N f(\eta) := \sum_{x \in \mathbb{L}_N} c_{x,x+1}^N(\eta) \{f(\eta^{x,x+1}) - f(\eta)\}, \quad (\text{I.1})$$

where  $\eta^{x,x+1}$  is the configuration where the values at sites  $x$  and  $x+1$  have been exchanged defined in (3). In order to encompass both symmetric and asymmetric cases, the jump rates are given by

$$c_{x,x+1}^N(\eta) := p_N \eta_{x-1} \eta_x (1 - \eta_{x+1}) + q_N \eta_{x+2} \eta_{x+1} (1 - \eta_x), \quad (\text{I.2})$$

and exhibit both

- the *exclusion constraint*: jumps can only occur towards empty sites.
- The *kinetic constraint*: a particle can only jump to a neighboring site if its other neighboring site is occupied.

We now define the FEP as a continuous time Markov Process  $(\eta(t))_{t \geq 0}$  driven by the generator  $\mathcal{L}_N$ , and we denote by  $\mathbb{P}_{\mu^N}$  its distribution starting from an initial distribution  $\mu^N$ , and by  $\mathbb{E}_{\mu^N}$  the corresponding expectation.

## 5 Transience time and cutoff phenomenon

The results presented in this section were derived in [BESS20], [BES21] and [EM24]. We consider in this entire section the symmetric case, and for convenience we do not accelerate the process diffusively, meaning that we set throughout this section

$$p_N = q_N = 1 \quad (\text{I.3})$$

in (I.2).

## 5.1 Transient, ergodic, and frozen configurations

Because of the kinetic constraint, the FEP's configurations can be split into 4 categories. Consider for example the case of the torus  $\mathbb{L}_N = \mathbb{T}_N$ , and given a configuration  $\eta$ , denote by  $J = \sum_x \eta_x$  its number of particles, and call  $\rho := J/N$  its density. Denote by

$$\Omega_{N,J} := \left\{ \eta \in \Omega_N, \sum_x \eta_x = J \right\} \quad (\text{I.4})$$

the set of configurations with  $J$  particles on  $\mathbb{T}_N$ . Note that when particles are all isolated, the system is frozen, which can only happen up to density  $\rho_c := 1/2$ , which is therefore critical for the FEP. Furthermore, the dynamics can only break apart neighboring empty sites, because two empty sites becoming neighbors would require an isolated particle between them jumping out, which is not possible due to the kinetic constraint. As represented in Figure I.1, these observations lead to the following classification of configurations

i) For  $J \geq N/2$  (*supercritical density*), a configuration can either be

- *ergodic* if all its empty sites are isolated, meaning there are no two consecutive empty sites. We denote by

$$\mathcal{E}_{N,J} := \{ \eta \in \Omega_{N,J}, \eta_x + \eta_{x+1} \geq 1 \ \forall x \in \mathbb{T}_N \}, \quad (\text{I.5})$$

the set of ergodic configurations with  $J$  particles, and by  $\mathcal{E}_N := \cup_{J \geq N/2} \mathcal{E}_{N,J}$  the set of ergodic configurations, or *ergodic component*.

- *Transient supercritical* if it is supercritical but not ergodic. We denote by

$$\mathcal{T}_{N,J}^+ = \Omega_{N,J} \setminus \mathcal{E}_{N,J}$$

the set of supercritical transient configurations with  $J$  particles, and further denote by  $\mathcal{T}_N^+ = \cup_{J \geq N/2} \mathcal{T}_{N,J}^+$  the set of all supercritical transient configurations.

ii) For  $J \leq N/2$  (*subcritical density*), a configuration can either be

- *frozen* if all its particles are isolated, meaning no particle has an occupied neighbor. We denote by

$$\mathcal{F}_{N,J} := \{ \eta \in \Omega_{N,J}, \eta_x + \eta_{x+1} \leq 1 \ \forall x \in \mathbb{T}_N \}, \quad (\text{I.6})$$

the set of frozen configurations with  $J$  particles, and by  $\mathcal{F}_N := \cup_{J \leq N/2} \mathcal{F}_{N,J}$  the set of frozen configurations.

- *Transient subcritical* if it is subcritical but not frozen. We denote by

$$\mathcal{T}_{N,J}^- = \Omega_{N,J} \setminus \mathcal{F}_{N,J}$$

the set of subcritical transient configurations with  $J$  particles, and we further denote by  $\mathcal{T}_N^- = \cup_{J \leq N/2} \mathcal{T}_{N,J}^-$  the set of all subcritical transient configurations.

Because pairs of empty sites can only be broken up, the ergodic component is stable under the dynamics. Further note that a critical alternated configuration  $\cdots \circ \bullet \circ \bullet \cdots$  is considered both *ergodic* and *frozen*. This is by design, since such a configuration is indeed frozen (no

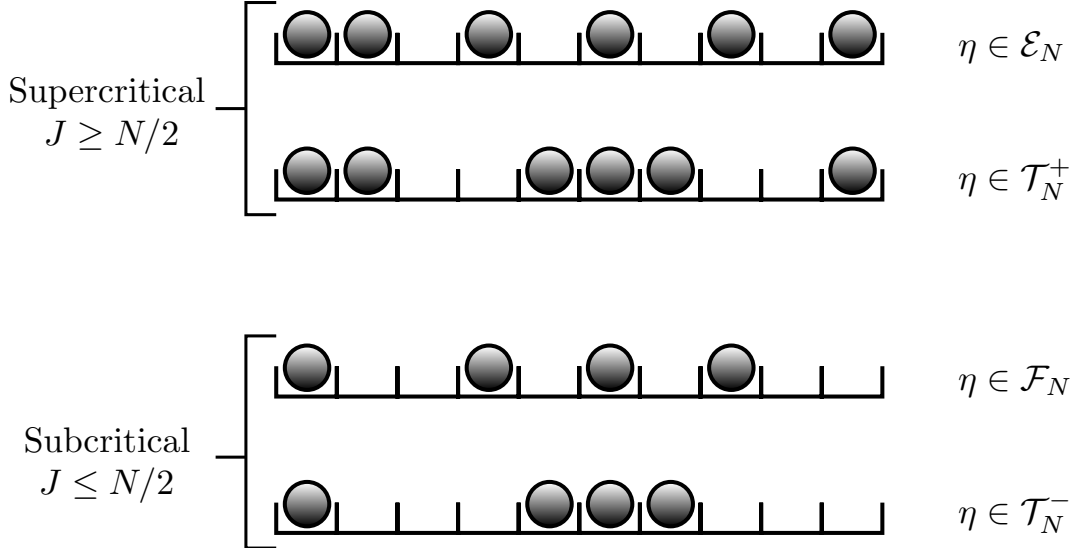


**Figure I.1:** Representation of the four different types of configurations for the FEP

particle can jump), but it is in the ergodic component in the sense that it is in the support of the FEP's stationary states (cf. Section 6.1).

Starting from a Bernoulli product measure, various aspects of the nature of the stationary states ultimately reached by the FEP, in both symmetric and asymmetric settings, were studied by Goldstein et al. [36, 35, 4], in particular the hyperuniform nature of the FEP's frozen state [37]. Another central question in understanding the macroscopic behavior of the FEP is to estimate the timescale, starting from a transient state on the torus  $\mathbb{T}_N$ , to reach either the ergodic component or a frozen state. In Sections 5.2 and 5.6, we answer this question, first starting from a Bernoulli product measure fitting a given macroscopic profile, then uniformly in the initial transient configuration to show a cutoff phenomenon on the transience time.

## 5.2 Transience time starting from a Bernoulli product measure

In order to derive the hydrodynamic limit for the FEP, the first case in which we estimated the transience time for the facilitated exclusion process is that of a product initial distribution  $\mu^N \sim \rho_0$  fitting a smooth uniformly supercritical profile.

**Theorem 5.1 (Theorem 2.4 in [BESS20])** *Fix a uniformly supercritical smooth profile  $\rho_0 : \mathbb{T} \rightarrow (1/2, 1]$  in  $C^1(\mathbb{T})$ , and consider the associated product state  $\mu^N$  on  $\Omega_N$  given by (9). Then, defining  $t_N := (\log N)^{32} \ll N^2$ , we have*

$$\lim_{N \rightarrow \infty} \mathbb{P}_{\mu^N}(\eta(t_N) \in \mathcal{E}_N) = 1,$$

where  $\mathcal{E}_N$  is the ergodic component defined after (I.5). In other words, starting from a supercritical product state, the ergodic component is reached well before the diffusive timescale.

Although we did not give a formal statement, the strategy of the proof of Theorem 5.1 applies fairly straightforwardly in order to show that a frozen state is reached w.h.p. in time  $t_N$  as well, starting from a product distribution fitting a uniformly subcritical profile  $\rho_0 : \mathbb{T} \rightarrow [0, 1/2)$ .

We then refined this result, and studied in a subsequent article the transient behavior in a two-phased profile.

**Theorem 5.2 (Theorem 2.6 in [BES21])** *Fix a smooth profile  $\rho_0 : \mathbb{T} \rightarrow [0, 1] \in C^1(\mathbb{T})$ , and assume that  $\rho_0$  has one supercritical and one subcritical segment, meaning that there exists  $u_1, u_2 \in \mathbb{T}$  such that*

$$\rho_0(u) \in \begin{cases} (1/2, 1] & \text{for } u \in (u_1, u_2) \\ [0, 1/2) & \text{for } u \in (u_2, u_1) \end{cases}$$

*Note in particular that this defines two macroscopic interfaces  $u_1$  and  $u_2$  with critical density  $\rho_0(u_1) = \rho_0(u_2) = \rho_c = 1/2$ . Further assume that these interfaces are not locally flat, namely*

$$\partial_u \rho_0(u_1) \neq 0 \quad \text{and} \quad \partial_u \rho_0(u_2) \neq 0.$$

*Then, considering once again an initial product distribution  $\mu^N$  given by (9), there is a microscopic phase separation in a subdiffusive time  $s_N = N^{7/4} \ll N^2$ , meaning*

$$\lim_{N \rightarrow \infty} \mathbb{P}_{\mu^N}(\exists \text{ segment } E \subset \mathbb{T}_N \text{ s.t. } \eta(s_N) \text{ is ergodic on } E \text{ and frozen on } \mathbb{T}_N \setminus E) = 1,$$

*In other words, after time  $s_N$ , w.h.p. there exists in the configuration at most one ergodic segment, and one frozen segment.*

We assume in this result that there are only two macroscopic critical interfaces. However, this could be straightforwardly generalized to a finite (even) number of critical interfaces, assuming however that at each interface, the space derivative of the density is not zero. We stated the result this way because the notations become much more burdensome with an arbitrary number of interfaces.

Before sketching the proof of these two results, we introduce a classical mapping between exclusion processes and zero-range processes, that we exploited repeatedly to characterize the macroscopic behavior of the facilitated exclusion process.

### 5.3 Mapping with an attractive zero-range process

We will define the mapping for configurations defined on the whole line, but this construction can straightforwardly be adapted to a periodic setting. Not to burden this section, we will not give an explicit construction in the periodic case.

#### A) Static mapping

Fix an (infinite) exclusion configuration  $\eta \in \{0, 1\}^{\mathbb{Z}}$  with infinitely many empty sites on both half-lines, and denote by  $X_0 \in \mathbb{T}_K$  the position of the first empty site to the left of (or at) the origin. We then denote by  $\cdots < X_{-1} < X_0 < X_1 < X_2 < \cdots$  the successive positions of the empty sites in  $\eta$  and we define for  $y \in \mathbb{Z}$

$$\omega_y := X_{y+1} - X_y - 1, \tag{I.7}$$

which is the number of particles between the  $y$ -th and  $y + 1$ -th empty sites. Recall that  $\mathbb{N} = \{0, 1, 2, \dots\}$  is the set of non-negative integers, so that the identity above defines a zero-range configuration  $\omega \in \mathbb{N}^{\mathbb{T}_K}$ . Of course, the mapping  $\eta \mapsto \omega$  is not 1-to-1, since knowledge of the position of the initial empty site  $X_0$  is necessary to revert the construction.

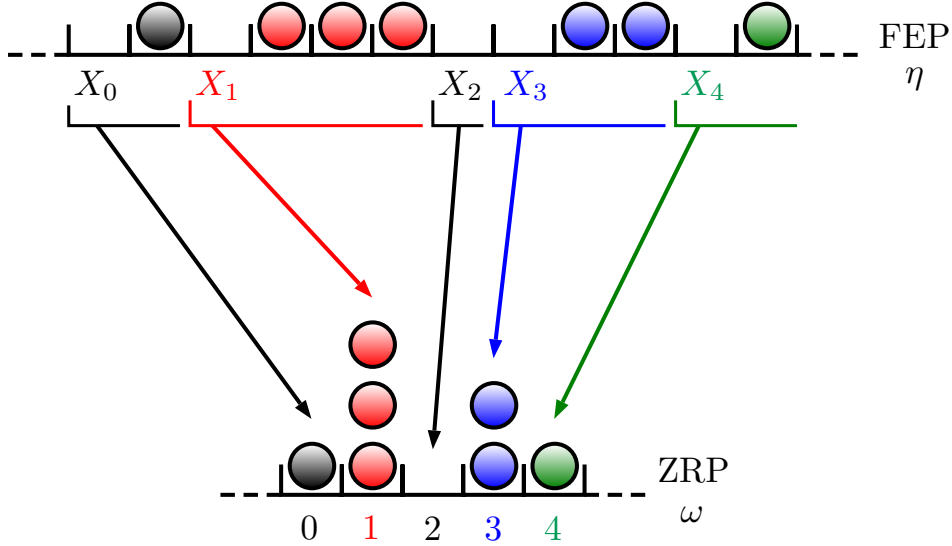


**Figure 1.2:** Representation of the mapping  $\Pi$  between a FEP ergodic configurations  $\eta$  and zero-range configuration  $\omega$

Instead, denote by  $\Pi : \eta \mapsto (\omega, X_0)$ , the mapping represented in Figure 1.2 which, with an exclusion configuration  $\eta$ , associates the zero-range configuration  $\omega \in \mathbb{N}^{\mathbb{Z}}$  built through (I.7) and the position of the first empty site left of the origin. It is straightforward to show that the mapping  $\Pi$  is a bijection between the FEP's ergodic configuration  $\mathcal{E}_{\mathbb{Z}}$ , and the set

$$\widehat{\mathcal{E}}_{\mathbb{Z}} := \{(\omega, X_0) \in \mathbb{N}^{\mathbb{Z}} \times \mathbb{Z} \mid -\omega_0 - 1 \leq X_0 \leq 0\}. \quad (\text{I.8})$$

The reverse mapping  $\Pi^{-1}$  is easily defined; choose a zero-range configuration  $\omega \in \mathbb{N}^{\mathbb{Z}}$  and an integer  $-\omega_0 - 1 \leq X_0 \leq 0$ . The associated ergodic configuration  $\eta$  is then built by placing an empty site in  $\eta$  at site  $X_0$ , and then choosing the consecutive positions  $X_y$  of empty sites in  $\eta$  according to  $\omega$  and (I.7). We then have as wanted  $\eta = \Pi^{-1}(\omega, X_0)$ . In most cases, we will not need to keep track of the position of the empty site, so that we will abuse our notations and simply denote by  $\Pi(\eta)$  the zero-range configuration associated with an exclusion configuration  $\eta$ .

In the periodic setting, the mapping  $\pi$  can be defined analogously on the set of exclusion configurations  $\eta$  with fixed number of empty sites  $K = K(\eta) := N - J$ ,

$$\Pi_K : \Omega_{N, N-K} \longrightarrow \mathbb{N}^{\mathbb{T}_K},$$

where  $\Omega_{N, N-K}$  was introduced in (I.4). In other words, a periodic exclusion configuration with  $K$  empty sites is associated with a zero-range configuration  $\omega := \Pi_K(\eta)$  on  $\mathbb{T}_K$ . In the absence of ambiguity, given a non-empty configuration  $\eta$ , we will also denote by

$$\Pi(\eta) := \sum_{1 \leq K \leq N} \Pi_K(\eta) \mathbf{1}_{\{\eta \in \Omega_{N, N-K}\}}$$

the mapping on  $\Omega_N$ .

## B) Dynamic mapping to a Facilitated Zero-Range Process

We now consider a dynamical version of the mapping above : to do so, consider any given trajectory  $\{\eta(t), t \geq 0\}$  of the FEP starting from  $\eta(0) \in \{0, 1\}^{\mathbb{Z}}$ . Let  $X_0(0)$  be the position

of the first empty site in  $\eta(0)$  to the left of (or at) the origin at the initial time. Then, we define as before, for any  $y > 0$  (resp.  $y < 0$ ), the position  $X_y(0)$  of the  $y$ -th empty site to the right (resp. to the left) of  $X_0(0)$ . Since the dynamics is conservative, we can keep track of each of the trajectories  $\{X_y(t), t \geq 0\}$  of the  $y$ -th empty site for  $y \in \mathbb{Z}$  in  $\{\eta(t), t \geq 0\}$ . Since the jumps are nearest neighbor, the order of the empty sites is preserved along the evolution of the process, *i.e.* for any  $t \geq 0$ ,

$$\dots < X_{-1}(t) < X_0(t) < X_1(t) < \dots$$

We then define as in the static case

$$\omega_y(t) := X_{y+1}(t) - X_y(t) - 1 \quad \text{for } y \in \mathbb{Z}. \quad (\text{I.9})$$

In order not to confuse with the static mapping, we denote  $\Pi^*[\eta]$  this dynamic mapping between trajectories, meaning that  $\Pi^*[\eta](t) = \omega(t)$ . Note that we do not have in general that  $\Pi^*[\eta](t) = \Pi(\eta(t))$ , unless the tagged empty site that was at time 0 the first left of the origin is still the first left of the origin at time  $t$ .

It is straightforward to check that if  $\eta$  is a rate 1 symmetric FEP (meaning setting  $p_N = q_N = 1$  in (I.2)), then  $\{\omega(t), t \geq 0\} = \Pi^*[\eta]$  evolves as the symmetric non-ergodic zero-range process with generator  $\mathcal{L}^{\text{zr}}$ , which acts on local functions  $f : \mathbb{N}^{\mathbb{Z}} \rightarrow \mathbb{R}$  as

$$\mathcal{L}^{\text{zr}} f(\omega) = \sum_{y \in \mathbb{Z}} \mathbf{1}_{\{\omega_y \geq 2\}} \{f(\omega^{y,y+1}) + f(\omega^{y,y-1}) - 2f(\omega)\}. \quad (\text{I.10})$$

Since we use different letters for exclusion ( $\eta$ ) and zero-range ( $\omega$ ) configurations, without confusion, we also denote  $\omega^{y,y \pm 1}$  the zero-range configuration obtained from  $\omega$  after a particle jumps from  $y$  to  $y \pm 1$ ,

$$\omega_{y'}^{y,y \pm 1} = \begin{cases} \omega_y - 1 & \text{if } y' = y, \\ \omega_y + 1 & \text{if } y' = y \pm 1, \\ \omega_{y'} & \text{otherwise.} \end{cases}$$

Note that this is a *constrained* zero-range process, because particles can only jump if they are not alone on their site, we will call it *Facilitated Zero-Range Process* (FZRP) in what follows. Given a distribution  $\nu$  on  $\mathbb{N}^{\mathbb{Z}}$  or on  $\mathbb{N}^{\mathbb{T}_K}$ , we denote by  $\mathbf{P}_\nu$  the distribution of the facilitated zero-range process started from the initial state  $\omega(0) \sim \nu$  and driven by the generator  $\mathcal{L}^{\text{zr}}$  and by  $\mathbf{E}_\nu$  the corresponding expectation. In each instance, we will make clear which setting, periodic or infinite line, we consider. When  $\nu = \delta_\omega$  is a Dirac distribution on a single configuration  $\omega$ , we write  $\mathbf{P}_\omega, \mathbf{E}_\omega$  instead.

### C) Stationary states and attractiveness for the FZRP

One easily checks that as the FEP, the FZRP on  $\mathbb{T}_K$  has four different kind of configurations, so that we introduce

$$\mathbf{E}_K := \{\omega \in \mathbb{N}^{\mathbb{T}_K}, \omega_y \geq 1 \forall y \in \mathbb{T}_K\} \quad (\text{I.11})$$

$$\mathbf{T}_K^+ := \left\{ \omega \in \mathbb{N}^{\mathbb{T}_K} \setminus \mathbf{E}_K, \sum_{y \in \mathbb{T}_K} \omega_y \geq K \right\}, \quad (\text{I.12})$$

$$\mathbf{F}_K := \{\omega \in \mathbb{N}^{\mathbb{T}_K}, \omega_y \leq 1 \forall y \in \mathbb{T}_K\} \quad (\text{I.13})$$

$$\mathbf{T}_K^- := \left\{ \omega \in \mathbb{N}^{\mathbb{T}_K} \setminus \mathbf{F}_K, \sum_{y \in \mathbb{T}_K} \omega_y \leq K \right\}, \quad (\text{I.14})$$

which are respectively the sets of *ergodic*, *transient supercritical*, *frozen*, and *transient subcritical* zero-range configurations.

Furthermore, for any  $0 < a < 1$ , the FZRP is reversible w.r.t. the geometric product measure supported on the set of ergodic configurations  $\mathbf{E}_K$  with marginals

$$\mu_a(\omega_y = k) = a^{k-1}(1-a) \quad \text{for } k \geq 1. \quad (\text{I.15})$$

We will typically denote by  $\alpha$  the local zero-range particle density. In the case of those stationary measure, it is given by

$$\alpha := \mathbb{E}_{\mu_a}(\omega_y) = \frac{1}{1-a}. \quad (\text{I.16})$$

Furthermore, since the function  $g(k) = \mathbf{1}_{\{k \geq 2\}}$  is non-decreasing, the FZRP is attractive, meaning in particular that given two initial zero-range configurations  $\omega(0)$  and  $\xi(0)$  such that  $\omega(0) \leq \xi(0)$ , there exists a coupling  $\mathbb{Q}$  such that under  $\mathbb{Q}$ , both  $\omega$  and  $\xi$  are distributed as FZRPs, and such that at any time  $t \geq 0$ ,  $\mathbb{Q}$ -a.s. we still have

$$\omega(t) \leq \xi(t). \quad (\text{I.17})$$

The construction for  $\mathbb{Q}$  is referred to as *basic coupling*, and is built in the following way:

- Under  $\mathbb{Q}$ , each site  $y$  is associated with two rate 1 Poisson clocks  $\mathcal{N}_{y,y-1}$  and  $\mathcal{N}_{y,y+1}$ .
- When a clock  $\mathcal{N}_{y,y \pm 1}$  rings at site  $y$ , each process that has at least two particles at site  $y$  makes one of them jump to  $y \pm 1$ .
- This construction ensures that order between processes is preserved throughout the dynamics so that (I.17) holds.

Not to introduce burdensome notation, we do not explicitly build the coupled process's Markov generator, it is straightforward to write down.

## 5.4 Strategy of the proof in the supercritical case : Theorem 5.1

As assumed in Theorem 5.1, consider a supercritical profile  $\rho_0 > 1/2$  bounded away from the critical density, and the corresponding product state  $\mu^N$ . Then, we can write according to the dynamic mapping

$$\mathbb{P}_{\mu^N}(\eta(t_N) \in \mathcal{E}_N) = \mu^N(\eta \equiv 1) + \sum_{K \geq 1} \sum_{\omega \in \mathbb{N}^{\mathbb{T}_K}} \mu^N(\Pi(\eta) = \omega) \mathbf{P}_\omega(\omega(t_N) \in \mathbf{E}_K).$$

Note that the first term in the right hand side accounts for the degenerate case where the FEP configuration contains no empty site, in which case the mapping is not well defined. From this identity, the strategy of the proof is the following:

**Step 1: Reduction to regular configurations.** If the initial profile is identically equal to 1, the result is clearly true because the initial configuration will be full a.s.. Otherwise, since

$\rho_0$  is smooth, by a standard large deviations estimate, any configuration  $\eta$  must have with high probability at least

$$K(\eta) \geq \ell_N := (\log N)^8 \quad (\text{I.18})$$

empty sites (in reality, it will very likely have  $O(N)$  empty sites). Recall that we assume the initial profile for  $\eta$  to be supercritical ( $\rho_0 \geq 1/2$ ), so that the average (zero-range) density  $K/(N-K)$  in  $\Pi(\eta)$  must be w.h.p. larger than 1. Given a configuration  $\eta$  with more than  $\ell_N$  empty sites, still by a large deviations argument, in any box  $B := B_{\ell_N}(y)$  of size  $\ell_N$  centered in  $y$  of the associated zero-range configuration  $\omega := \Pi(\eta)$ , we must therefore have at least  $\delta\ell_N$  particles which are distributed rather evenly. More precisely, w.h.p. there exists  $\omega' \leq \omega$  with  $(1 + \delta)\ell_N$  particles such that in  $\omega'$

$$\sum_{y' \in B} (y' - y)\omega'_y \leq (1 + \delta/2) \frac{(1 + \delta)\ell_N(\ell_N + 1)}{2}. \quad (\text{I.19})$$

One can check that the fraction above is the standard deviation one would expect in the average position of the particles, if they were indeed distributed evenly in the box  $B$ , so that having a deviation which is less than  $1 + \delta/2$  times the standard value is very likely indeed.

In what follows, given  $\eta$ , if (I.18) holds and for any box  $B$  of size  $\ell_N$  in  $\mathbb{T}_K$  there exists  $\omega' \leq \Pi(\eta)$  satisfying (I.19), we call  $\eta$  “ $\ell_N$ -regular”. By slight abuse of language, we also call the associated zero-range configuration  $\omega = \Pi(\eta)$  regular. Then, as stated in [BESS20, Lemma 4.2],

$$\lim_{N \rightarrow \infty} \mu^N(\eta \text{ is } \ell_N\text{-regular}) = 1. \quad (\text{I.20})$$

**Step 2: Estimation of the FZRP transience time started from a  $\ell$ -regular configuration.** From this point on, we do not need to keep the explicit value of  $\ell_N$ , so that we replace it by any large positive integer that we denote  $\ell$ . Let  $K$  denote the size of the zero-range lattice, we show with [BESS20, Proposition 4.1] that

$$\sup_{\omega \text{ } \ell\text{-regular}} \mathbf{P}_\omega(\omega(T_\ell) \notin \mathbf{E}_K) \leq K e^{-\ell^{1/4}}, \quad (\text{I.21})$$

where  $T_\ell = \ell^4$ . In other words, starting from a  $\ell$ -regular ZR configuration, the ergodic component is reached w.h.p. in a time  $\ell^4$ . Together, (I.20) and (I.21) are enough to prove Theorem 5.1. Proving equation (I.21) is tricky, however, because in the zero-range process, particles trajectories are not independant : if many particles have exited a box on one side, other particles initially in this box will have an easier time exiting by the same side, because close to the boundary, at least one particle must be present at each site.

Keep in mind that in the FZRP, particles jump symmetrically while they are active, until they reach an empty site where they become inactive and remain stuck forever. Furthermore, by making an active particle chosen at random jump when the Poisson clocks ring, we see that an active particle at site  $y$  effectively jumps at a rate  $1/(\omega_y - 1)$ .

The structure of the proof of (I.21) is the following:

- Fix a box  $B$  of size  $\ell$  in  $\mathbb{T}_K$ , since the initial configuration  $\omega$  was assumed regular, by attractiveness, we can keep exactly  $(1 + \delta)\ell$  particles in this box and remove all other particles from the system. Furthermore, those particles are spread out evenly enough to satisfy (I.19). This defines a new configuration  $\omega'$ , and we will prove that in  $\omega'$ , at time  $\ell^4$ , at least one particle must have exited  $B$  to the left w.p.  $1 - e^{-\ell^{1/4}}$ .

- By attractiveness, this means that this is also the case in  $\omega$ , so that site  $x$  is empty at time  $\ell^4$  with probability at most  $e^{-\ell^{1/4}}$ . By union bound, this proves (I.21).
- To prove that in  $\omega'$ , w.h.p. a particle has exited to the left before time  $\ell^4$ , we prove the following. First, no site can contain more than the total number of particles which is  $(1 + \delta)\ell$ . In particular, particles jump, at the least, at an effective rate  $1/(1 + \delta)\ell$ . Since particles behave as symmetric random walkers (with time distortion due to other particles on the same site), this means that with high probability, in a time of order  $(1 + \delta)\ell^4$ , all particles either got stuck alone on a site, or remained active the whole time and therefore at some point exited the box  $B$  [BESS20, Lemma 4.4].
- Since at most  $\ell$  particles remained stuck in  $B$ , this means that at least  $\delta\ell$  particles remained active until they exited  $B$ . If they all exited to the right-hand side, this would mean one of two things : either particles were initially on average much closer to the right hand-side of  $B$ , but this is not possible because we assumed that  $\omega$  is regular. Or, during the dynamics, the total number of jumps to the right performed by all particles must have been much larger than the number of jumps to the left, the probability of which can be estimated by a large deviations argument [BESS20, Lemma 4.5].

To summarize, our proof strongly relies on the zero-range mapping, in which particles either get stuck because they jumped to an empty site, or roughly behave as random walkers that are slowed down by other particles. Starting from a uniformly supercritical profile, in  $\omega$ , any mesoscopic box of size  $\ell_N$  contains w.h.p. at least  $(1 + \delta)\ell_N$  particles distributed evenly in the box. Before time  $\ell_N^4$ , all those particles either got stuck or exited the box at some point, and if they all exited to the right, an abnormal number of rightwards jumps must have occurred in the system. In particular, each site in  $\mathbb{T}_K$  being the extremity of such a box, this proves that at time  $\ell_N^4 = \log(N)^{32}$ , w.h.p., each site in the zero-range configuration is non-empty.

## 5.5 Microscopic front creation : Theorem 5.2

In the general case where the density is not assumed uniformly supercritical, we are interested in the time the microscopic system takes to define microscopic interfaces between phases. As in Theorem 5.2, assume that we have initially two macroscopic phases, separated by two macroscopic interfaces. This time, not to burden the arguments, we will look at the problem straight from the point of view of the zero-range process, getting back to the FEP will be a matter of using similar arguments as in the supercritical case. From the standpoint of the zero-range process, we therefore have a subcritical phase  $(v_1, v_2)$  where the zero-range density  $\alpha$  is less than 1, and a supercritical phase  $(v_2, v_1)$  where it is larger than 1. Without loss of generality, we assume that  $v_1 = 0$  and we simply denote  $v_2 = v$ .

As represented in Figure I.3, we define  $\ell_K = K^{3/4}$ , and consider the  $\ell_K$ -interior of the subcritical region

$$B_K := \{\ell_K, \dots, Kv - \ell_K\},$$

as well as its complementary set  $A_K := \mathbb{T}_K \setminus B_K$ . To prove that the interfaces are created before time  $K^{7/4}$ , it is enough to show the following statements:

- The number of empty sites in the FEP,  $K$ , is close to  $N$ . Furthermore, by attractiveness and comparison with an equilibrium FZRP, up until time  $T_K$  we have  $\omega_y(t) \leq (\log K)^2$  for any  $y \in K$ .

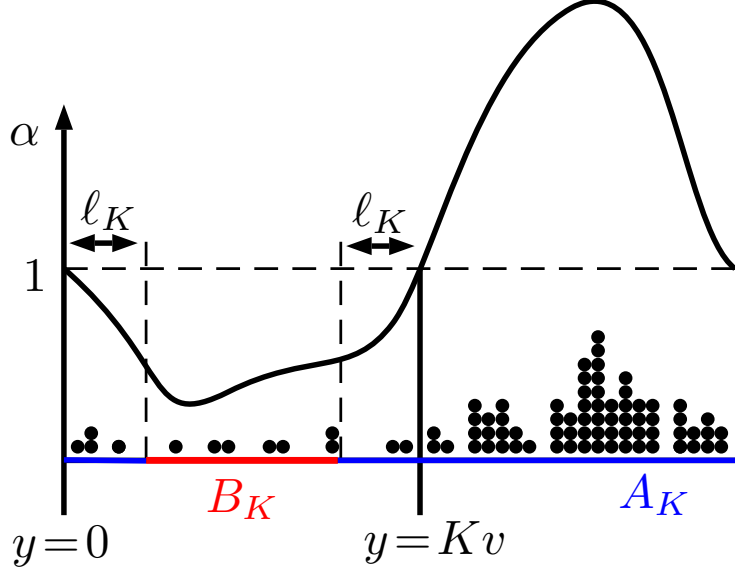


**Figure I.3:** Representation of the sets  $A_K$  (supercritical region and its subcritical boundary, in blue) and  $B_K$  (subcritical region, in red). Before time  $T_K$ ,  $A_K$  becomes ergodic (no empty sites) w.h.p., whereas in  $B_K$  only one subcritical region can remain, and the latter freezes before time  $T_K$ . The black dots represent a typical zero-range configuration fitting the density profile  $\alpha$ .

- In the zero-range process, any box of size  $\ell_K$  contained in  $B_K$  has w.h.p. a subcritical number of particles (i.e. less than  $\ell_K$ ). Similarly, there exists a constant  $c^*$  such that any box of size  $10\ell_K$  included in  $A_K$  initially contains at least  $1 + c^*\ell_K/K$ , and we can choose those particles in such a way that they are evenly distributed in the box (in an analogous sense to (I.19)). Of course, the latter would not be true close to the boundaries of  $A_K$ , which are slightly subcritical, if the box was taken of size  $\ell_K$ . Since the box is chosen of size  $10\ell_K$ , however, this is not an issue. A zero-range configuration satisfying these conditions is called *typical*. Under the static mapping,  $\Pi(\eta)$  is typical w.h.p. [BES21, Lemma 4.2].
- The set  $A_K$  becomes ergodic before time  $T_K = K^{7/4}$  with high probability [BES21, Lemma 4.6]. The proof of this statement follows the exact same steps as in the supercritical case, albeit with refined estimates.
- After time  $T_K$ , there exists at most a single subcritical connected set, meaning that w.h.p. one cannot find  $x < y < z \in B_K$  satisfying

$$\omega_x(T_K) = \omega_z(T_K) = 0 \quad \text{and} \quad \omega_y(T_K) > 1. \quad (\text{I.22})$$

This last statement is the content of [BES21, Lemma 4.7]. Its proof is fairly straightforward. Summing over all possible  $x, y, z$ , we loose a factor  $K^3$  by union bound. Now, two cases can arise: either  $z - x \leq \ell_K$ , in which case the particle that is at  $y$  at time  $T_K$  has been moving freely up until time  $T_K$ , but even so has not hit either  $z$  or  $x$ , otherwise it would have remained stuck there. Since at each site, there is never more than  $(\log K)^2$  particles, the effective jump rates of particles is at least  $1/(\log K)^2$ , so that in a time  $T_K \gg \ell_K^2 (\log K)^2$ , the probability that a particle remained stuck between  $x$  and  $z$  is exponentially small in  $K$ . If instead  $z - x \leq \ell_K$  and there are no other empty sites in between, the average number of particles per site initially in  $\{x + 1, z - 1\}$

was more than 1, which occurs with exponentially small probability in the subcritical region. These exponentially small probabilities compensate for the  $K^3$  coming from the union bound, and shows that (1.22) cannot occur in  $B_K$ .

## 5.6 Sharp uniform estimate of the transience time and cutoff

In the previous section, we gave a fairly exhaustive characterization of the transience time's behavior starting from a product measure with smooth parameter. This, however, only gives a partial picture of the way the FEP leaves its transience component, and it is natural to try and obtain information on its transience time uniformly in the initial configuration. Although one expects that the transience time starting from a configuration with  $J$  particles closely packed together should stochastically dominate that of any other configuration with  $J$  particles, this is by no means straightforward to show, absent coupling or attractiveness arguments. Similarly, the dependency of the transience time on  $J$  is not *a priori* obvious.

Naturally, one hopes that the lack of attractiveness can be solved by mapping to the FZRP defined in Section 5.3. This option, however, is not very satisfactory if one hopes to obtain sharp estimates on the transience time, because particles in the FZRP jump at an effective rate which decreases with the density, so that estimating the transience time would require some very fine and microscopic estimates on the local density throughout the system. In practice, this is very hard to do, especially for a worst-case scenario where up to  $O(N)$  particles can momentarily coexist on the same site.

For this reason, we introduce in [EM24] a new mapping to a process that we call SSEP with traps (SWT). Once again, we use here different notations to the ones of [EM24] in order to have coherent notations throughout the manuscript. We define a SWT configuration as an element, denoted  $\xi$ , of the set  $\{n \in \mathbb{Z} \mid n \leq 1\}^{\mathbb{T}_J}$ , whose value at each site  $j$  is either

- $\xi_j = 1$  to represent site  $j$  being occupied by a particle.
- $\xi_j = 0$  to represent site  $j$  being empty.
- $\xi_j = -d < 0$  to represent site  $j$  containing a trap of depth  $d$ .

Fix a FEP configuration  $\eta$  on the ring  $\mathbb{T}_N$ , recall that we denote by  $J$  its number of particles, and denote by  $Y_1 < Y_2 < Y_3 < \dots < Y_J < Y_1$  their successive positions in the ring, the first one being chosen arbitrarily. The static mapping from  $\eta$  (FEP on  $\mathbb{T}_N$ ) to  $\xi$  (SWT on  $\mathbb{T}_J$ ) is represented in Figure 1.4, each value  $\xi_j$  being determined by what immediately follows the  $j$ -th particle in  $\eta$ . More precisely, recalling that by construction,  $\eta_{Y_j} = 1$ , we define

$$\xi_j = 2 + Y_j - Y_{j+1},$$

meaning that

- $\xi_j = 1$  if the  $j$ -th particle in  $\eta$  is immediately followed by another particle.
- $\xi_j = 0$  if the  $j$ -th particle in  $\eta$  is followed by a single empty site
- $\xi_j = -d < 0$  if the  $j$ -th particle in  $\eta$  is followed by  $d + 1$  consecutive empty sites.

This static construction can be translated as a dynamic mapping for the SWT. Assume that  $\eta(t)$  is a rate 1 FEP on  $\mathbb{T}_N$  (driven by the generator (1.1) with  $p_N = q_N = 1$ ), and keep at all time the same tagged particle as the position  $Y_1(t)$  to start the mapping. Then, the

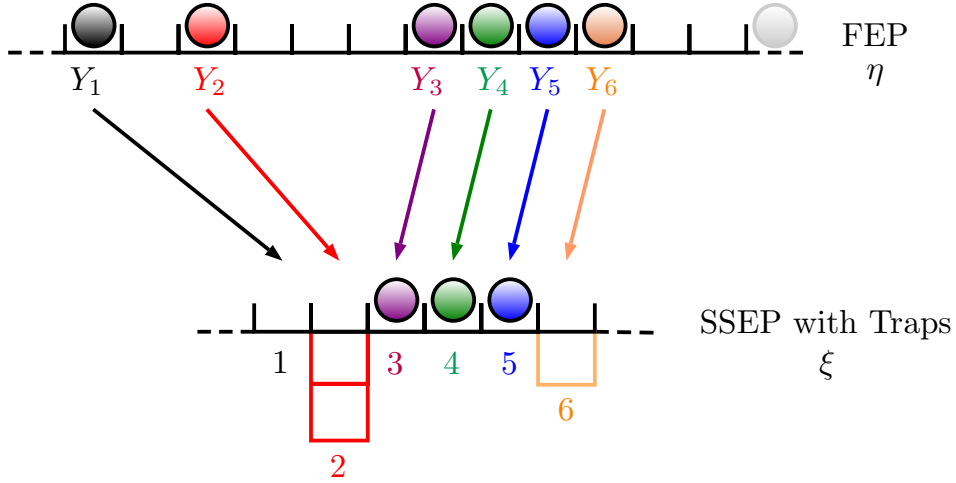


**Figure I.4:** Representation of the mapping  $\Gamma$  between a FEP configuration  $\eta$  and a SWT configuration  $\xi$

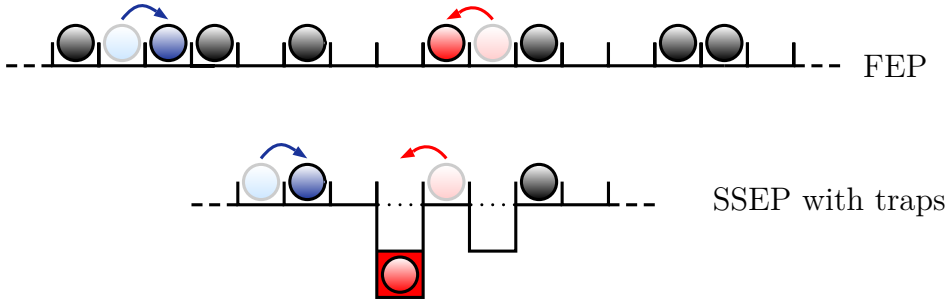


**Figure I.5:** Representation of the dynamic mapping between a FEP  $\eta$  and a SWT  $\xi$

corresponding SWT  $\xi(t)$  is ruled by the following evolution : particles and empty sites in  $\xi$  interact exactly as in a rate 1 SSEP. On top of that, still at rate 1, a particle in  $\xi$  can jump to a neighboring trap, at which point the trap's depth decreases by one (in particular, it becomes an empty site if it was of depth exactly one), and the particle is removed. Any decrease in trap depth in the SWT then corresponds to a neighboring pair of empty sites being broken up in the FEP.

Like the FZRP, this SWT is attractive : starting from two (ordered site-by-site) configurations  $\xi \leq \xi'$ , we can couple their respective evolutions in such a way that  $\xi(t) \leq \xi'(t)$  at any later time  $t > 0$ , by simply using the same clocks so that two particles present at the same site in both processes jump in the same direction at the same time. This big upside, however, w.r.t. the FZRP, is that particles in the SWT behave as rate 1 random walkers until they encounter a trap, which allows for much sharper estimates on the transience time. Once all traps are removed, the SWT simply becomes a standard SSEP. If instead, there are initially not enough particles to fill all traps, then at some point the last particle will get absorbed and the SWT will reach an absorbing state. The transience time for the SWT is therefore defined as the maximal time traps (of positive depth) and particles coexist. Given an initial configuration  $\xi$ , denote by  $p_\xi(t)$  the probability that a SWT started from  $\xi$  is still transient at time  $t$ , namely

$$p_\xi(t) = \mathbb{P}_\xi(\exists j, j' : \xi_j(t) > 0, \xi_{j'}(t) < 0).$$

We then define the maximal transience probability as

$$p_J^{\text{SWT}}(t) := \sup_{\xi} \{p_{\xi}(t)\},$$

where the supremum is taken over all SWT configurations on  $\mathbb{T}_J$ . The first results we obtain in [EM24] is the following;

**Theorem 5.3 (Theorem 1.1 in [EM24])** *The transience probability vanishes over large time scales  $tJ^2 \log J$ , meaning*

$$p_J^{\text{SWT}}(tJ^2 \log J) \xrightarrow[t \rightarrow \infty]{} 0.$$

Given the SWT mapping, this theorem is not very hard to prove: first, one checks that the maximal transience probability is achieved for critical configurations containing as many trap depth as particles, meaning for configurations  $\xi$  such that  $\sum_j \xi_j = 0$ . Indeed, by attractiveness, adding either trap depth or adding particles to a critical configuration will only decrease its transience time. Given this observation, proving Theorem 5.3 amounts to carefully labeling particles, and coupling the SWT with the so-called interchange process [59, 43], and then estimating its full exploration time. This result, however, only yields an asymptotic control of the transience probability over the correct timescale  $J^2 \log J$ . In our second result, we go much further in our estimation of the transience time, and prove that the maximal transience probability for the SWT undergoes a cutoff at time

$$t_J^* := \frac{1}{\pi^2} J^2 \log J.$$

**Theorem 5.4 (Theorem 1.2 in [EM24])** *Define the maximal transience time  $\theta_J^{\text{SWT}} : [0, 1] \rightarrow [0, +\infty]$  as the inverse function of the transience probability  $p_J^{\text{SWT}}$ . There exists a constant  $C > 0$  such that for any  $J$  and any  $\varepsilon \in (0, 1)$ ,*

$$|\theta_J^{\text{SWT}}(\varepsilon) - t_J^*| \leq \delta(J, \varepsilon) := CJ^2 \left( 1 + \log \log \frac{J}{\varepsilon \wedge (1 - \varepsilon)} \right).$$

This theorem proves the transience time undergoes cutoff, in the sense that the maximal transience probability  $p_J^{\text{SWT}}(t)$  goes from 1 to 0 in a time-window of size  $\delta(J, \varepsilon) \ll t_J^*$  around  $t_J^*$ . Because it contains a much sharper bound on the transience probability, this theorem is much more difficult to prove.

Once again, since we are interested in the maximal transience probability, we can focus on critical configurations. However, among critical configurations, it is not clear which one is the worst. For this reason, we need to consider any trap layout. The core set of arguments to prove Theorem 5.4 is the following; Fix an initial critical configuration  $\xi$ , a segment  $A \subset \mathbb{T}_J$ , and call  $B = \mathbb{T}_J \setminus A$  the complementary set of  $A$ . Assume that at time  $t$ , there is still trap (of positive depth) left in  $A$ , then we can be sure that

- at least one live particle (meaning one that was never trapped) remains at time  $t$ , since we started from a critical configuration, and by assumption there remains at least one trap with positive depth.
- This particle has never fully crossed, in either direction, set  $A$  before time  $t$ , otherwise it would have become trapped.

For this reason, the remaining trap in  $A$  breaks in some sense the periodicity of the ring, and allow us to build a SWT on a larger *non-periodic* segment  $S$  of size  $J + |A|$ , where the ring was “cut” at one of the extremities of  $A$ , and another copy of  $A$  is added to the other extremity of  $B$ . This procedure, that we call *unrolling the circle*, allows us to couple up to time  $t$ , any trajectory of the SWT with a trap still in  $A$  at time  $t$ , with a SSEP  $\sigma$  on  $S$  started from the same paired positions  $\mathbb{T}_J \rightarrow S$ , and in contact at both extremities with empty equilibrium reservoirs (see (39)).

Then, under our coupling, the presence of a trap in  $A$  translates as the survival of one of the  $\sigma$  particles up to time  $t$  without being absorbed by either reservoirs. However, the probability for a SSEP in contact with empty reservoirs to still have a particle up to time  $t$  is well known [71], and exhibits cutoff. Once this is done, only remains to divide  $\mathbb{T}_J$  into segments  $A_1, \dots, A_Q$ , each of size  $J/\log J \ll J$ , and carefully use a union bound to the previous result, depending on which of the  $A_q$ 's still contains a trap at time  $t$ . The main technical challenge to achieve this program is to couple particle's trajectories in  $\xi$  and  $\sigma$ , at least until the  $\xi$ -particle gets trapped. To build  $\sigma$  this way, one needs to copy the same Poisson clocks in both  $A$  and its copy, while keeping a SSEP dynamics with independent jumps.

Once this is done, we can get back to the FEP on  $\mathbb{T}_N$ : define analogously to the SWT the maximal transience probability  $p_N^{\text{FEP}}(t)$  and the associated maximal transience time  $\theta_N^{\text{FEP}} : [0, 1] \rightarrow [0, +\infty]$ . We do not state the analogous result to the weaker Theorem 5.3 to focus on the transience time's cutoff;

**Theorem 5.5 (Theorem 2.2 in [EM24])** *The FEP's maximal transience time also exhibits cutoff, in the sense that there exists a constant  $C > 0$  such that for any  $N$  and any  $\varepsilon \in (0, 1)$ ,*

$$|\theta_N^{\text{FEP}}(\varepsilon) - t_{N/2}^*| \leq \delta(N, \varepsilon) := CN^2 \left( 1 + \log \log \frac{N}{\varepsilon \wedge (1 - \varepsilon)} \right).$$

By the previous mapping, any critical FEP configuration on  $\mathbb{T}_N$  is mapped to a critical SWT configuration on  $\mathbb{T}_{N/2}$ . Since transience in both processes is completely equivalent, Theorem 5.4 yields that the *critical maximal transience probability* for the FEP undergoes cutoff at time  $t_{N/2}^*$  as wanted. To prove Theorem 5.5, only remains to compare to non-critical configurations. However, since the FEP is not attractive, this is not completely trivial, and requires a couple more arguments.

- Given a subcritical configuration  $\eta$ , containing  $J < N/2$  particles, its transience time will be that of a mapped SWT  $\xi$  on  $\mathbb{T}_J$ , which will be less than that of a *critical* SWT  $\xi' \geq \xi$  on  $\mathbb{T}_J$ , which is at most  $t_J^*$ , itself less than  $t_{N/2}^*$  because  $J < N/2$ . This proves that a subcritical FEP configuration will freeze faster than a critical one.
- The same argument cannot be repeated for supercritical configurations, however, because for those  $J \geq N/2$ , and therefore we overestimate the corresponding transience time  $t_J^* \geq t_{N/2}^*$ . Instead, for this part of the argument, we use the previous FZRP mapping : Given a supercritical configuration  $\eta$ , we map it to a supercritical FZR configuration  $\omega$  on  $\mathbb{T}_K$  with  $K \leq N/2$ . Then, by the FZRP's attractiveness, there exists a *critical* configuration  $\omega' \leq \omega$  on  $\mathbb{T}_K$  such that  $p_\omega(t) \geq p_{\omega'}(t)$ . We then switch back to a critical FEP  $\eta'$  on  $\mathbb{T}_{2K}$ , then to a critical SWT  $\xi'$  on  $\mathbb{T}_K$ , this time with  $K \leq N/2$ . This time, starting from  $\xi'$  the transience time is at most  $t_K^* \leq t_{N/2}^*$ , which proves as wanted that a supercritical FEP configuration will become ergodic faster than a critical one.

## 6 Hydrodynamic limit in the symmetric case

We now characterize the macroscopic behavior of the FEP on the ring  $\mathbb{T}_N$  and in particular its hydrodynamic limit in the symmetric case. The results presented in this section were obtained in [BESS20], [BES21] and [ESZ23b], and rely in parts on the transience time estimates obtained in the previous section. We focus in this section on the symmetric case, we therefore choose a diffusive timescale and set

$$p_N = q_N = N^2. \quad (\text{I.23})$$

in (I.2). Accelerating thusly the generator by  $N^2$  allows particle (roughly behaving as symmetric random walks) to travel macroscopic distance in times of order 1, so that the macroscopic process will be on the correct timescale already. We consider throughout this section a Markov process  $\{\eta(t), t \geq 0\}$  with *accelerated generator*  $\mathcal{L}_N$  defined by the previous jump rates, and started from a product measure  $\mu^N$  fitting an initial profile  $\rho_0$ , in the sense of (9).

### 6.1 Grand canonical and canonical states for the FEP

As previously emphasized, in order to state a Replacement Lemma similar to Lemma 1.2, one needs first to understand the canonical and grand canonical states for the considered process;

- The *canonical states*  $\mu_{J,B}$  in any given box  $B$  are defined as the stationary state with fixed number of particles  $J$  in  $B$ .
- The *grand-canonical states*  $\mu_{\rho,B}$  are parametrized by the density  $\rho$ . By the *equivalence of ensembles*, they are defined by taking a much larger box  $\Lambda \ni B$  in which the number of particles is set to  $J_\rho := \rho|\Lambda|$ , and observing it on  $B$ ,

$$\mu_{\rho,B}(\sigma) = \lim_{\Lambda \uparrow \mathbb{Z}} \mu_{J_\rho, \Lambda}(\eta|_B = \sigma).$$

For the Simple Exclusion Process, the canonical states are given by uniform distributions on  $\Omega_{N,J}$  (cf. (I.4)), and the grand-canonical states are given by Bernoulli product measures (6). For the FEP, this is not the case, since stationary states must be supported either by the frozen or ergodic components defined in (I.5) and (I.6). Clearly, in the supercritical region, the stationary states are exactly the probability measures supported on frozen states. In the subcritical region, since all jumps occur at rate 1, the canonical states are the uniform distributions  $\pi_{N,j}$  over the ergodic components  $\mathcal{E}_{N,j}$  defined in (I.5), so that for example on the circle  $\mathbb{T}_N$

$$\pi_{N,j}(\eta) = \frac{\mathbf{1}_{\{\eta \in \mathcal{E}_{N,j}\}}}{|\mathcal{E}_{N,j}|} = \frac{\mathbf{1}_{\{\eta \in \mathcal{E}_{N,j}\}}}{\binom{N-k}{k} + \binom{N-k-1}{k-1}}. \quad (\text{I.24})$$

To obtain the last identity, one only needs to check that the first site of the ring can either be occupied or empty, and once this is chosen, the remaining empty sites must be placed in-between particles to be in the ergodic component.

To define the grand canonical state for  $\rho > 1/2$ , we take the canonical state over a very large box  $\Lambda$  with  $\rho|\Lambda|$  particles, and consider its marginal in a small box inside of it as  $|\Lambda| \rightarrow \infty$ . We obtain an infinite volume, translation invariant distribution  $\pi_\rho$  with finite size marginals given by

$$\pi_\rho(\eta|_{\{1, \dots, \ell\} = \sigma}) = \mathbf{1}_{\{\sigma \in \mathcal{E}_\ell\}} (1 - \rho) a(\rho)^{2J - \ell + 1 - \sigma_1 - \sigma_\ell} (1 - a(\rho))^{\ell - 1 - J}, \quad (\text{I.25})$$

where  $\mathcal{E}_\ell$  is the set of ergodic configurations on  $\{1, \dots, \ell\}$ ,  $J := \sum_{x=1}^\ell \sigma_x$  is the number of particles in  $\sigma$ , and

$$a(\rho) := \frac{2\rho - 1}{\rho}. \quad (\text{I.26})$$

One easily checks that  $a(\rho)$  represents the density under  $\pi_\rho$  of active particles, namely

$$a(\rho) = \pi_\rho(\eta_{x-1}\eta_x + \eta_x\eta_{x+1} \geq 1). \quad (\text{I.27})$$

In the critical case  $\rho = 1/2$ , the grand canonical state is simply given by  $\pi_{1/2} = (\delta_{\circ\bullet} + \delta_{\bullet\circ})/2$  where  $\circ\bullet$  and  $\bullet\circ$  represent the two possible alternated configurations with particles at odds (resp. even) sites.

The construction (I.25) of the grand-canonical states, however, is in many cases not very convenient, because it is a global construction over a given box rather than a local one. For this reason, it is very useful to build  $\pi_\rho$  in a sequential, Markovian way. More precisely, if  $(\eta_x)_{x \geq 0}$  and  $(\eta_x)_{x \leq 0}$  are distributed as independent Markov chains on  $\{0, 1\}$ , both starting from  $\eta_0 = \text{Ber}(\rho)$ , and with transition probabilities

$$\mathbb{P}(\eta_{x\pm 1} = 1 \mid \eta_x = 1) = a(\rho) \quad \text{and} \quad \mathbb{P}(\eta_{x\pm 1} = 1 \mid \eta_x = 0) = 1. \quad (\text{I.28})$$

then,  $(\eta_x)_{x \in \mathbb{Z}} \sim \pi_\rho$ .

## 6.2 Hydrodynamic limit for the supercritical symmetric FEP

Now that the canonical and grand canonical states of the FEP are characterized, we describe its hydrodynamic limit, and start by the easier setting, when the initial profile  $\rho_0$  is uniformly supercritical as in Theorem 5.1. More precisely, we have the following result, which is the analogous to Theorem 1.1 for the supercritical FEP.

**Theorem 6.1 (Theorem 2.2 of [BESS20])** *Fix  $\rho_0 \in C^1(\mathbb{T})$  taking values in  $(1/2, 1]$  and  $\mu^N$  the associated product state (9). Then, in the sense of Definition 1.3, the hydrodynamic limit of  $\{\eta(t), t \geq 0\}$  is given by the unique weak solution  $\rho(t, u) : [0, +\infty) \times \mathbb{T} \rightarrow [0, 1]$  to the hydrodynamic equation*

$$\begin{cases} \partial_t \rho = \partial_u^2 a(\rho) \\ \rho(0, \cdot) = \rho_0, \end{cases} \quad (\text{I.29})$$

where  $a(\rho)$  is the equilibrium active density defined in (I.26).

We now sketch the proof of this result, which thanks to the subdiffusive estimate of the transience time given in Theorem 5.1, is an adaptation of Guo Papanicolaou and Varadhan's entropy method (see Section 1.3). Here are the main steps;

- Because our process is now accelerated by a diffusive factor  $N^2$ , according to Theorem 5.1, with high probability the process is at time  $\tilde{t}_N = (\log N)^{32}/N^2$  in an ergodic state. Furthermore, since  $\tilde{t}_N \ll 1$  the process  $\eta(\tilde{t}_N)$  at that time is still associated with the initial profile  $\rho_0$ , because particles have not had the time to travel over macroscopic distances. In particular, the distribution

$$\tilde{\mu}^N(\cdot) := \mathbb{P}_{\mu^N}(\eta(\tilde{t}_N) = \cdot \mid \eta(\tilde{t}_N) \in \mathcal{E}_N)$$

of the process at time  $\tilde{t}_N$  conditioned to being in the ergodic component is very close to the the unconditioned distribution  $\mu_{\tilde{t}_N}$ , so that the process started from  $\tilde{\mu}^N$  and the one started from  $\mu^N$  have the same hydrodynamic limit.

- We therefore now consider instead the process started from  $\tilde{\mu}^N$ , and define  $\tilde{\mu}_t^N$  its distribution at time  $t$ . Its relative entropy w.r.t. a grand canonical state, defined in (18),  $H(\tilde{\mu}_t^N \mid \pi_\rho)$  on the ring  $\pi_\rho$  (defined analogously to its infinite volume counterpart (I.25)) is now of order  $O(N)$  for any time  $t$  because both distributions are supported on the ergodic component. This allows us to derive a standard estimate for the Dirichlet form

$$D_N(f) := \mathbb{E}_\rho(\sqrt{f}(-\mathcal{L}_N)\sqrt{f}) = \frac{1}{2} \sum_{x \in \mathbb{T}_N} c_{x,x+1}^N(\eta) \left\{ \sqrt{f}(\eta^{x,x+1}) - \sqrt{f}(\eta) \right\}^2 \quad (\text{I.30})$$

of the density  $f_t^N := d\tilde{\mu}_t^N/d\pi_\rho$  w.r.t.  $\pi_\rho$ . More precisely, recalling that the  $c_{x,x+1}^N$  are the *accelerated jump rates* one obtains that

$$D_N \left( \int_0^t f_s^N ds \right) = O(N).$$

- This estimate of the Dirichlet form allows us to apply the entropy method by obtaining the classical one and two-blocks estimates. The main hurdle to do so is the fact that the grand canonical state  $\pi_\rho$  is not product, so that we need to estimate its correlation decay [BESS20, Lemma 6.5], which is exponential, as well as its equivalence of ensembles [BESS20, Proposition 6.9].
- Once this is done, it remains to exploit the fact that the FEP is gradient, meaning that (7) holds for the function

$$\tau_x h = \eta_{x-1}\eta_x + \eta_x\eta_{x+1} - \eta_{x-1}\eta_x\eta_{x+1} = \mathbf{1}_{\{x \text{ is occupied by an active particle}\}} \quad (\text{I.31})$$

whose expectation under the grand canonical state  $\pi_\rho$  is  $a(\rho)$  according to (I.27).

### 6.3 Stephan problem for the symmetric FEP

As outlined in the previous section, once the ergodic component is reached, the hydrodynamic limit for the FEP is derived using classical tools. In the general setting where the initial profile is not uniformly supercritical however, and also charges the subcritical region, entropy-based techniques no longer straightforwardly apply, because there is no single reference state to which the two-phased system can be locally compared. More precisely, we derive the following result.

**Theorem 6.2 (Theorem 2.4 of [BES21])** *Fix a measurable initial profile  $\rho_0$  and  $\mu^N$  the associated product state (9). The hydrodynamic limit for  $\{\eta(t), t \geq 0\}$  is given by the unique weak solution  $\rho(t, u) : [0, +\infty) \times \mathbb{T} \rightarrow [0, 1]$  to the Stefan problem*

$$\begin{cases} \partial_t \rho = \partial_u^2 \mathcal{H}(\rho) \\ \rho(0, \cdot) = \rho_0, \end{cases} \quad (\text{I.32})$$

where we define  $\mathcal{H}(\rho) = a(\rho)\mathbf{1}_{\{\rho \geq 1/2\}}$  (cf. (I.26)).

Since entropy methods are not well-suited to phase separated hydrodynamics, we relied instead on a scheme of proof introduced by Funaki [31] involving Young measures. The key arguments are the following;

- First, we characterize local equilibrium [BES21, Proposition 3.8], namely the one-block estimate that states that for a local function  $g$ , any test function  $H$  and any  $T > 0$

$$\int_0^T ds \frac{1}{N} \sum_{x \in \mathbb{T}_N} H(x/N) \{ \tau_x g(s) - \mathbb{E}_{\rho_x^\ell(s)}(g) \} \quad (\text{I.33})$$

vanishes in probability as  $N \rightarrow \infty$  then  $\ell \rightarrow \infty$ , where  $\rho_x^\ell$  is defined as in (15) as the local density in a box of size  $\ell$  around  $x$ . The one-block estimate amounts to a replacement Lemma 1.2, but at a microscopic scale going to infinity *after*  $N$  rather than *jointly with*  $N$ . The main point to obtain this one-block estimate in Funaki's scheme is to characterize the infinite volume translation invariant stationary distributions  $\bar{\mu}$  for the process. For the FEP, we prove using the zero-range mapping laid out in Section 5.3 a De-Finetti type decomposition [BES21, Lemma 3.6], meaning that any such distribution can be written

$$\bar{\mu} = \mu_{\mathcal{F}} + \int_{\rho \geq 1/2} dq(\rho) \pi_\rho,$$

where  $\mu_{\mathcal{F}}$  is supported on the frozen component and  $q$  is a distribution on  $[1/2, 1]$ . the one block estimate then follows, because in any frozen state (I.33) gives a null contribution, whereas any  $\pi_\rho$  satisfies a law of large numbers which yields that (I.33) vanishes in the limit  $N \rightarrow \infty$  then  $\ell \rightarrow \infty$ .

- Once the one-block estimate is obtained, one needs to show that  $\rho_x^\ell$  does not change much when  $x$  remains in a small mesoscopic box of size  $\varepsilon N$ . In the absence of Dirichlet estimate, we cannot show it by the standard two-blocks estimate, so that instead we exploit Young measures, and define analogously to the empirical measure (13) the Young measure on  $\mathbb{T} \times [0, 1]$

$$\pi_t^{N,\ell}(du, dr) := \frac{1}{N} \sum_{x \in \mathbb{T}_N} \delta_{x/N}(du) \delta_{\rho_x^\ell(t)}(dr). \quad (\text{I.34})$$

- At this point, the main missing piece is to show that in the limit  $N \rightarrow \infty$  then  $\ell \rightarrow \infty$ , the Young measure  $\pi_t^{N,\ell}$  converges  $\mathbb{P}_{\mu_N}$ -a.s. to a measure that is Dirac in  $r$ , meaning, as stated in [BES21, Proposition 3.4], that there exists a function  $\rho$  such that

$$\pi_t^{N,\ell}(du, dr) \xrightarrow{N,\ell \rightarrow \infty} m_t(du) \delta_{\rho_t(u)}(dr).$$

The proof of this convergence is quite intricate, however the main idea is to compare small mesoscopic  $t_\theta \simeq \theta \rightarrow 0$  after  $N \rightarrow \infty$  timescales and large microscopic timescales  $t_{\Theta,N} \simeq \Theta/N^2$  with  $\Theta \rightarrow \infty$  after  $N \rightarrow \infty$ . Roughly speaking, consider around  $u \in \mathbb{T}$  a large microscopic box in the system, at a microscopic time  $t_{\Theta,N}$  with density  $r$ . Letting now time evolve over a time  $t_\theta$ , particles will diffuse and locally mix in the system, so that the density in that same box is no longer fixed and given by a Young distribution  $p_t(u, dr')$ . However, because the timescale is small in the limit  $\theta \rightarrow 0$ , mass does not have time to actually move around the system, so that on average over  $r$  and  $u$  and in the proper limit, we must have that  $r - \int r' p_t(u, dr')$  vanishes, meaning that in the limit  $p_t$  actually converges to a Dirac measure.

This strategy proves the hydrodynamic limit in the Stefan regime where the initial profile exhibits both supercritical and subcritical phases. Of course, the weak construction, obtained in the hydrodynamic limit, of solutions to (I.32) is not very explicit, therefore we also proved in [BES21, Proposition 2.5] that under reasonable assumptions on the initial profile  $\rho_0$ , one can define macroscopic interfaces  $u_k(t)$  between phases  $\rho \geq 1/2$  and  $\rho < 1/2$ , and compute their velocity as a function of the densities on both sides of the interface. This is by no means trivial, in particular because this velocity

$$v_k(t) := \frac{4\partial_u \rho_k^+(t)}{1/2 - \rho_k^-(t)}$$

depends on the inverse of the criticality gap  $1/2 - \rho_k^-(t)$ , where  $\rho_k^-(t)$  is the density in the subcritical region right next to the interface and can be very close to  $1/2$  if for example the initial data is smooth.

## 6.4 Critical behavior in two dimensions

Because we loose access to the mapping arguments, and to explicit formulas for the stationary states, the higher dimensional case is much harder to tackle. Several different models can be put forward as higher-dimensional versions of the FEP. One of them is the two-dimensional Constrained Lattice Gas considered in [65], an exclusion process in which particles jump at rate one to empty neighbors provided any other neighboring site is occupied, whose critical behavior we scrutinize in [25]. In the same way that the alternate configuration  $\bullet\circ\bullet\circ$  is critical for the 1-dimensional FEP, the checkerboard configuration  $\begin{smallmatrix} \bullet & \circ & \bullet \\ \circ & \bullet & \circ \\ \bullet & \circ & \bullet \end{smallmatrix}$  is critical for the CLG, in the sense that it is the most dense frozen configuration, so that  $\bar{\rho} := 1/2$  is still a critical density threshold. However, unlike in the 1-dimensional case, we observe in [25] that diffusive behavior can be sustained below  $\bar{\rho}$  down to a second critical density  $\rho_c \simeq 0.3257$ , under which no diffusive behavior occurs and the system quickly freezes.

The reason for these separated critical densities is that the 2-dimensional checkerboard is a highly structured configuration, which is much easier to break down than to create. To illustrate this, consider that when a configuration with density  $\rho < 1/2$  is close to the checkerboard one, many more jumps will drive the configuration *away* from that checkerboard than *towards* it. For this reason, in the density range between the two critical densities  $\rho_c < \rho < \bar{\rho}$ , starting from a disordered state in a system of size  $N$ , activity is sustained over much longer timescales than the diffusive one, thus resulting in a diffusive behavior over diffusive timescales  $t \sim O(N^2)$ . Unlike for high densities, however, for  $\rho_c < \rho < \bar{\rho}$  a frozen state is ultimately reached and no truly active stationary state exists. Like in the one-dimensional case (see [BESS20]), under  $\rho_c$ , activity dies down over logarithmic timescales and the system quickly freezes.

Although it cannot be straightforwardly proved using the same tools as for Theorems 6.1 and 6.2, we fully expect that under diffusive scaling, and starting from a Bernoulli product measure fitting a given initial profile  $\rho_0$ , the two-dimensional CLG's macroscopic evolution is ruled by a Stefan diffusion equation  $\partial_t \rho = \text{div}(D(\rho)\nabla \rho)$  (where  $D(\rho)$  vanishes in the frozen phase  $\rho < \rho_c$ ) with initial condition  $\rho_0$ . Mathematically speaking, this is very difficult to prove in parts because, as explained in the previous paragraph, in the regime  $\rho_c < \rho < \bar{\rho}$ , no active stationary state exists. Instead, we expect that microscopically, an infinite system reaches over large diffusive timescales a quasi-stationary state  $\tilde{\mu}_\rho$ . For  $\rho > \bar{\rho}$  instead, the quasi-stationary state becomes an actual stationary state  $\tilde{\mu}_\rho$ .

In the supercritical phase, as conjectured in [44], two different correlation lengths exist: first, the classical, probabilistic, correlation length  $\xi_{\times} = \xi_{\times}(\rho)$  over which the two-points stationary correlations vanish under  $\tilde{\mu}_{\rho}$ . And second, the geometric correlation length  $\xi_{\perp}$ , which is the one mostly used in the physics literature [19], which is the scale of the activation chains that sustain activity. In particular, for any system of size  $N \ll \xi_{\perp}(\rho)$ , activity decays until dying out. These two length-scales diverge as  $\rho \searrow \rho_c$ , and we denote by  $\nu_{\times}, \nu_{\perp} \geq 0$ , the corresponding critical exponents, meaning that

$$\xi_{\times} \sim (\rho - \rho_c)^{-\nu_{\times}} \quad \text{and} \quad \xi_{\perp} \sim (\rho - \rho_c)^{-\nu_{\perp}}.$$

Activity in the system is also ambiguously defined (because particles in dense regions are active but cannot jump because of the exclusion constraint), so that we distinguish between the density of active particles (with an occupied neighbor)  $\rho_a(\rho) \sim (\rho - \rho_c)^{\beta}$ , and the activity  $a \sim (\rho - \rho_c)^b \leq 3\rho_a$ , namely the total rate at which jumps occur in the system. We numerically show in [25] that the two critical exponents actually coincide, meaning  $\beta = b$ .

To get a full picture at criticality, other macroscopic quantities need to be taken into account. First, because the stationary state for the CLG is locally correlated, its compressibility

$$\chi(\rho) := \sum_{x \in \mathbb{Z}^2} \text{Cov}_{\tilde{\mu}_{\rho}}(\eta_0, \eta_x) \sim (\rho - \rho_c)^{\gamma}$$

is different from that of the SSEP. Furthermore, as evidenced by [65, 44] the CLG's absorbing state is hyperuniform, meaning the number  $N$  of particles in a typical box of size  $R$  in the absorbing state has variance  $\sim R^{\zeta}$ , for  $\zeta < 1$ . Finally, we denote by  $\alpha$  the diffusion coefficient's critical exponent,  $D(\rho) \sim (\rho - \rho_c)^{\alpha}$ . Because some of these critical exponents are difficult to approach numerically, in [25] we supplement our simulations with a number of theoretical relationships between exponents.

- The Einstein relation  $D\chi = \sigma$ , together with the fact that the current's fluctuations' amplitude are ruled by the activity, yields

$$\alpha + \gamma = b.$$

- At smaller scales than  $\xi_{\perp}$ , the system looks critical, so that critical density fluctuations must be of order  $\rho - \rho_c$  to hide the off-criticality. This yields the identity  $\xi_{\perp}^{\zeta} \approx (\rho - \rho_c)\xi_{\perp}^2$  and in turn

$$\nu_{\perp}(2 - \zeta) = 1.$$

- Exploiting the structure factor [34] yields the identity

$$\gamma = 2\nu_{\times}(1 - \zeta).$$

- The gradient nature of the process yields that  $\rho'_a = D$ , so that

$$\alpha = \beta - 1.$$

We regroup in table I.1 the related observables and critical exponents whose numerical value was determined in [25], and which are in excellent agreement with previous results [65, 44].

obs.	$D$	$\chi$	$\xi_{\perp}$	$\xi_{\times}$	$\text{Var}(N)$	$\rho_a$	$a$
exp.	$\alpha$	$\gamma$	$\nu_{\perp}$	$\nu_{\times}$	$\zeta$	$\beta$	$b$
	-0.38	1 and 1.07	0.77	1.8	0.70	0.62	0.62

**Table I.1:** Critical exponents related to observables for the two-dimensional CLG.

## 7 Hydrodynamics and fluctuations for the asymmetric FEP

As outlined in the introduction (see Section 2.3), the most straightforward tools to derive the macroscopic behavior of *asymmetric* interacting lattice gases only hold for *attractive systems* [48, Section 9]. The FEP is not attractive, but the mapped zero-range process described in Section 5.3 is, so that to characterize the macroscopic limit of the FEP in the asymmetric case, we map back and forth that of the facilitated zero-range process.

### 7.1 Hydrodynamic limit for the AFEP

We now consider the asymmetric case of the FEP on  $\mathbb{L}_N = \mathbb{Z}$ , on a hyperbolic timescale, so that we choose  $p \in (1/2, 1]$  and set in this section

$$p_N := pN \quad \text{and} \quad q_N = (1 - p)N$$

in the jump rates I.2. Define the macroscopic drift

$$\mathfrak{H}(r) = (1 - r)a(r)\mathbf{1}_{\{r \geq 1/2\}}, \quad (\text{I.35})$$

where the active density  $a$  was defined in (I.27). In the asymmetric case, the hydrodynamic equation is hyperbolic, so that the weak formulation of solutions needs to be supplemented by an entropy condition, as given by the following definition.

**Definition 7.1 (Entropy solutions to the hyperbolic Stefan problem)** *Fix a measurable initial profile  $\rho_0$  on  $\mathbb{R}$ . A measurable function  $\rho$  is an entropy solution to the hyperbolic equation*

$$\partial_t \rho + (2p - 1)\partial_u \mathfrak{H}(\rho) = 0 \quad (\text{I.36})$$

with the initial condition  $\rho_0$  if

1. (entropy inequality) for any non-negative test function  $\varphi \in C^{1,1}(\mathbb{R}_+ \times \mathbb{R})$  with compact support in  $(0, \infty) \times \mathbb{R}$ , for any  $0 \leq c \leq 1$ ,

$$\int_0^\infty \langle |\rho(t, \cdot) - c|, \partial_t \varphi_t \rangle + (2p - 1) \langle \mathfrak{q}(\rho(t, \cdot); c, \mathfrak{H}), \partial_u \varphi_t \rangle dt \geq 0, \quad (\text{I.37})$$

where  $\mathfrak{q}(\rho; c, \mathfrak{H}) = \text{sign}(\rho - c)(\mathfrak{H}(\rho) - \mathfrak{H}(c))$ ;

2. (initial condition) for any  $A > 0$ ,  $\lim_{t \rightarrow 0} \int_{-A}^A |\rho(t, u) - \rho_0(u)| du = 0$ .

Nonlinear hyperbolic problems can create shocks, after which there is in general more than one weak solution to the equation. However, the entropy solution is *unique*, and is the physically relevant solution because it can be seen as the vanishing viscosity limit solution to the equation, meaning the limit as  $\varepsilon \rightarrow 0$  of the solution to the viscous equation

$$\partial_t \rho + (2p - 1)\partial_u \mathfrak{H}(\rho) = \varepsilon \partial_u^2 \rho, \quad (\text{I.38})$$

where  $\mathcal{H}$  was introduced in Theorem 6.2. We are now ready to state the hydrodynamic limit in the asymmetric case.

**Theorem 7.1 (Theorem 2.3 - (II) of [ESZ23b])** Fix a measurable initial profile  $\rho_0$  and  $\mu^N$  the associated product state (9). The hydrodynamic limit for the asymmetric FEP  $\{\eta(t), t \geq 0\}$  started from  $\mu^N$  is given by the unique entropy solution to (I.36), with  $\mathfrak{H}$  given by (I.35).

## 7.2 Sketch of the proof

The proof of this result strongly relies on the mapping with the attractive zero-range process introduced in Section 5.3. More precisely, it is straightforward to check that the zero-range process  $\omega := \Pi^*[\eta]$  defined on  $\mathbb{Z}$  through the dynamic mapping (I.9) is driven by the asymmetric zero-range generator

$$\mathcal{L}^{\text{ZR}} f(\omega) = \sum_{y \in \mathbb{Z}} \mathbf{1}_{\{\omega_y \geq 2\}} \left\{ p_N (f(\omega^{y,y+1}) - f(\omega)) + q_N (f(\omega^{y,y-1}) - f(\omega)) \right\}. \quad (\text{I.39})$$

Since this zero-range is attractive, we derive [ESZ23b, Theorem 2.4 - (II)] its hydrodynamic limit  $\alpha(t, v) \simeq \mathbb{E}(\omega_{\lfloor Nv \rfloor}(t))$  following [64], which is given by the unique entropy solution, in the sense of Definition 7.1, of the hyperbolic equation

$$\partial_t \alpha + (2p - 1) \partial_v \left\{ \frac{\alpha - 1}{\alpha} \mathbf{1}_{\{\alpha \geq 1\}} \right\} = 0. \quad (\text{I.40})$$

The first hurdle to get this hydrodynamic limit is that the initial distribution  $\tilde{\mu}^N := \mu^N \circ \Pi^{-1}$  for the zero-range process, which is the pushforward through the static mapping of the initial distribution  $\mu^N$  of the FEP, is not a simple product state, therefore we need to approximate it by a product distribution. Then, using attractiveness, we estimate the number of discrepancies  $\delta \ll N$  between the two processes. This strategy shows that the mapped FZRP and its approximation must have the same hydrodynamic limit [ESZ23b, Lemma 5.2]. Once this issue is solved, we locally compare the zero-range process with its local equilibrium state, and show that both in the supercritical and the subcritical regions, local mixing is quickly enforced [ESZ23b, Proposition 5.9]. The core idea of the proof is that because of attractiveness, two coupled zero-range processes  $\omega$  and  $\omega'$  become quickly ordered, in the sense that in any large local neighborhood  $B_\ell(y)$  of a site  $y$ , after a time of order  $t_\ell := \ell^3/N^2 \ll 1$ , we have w.h.p.

$$\left\{ \omega(t_\ell) \leq \omega'(t_\ell) \quad \text{on} \quad B_\ell(y) \right\} \quad \text{or} \quad \left\{ \omega(t_\ell) \geq \omega'(t_\ell) \quad \text{on} \quad B_\ell(y) \right\}.$$

In particular, consider a local box  $B_\ell(y)$  of the zero-range process  $\omega$  with supercritical initial density  $\alpha := \alpha_0(y/N)$ . After a time  $t_\ell$ , with high probability, we will be able to “sandwich”  $\omega$  on  $B_\ell(y)$  in between two *equilibrium* zero-range processes with respective distributions  $\mu_{\alpha-\varepsilon}$  and  $\mu_{\alpha+\varepsilon}$  defined by (I.15). Letting then  $\varepsilon \rightarrow 0$ , proves local equilibrium in the diffusive phase, whereas the subcritical phase is not too challenging because everything freezes out pretty quickly. We thus derive the microscopic counterpart to the entropy inequality (I.37) [ESZ23b, Lemma 5.7], and, in turn, the FZRP’s hydrodynamic limit.

Given the zero-range process’s hydrodynamic limit, we then need to map it back and forth to derive that of the AFEP. The space mapping, unfortunately is not homogeneous nor smooth. Indeed, recall that the sites in the zero-range processes sites  $y$  are defined as empty sites in the exclusion process, starting from a tagged empty site with position  $X_0(t)$ . At the macroscopic level, we denote by  $\sigma = \sigma_t := \lim_{N \rightarrow \infty} X_0(t)/N$  the macroscopic position of the tagged empty site in the exclusion process, and we obtain the following identity between

the exclusion process's macroscopic space variable  $u = u_t = x/N$  and  $v = v_t = y/N$ , that of the FZRP:

$$v = \int_{\sigma}^u (1 - \rho(u')) du'.$$

Writing this relation from the FZRP's standpoint is more convenient, because it is the hydrodynamic limit we actually have access to. This yields

$$u := \sigma + \int_0^v (1 + \alpha(v')) dv'. \quad (\text{I.41})$$

Next, we want to express  $\sigma$  as a function of the zero-range process as well, which is not hard, because the tagged empty site jumps left (resp. right) in the FEP every time a particle jump right (resp. left) over the origin in the FZRP. The variable  $\sigma$  can therefore be expressed as minus the total current that has crossed the origin in the zero-range process up to time  $t$

$$\sigma_t = - \int_0^{+\infty} (\alpha_t(v) - \alpha_0(v)) dv.$$

Once the space mapping  $u = u_t(v)$  is defined, one can then recover  $\rho$  by letting

$$\rho(t, u) := \frac{\alpha(t, v)}{1 + \alpha(t, v)}, \quad (\text{I.42})$$

which should be an entropy solution to (I.36) provided  $\alpha$  is solution to (I.40).

Because we are dealing with non-smooth functions (because of the interfaces between phases and of the hyperbolic shocks), however, this last statement is by no means straightforward, so that one needs to smooth out both  $\alpha$  and  $\rho$  in the spirit of the vanishing viscosity limit, and show that both smoothed out solution respectively converge to the actual solutions. More precisely, we consider the solution  $\alpha$  to the viscous equation

$$\partial_t \alpha^\varepsilon + (2p - 1) \partial_v \left\{ \frac{\alpha^\varepsilon - 1}{\alpha^\varepsilon} \mathbf{1}_{\{\alpha^\varepsilon \geq 1\}} \right\} = \varepsilon \partial_v^2 \left\{ \frac{\alpha^\varepsilon}{1 + \alpha^\varepsilon} \right\}, \quad (\text{I.43})$$

where both the interfaces and the shocks have been smoothed out. Then, we can define  $u^\varepsilon$ ,  $\sigma^\varepsilon$  and  $\rho^\varepsilon$  as in (I.41) and (I.42), and because everything is smooth, tedious but straightforward computations show [ESZ23b, Lemma 4.4] that  $\rho^\varepsilon$  is solution to the viscous equation (I.38). Proving that  $\alpha^\varepsilon$  and  $\rho^\varepsilon$  resp. converge as  $\varepsilon \rightarrow 0$  in  $L^1_{loc}$  to the entropy solutions to (I.40) and (I.36) ([ESZ23b, Lemma 4.3]) then completes the macroscopic mapping and proves Theorem 7.1.

Although the main upside of the strategy is that it allows to capture the hydrodynamic behavior of the FEP in the asymmetric case, which would be very difficult otherwise because the latter is not attractive, the strategy of mapping hydrodynamic limits is by no means restricted to the asymmetric case. In particular, we also use it to provide an alternative, simpler proof of Theorem 6.2 in the symmetric case [ESZ23b, Theorem 2.3 - (I)].

### 7.3 CLT stationary fluctuations for the FEP

We then exploited the same mapping strategy to derive the stationary fluctuations process for the FEP on  $\mathbb{Z}$  in the spirit of Theorem 1.3. We consider in this section the jump rates

$$p_N := \mathfrak{s}N^2 + N^\gamma \quad \text{and} \quad q_N = \mathfrak{s}N^2. \quad (\text{I.44})$$

The parameter  $\mathfrak{s}$  will be either 0 or 1 to help us distinguish between the weakly asymmetric and the totally asymmetric cases, whereas  $\gamma \leq 3/2$  tunes the strength of the asymmetry. We now consider, for  $\rho > 1/2$ , a facilitated exclusion process on  $\mathbb{Z}$  with those jump rates, and started from the stationary state  $\pi_\rho$  defined in (I.25).

As proved by the hydrodynamic limit of Theorem 7.1, in the asymmetric FEP at density  $\rho$ , particles travel on average at a macroscopic velocity

$$v = v(\rho) := \frac{d}{d\rho} \mathfrak{H}(\rho) = \frac{1 - 2\rho^2}{\rho^2} \quad (\text{I.45})$$

where  $\mathfrak{H}$  was defined I.35. Since the asymmetric jumps occur at rate  $N^\gamma$  and space is rescaled as  $1/N$ , the fluctuations process thus travels at an average speed  $vN^{\gamma-1}$ , so that we define the FEP's fluctuation field  $\mathcal{Y}_t^N \in \mathcal{S}'(\mathbb{R})$  in this moving reference frame, acting on smooth test functions  $H$  in the Schwartz space  $\mathcal{S}(\mathbb{R})$  as

$$\mathcal{Y}_t^N(H) := \frac{1}{\sqrt{N}} \sum_{x \in \mathbb{Z}} (\eta_x(t) - \rho) H \left( \frac{x}{N} - tvN^{\gamma-1} \right). \quad (\text{I.46})$$

In order to present our main results in [EZ24], we introduce for  $\rho > 1/2$  the diffusion coefficient

$$D(\rho) := a'(\rho) = \frac{1}{\rho^2}, \quad (\text{I.47})$$

the compressibility

$$\chi(\rho) := \rho(1 - \rho)(2\rho - 1), \quad (\text{I.48})$$

and the conductivity

$$\sigma(\rho) := \frac{(1 - \rho)(2\rho - 1)}{\rho}. \quad (\text{I.49})$$

Note that clearly, the Einstein fluctuation-dissipation relation  $\sigma = D\chi$  holds. In order not to burden this section unnecessarily, we now state in a formal setting our results from [EZ24]. First, we consider the weakly asymmetric case.

**Theorem 7.2 (Theorem 2.2 of [EZ24])** *Choose  $\mathfrak{s} = 1$  in (I.44), the FEP's fluctuation field's trajectory  $\{\mathcal{Y}_t^N, t \geq 0\}$  converges as  $N \rightarrow \infty$  in the uniform topology on  $D([0, T], \mathcal{S}'(\mathbb{R}))$  to a process  $\{Y_t, t \geq 0\}$  which is*

*i) solution to the stochastic heat equation*

$$\partial_t Y_t = D(\rho) \partial_u^2 Y_t + \sqrt{2\sigma(\rho)} \partial_u \dot{W}_t \quad (\text{I.50})$$

*for  $\gamma < 3/2$ , where  $D$  and  $\sigma$  are respectively given by (I.47) and (I.48).*

*ii) solution to the stochastic Burgers equation*

$$\partial_t Y_t = D(\rho) \partial_u^2 Y_t + \frac{1}{2} D'(\rho) \partial_u Y_t^2 + \sqrt{2\sigma(\rho)} \partial_u \dot{W}_t \quad (\text{I.51})$$

*for  $\gamma = 3/2$ .*

We do not give here the precise definition of the two limiting processes, and refer the reader to [EZ24, Definitions 2.1 and 2.3] for the details. Note that these two limits do not explicitly depend on the asymmetry exponent  $\gamma$ , because we are already looking at the fluctuation process  $\mathcal{Y}_t^N$  in a moving frame depending on  $\gamma$ . We now consider the totally asymmetric case.

**Theorem 7.3 (Theorem 2.3 of [EZ24])** Choose  $\varepsilon = 0$  and  $\gamma < 4/3$  in (I.44), the FEP's fluctuation field's trajectory  $\{\mathcal{Y}_t^N, t \geq 0\}$  converges as  $N \rightarrow \infty$  in  $D([0, T], \mathcal{S}'(\mathbb{R}))$ , in the weak topology, to a process  $Y_t = \sqrt{2\sigma(\rho)}\partial u\mathcal{W}_t$ , meaning a gaussian process with covariance

$$\mathbb{E}(Y_s(G)Y_t(H)) = \langle G, T_{t-s}H \rangle \quad \text{for} \quad t \geq s,$$

for  $G, H \in \mathcal{S}$ , where  $\{T_t, t \geq 0\}$  is the semi-group for the self adjoint operator  $A_\rho := D(\rho)\partial_u^2$ .

The derivation of these results relies on the same mapping strategy that allowed us to derive the FEP's hydrodynamic limit in the asymmetric case. More precisely, we exploit analogous results for attractive zero-range processes, namely the stationary fluctuations for the weakly asymmetric zero-range process derived in [40, Proposition 2.1 and Theorem 2.2] and for the totally asymmetric zero-range process derived in [38, Theorem 2.5]. Note that for these results, the two phased nature of the FZRP does not matter, because since the FEP is in a stationary state, it is in particular initially in the ergodic component, so that the FZRP in this case also starts from its ergodic component  $\mathbf{E}_K$  defined in (I.11), and therefore behaves as a “normal” constant-rate zero-range process, so that results in [40, 38] apply straightforwardly.

Given those results, proving Theorems 7.2 and 7.3 amounts to going through the mapping. Compared to the hydrodynamic setting, the macroscopic mapping is much more convenient because the density is constant, so that the macroscopic space variable  $u$  and  $v$  for the FEP and FZRP are related through the affine relation

$$v = (1 - \rho)(\sigma - u),$$

where as in the previous section  $\sigma$  is the macroscopic position of the tagged empty site. However, unlike for the hydrodynamic limit, at the macroscopic level fluctuations are obviously stochastic, so that we need to estimate the expectation and variance of the position of the tagged empty site  $X_0(t)$ . As mentioned before, this position is related to the total particle current going through edge  $(-1, 0)$  in the zero-range process before time  $t$ , denoted by  $J_{-1,0}^{\text{ZR}}(t)$ , for which we can write

$$J_{-1,0}^{\text{ZR}}(t) = X_0(0) - X_0(t).$$

With this identity, together with (I.9), one obtains that the position  $X_y(t)$  of the  $y$ -th empty site in the FEP can be expressed as a function of the zero-range process, namely

$$X_y(t) = X_0(0) - J_{-1,0}^{\text{ZR}}(t) + \sum_{y'=0}^{y-1} \omega_{y'}(t). \quad (\text{I.52})$$

Strikingly, the mapped zero-range process  $\omega(0) := \Pi(\eta(0))$  is *not* in its stationary state even though  $\eta(0)$  is, because of the degenerate way in which the origin's cluster is built. However the difference between  $\omega(0)$  and an stationary zero-range process only amounts to an a.s. finite number of particles at the origin. By attractiveness, those discrepancies do not impact the large scale behavior of the process [EZ24, Proposition 3.1], so that we can consider that the mapped zero-range process is in its stationary state  $\mu_a$ , where  $a = a(\rho)$  is the active density defined in (I.26) and  $\mu_a$  the FZRP's equilibrium distribution (I.15). Under this product measure, the last term in (I.52) can be sharply estimated by a large deviations

estimate. The main estimate is therefore that of the maximal variance of the current, and we prove in [EZ24, Lemma 3.2] that

$$\mathbb{E}_a \left( \sup_{0 \leq t \leq T} \{J_{-1,0}^{\text{ZR}}(t) - \mathbb{E}_a(J_{-1,0}^{\text{ZR}}(t))\}^2 \right) \leq CN^{3/2}(\log N)^3, \quad (\text{I.53})$$

where  $\mathbb{E}_a$  represents the expectation w.r.t.  $\mu_a$ . With this estimate, and thanks to (I.52),  $X_y(t)$  can be replaced by its expected value, so that we can show that

$$\sup_{0 \leq t \leq T} \left| \mathcal{Y}_t^N(H) - \mathcal{Z}_t^N(H_\rho) \right| \xrightarrow[N \rightarrow \infty]{} 0 \quad (\text{I.54})$$

in probability under  $\mathbb{P}_{\pi_\rho}$ . Here,  $H_\rho(v) = (1 - \rho)H(v/(1 - \rho))$  is the test function distorted by the mapping, and  $\mathcal{Z}_t^N$  is the zero-range process's fluctuation field,

$$\mathcal{Z}_t^N(H) := \frac{1}{\sqrt{N}} \sum_{y \in \mathbb{Z}} (\omega_y(t) - 1 - a) H \left( \frac{y}{N} - tv'N^{\gamma-1} \right),$$

where  $v'$  is the average velocity of a particle in the stationary zero-range process  $\omega \sim \mu_a$ . Thanks to (I.54), we only need to use the results [40, 38] for the FZRP to conclude the proof of Theorems 7.2 and 7.3.

In [EZ24], we further derive directly the equilibrium fluctuation process in the symmetric case  $\mathfrak{s} = 1$ ,  $\gamma = -\infty$ . This alternative proof does not rely on the mapping with the zero-range process, and instead roughly follows the classical strategy laid out e.g. in [48, Chapter 11] which is based on the Boltzmann-Gibbs principle. To obtain the latter for the FEP, we proved [EZ24, Proposition 5.5] a new equivalence of ensemble bound, which was much sharper than the one previously obtained in [BESS20].

## Conclusion and perspectives

Kinetically constrained lattice gases can roughly be split into two categories, *cooperative* and *non-cooperative* models [14]. In non-cooperative models such as the Kob-Andersen model [50], or the one considered in [41], *mobile clusters* allow to locally mix the configuration, therefore symmetric non-cooperative models roughly behave diffusively.

For this reason, in order to understand the behavior of non-cooperative models, it is crucial to understand the dynamical behavior of mobile clusters. For a model like the one considered in [41] (GLT), for example, mobile clusters in the vacuum roughly perform random walks. In the presence of other particles, however, the picture becomes much less clear, as the clusters interact among themselves and with isolated particles to form new mobile clusters. Controlling the spread of these mobile clusters, is, in fact, a key point in understanding the behavior of the GLT model in the presence of an empty region [11], as well as to be able to understand the hydrodynamic behavior of the non-gradient version of the model. Although we put the emphasis on the model studied in [41] because it is a particularly simple and rich example of non-cooperative lattice gas, the question of understanding the behavior and spread of random clusters is of interest for the class of non-cooperative models as a whole.

For cooperative models like the FEP, whose macroscopic behavior was thoroughly studied in the articles presented in this section, we observe a phase-separated behavior depending

on whether the kinetic constraint is typically satisfied or not at the considered density. The FEP is a very interesting prototype of cooperative model, because despite its strongly degenerate dynamics, its stationary states are still explicit, and its various mapping features allow to derive in great detail its macroscopic behavior. The FEP has attracted a lot of attention in recent years, both from the physics [8, 32] and mathematics [36, 35, 7] communities, however many open questions remain.

In [EM24], we describe in some detail the way the FEP reaches its ergodic or frozen components through a cutoff window, which was then used in [58] to derive the FEP’s mixing time on the ring in the symmetric setting. The SSEP with traps introduced in [EM24] to characterize the FEP’s transience time is a very interesting model in its own right, and raises a number of natural questions. First, although our estimates give a clear picture of its worst transience time, they do not identify which critical configuration realizes it. We conjecture that the configuration with a single deep trap should be the worst from a transience time perspective, but have not managed to prove it so far. Still, the SSEP with traps being attractive, we expect that some well-designed coupling arguments might yield this conclusion. One might also use its deep mapping features, in particular the mapping to the FEP or the FZR, to prove this. Identifying the worst configuration from a transience standpoint might also open the way to a more precise characterization of the transient behavior for the SWT. In the spirit of [51], where the cutoff profile for the SSEP’s mixing time is fully characterized in a diffusive time window around the cutoff time, we hope to characterize in more details the way the transient component is left by the FEP.

Another fundamental question is the effect of the underlying jump rates on both the FEP and the SWT’s transience and mixing time. It is not clear as of now if a cutoff remains in force for the transience time in the asymmetric case, for example. A specific question that deserves some consideration is that of the relaxation from the FEP to the SSEP: instead of imposing a hard constraint on “inactive” particles, one can consider a FEP with temperature, where the higher the temperature, the higher the rate for an inactive particle’s jump. Because of our Markovian description of the FEP’s equilibrium state, we should be able to explicitly build the stationary states for such a model as a ponderation of Markovian and independent transitions. Deriving those equilibrium states would then allow to derive the macroscopic behavior of the FEP with temperature in a fairly general setting. We expect that for fixed (positive) temperature, its hydrodynamic limit should then be easier than that of the FEP to derive, because of its single microscopic phase. For temperatures decaying with  $N$ , however, the picture is less clear and technical challenges may arise.

We are also interested in the behavior of similar kinetic constraints in higher dimensions. Two natural options, represented in Figure I.6, are available to define a two-dimensional FEP, depending on whether a neighboring particle only allows to jump in the opposite direction to the particle (referred to as  $FEP_2$ ) or whether a neighboring particle allows to jump on any neighboring empty site ( $CLG_2$ , studied in [25]). Simulations suggest that the behavior of these two-dimensional models is much richer than that of the FEP in one dimension, and that several phase transitions exist as the density increases, as represented in Figure I.7. The  $CLG_2$ ’s behavior at criticality was numerically studied in [25]. Unlike the FEP, the SWT can straightforwardly be defined on more general graphs than  $\mathbb{Z}$ , and we also hope to be able to characterize its transience and mixing regimes on different lattices, which may be done by comparing with analogous known results for the SSEP in contact with reservoirs [66].

Mathematically speaking, however, because we lose the mappings and the explicit stationary states that are specific features of dimension 1, two dimensional FEPs are very dif-

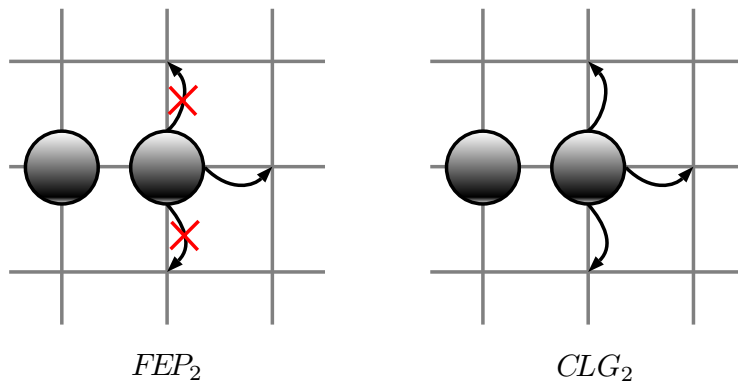


*Figure I.6*

difficult to study, and answering even basic questions require significant effort. For example, understanding the timescales over which the FEP freezes at low density is a delicate question. To answer it, a first step would be to understand the way a single dense particle cluster, in a large empty box, spreads out. This could open the way to use multi-scale analysis in the spirit of [47, 67], to show that starting from an arbitrarily low density product measure, the system eventually freezes, which although intuitively clear, is by no means easy to show. It is not obvious either that at high density (red region in Figure I.7), there is always only one ergodic component.

Overall, cooperative kinetically constrained lattice gases are still poorly understood, and the FEP remains one of the constraints on which the most is known. A much more ambitious goal is to try and categorize kinetically constrained lattice gases in broad categories determining their macroscopic behavior, in the same spirit of what was achieved in recent years for Glauber-type Kinetically Constrained Spin Models (KCSM) (see [56] and references therein).

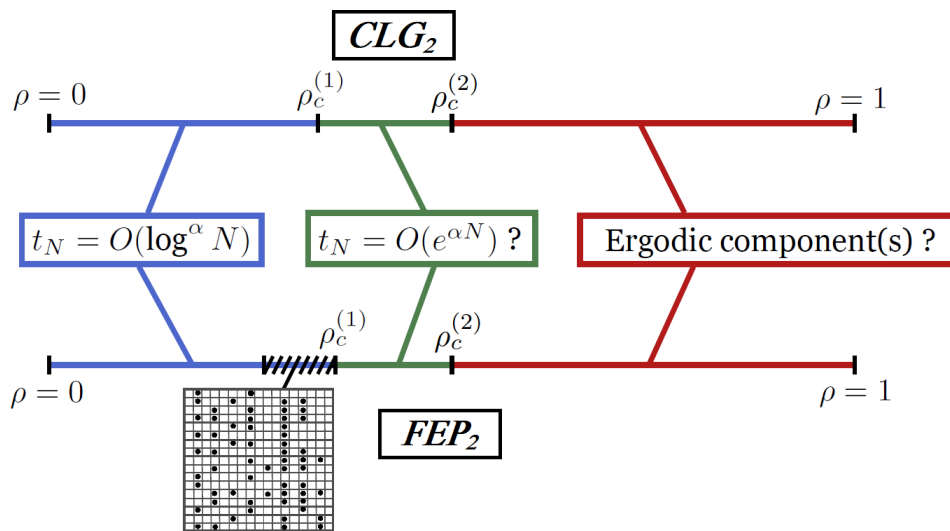


**Figure I.7:** A tentative phase diagram for the two dimensional counterparts to the FEP. In the blue region (low density), we expect that the system quickly freezes. In the red (high density) region, both models should exhibit roughly diffusive hydrodynamic behavior. In the green region, it seems the system eventually freezes, but over timescales that are much larger than the diffusive one, and therefore we expect that in the green region, starting from a Bernoulli product measure, a hydrodynamic limit holds. In the black hatched region for the  $FEP_2$ , particles seem to organize in a 1-D like pattern, where every other row or column is completely empty, so that particles remain active but only inside their row/column. It is not clear if the latter persists at high system sizes or is a finite-size feature of the  $FEP_2$ .

# Chapter II

---

## MACROSCOPIC BEHAVIOR OF BOUNDARY-DRIVEN LATTICE GASES

### Contents

---

<b>8</b>	<b>Hydrostat. and hydrodyn. limit for non-rev. boundary dynamics</b> . . . . .	<b>64</b>
8.1	Hydrostatics for a linear boundary dynamics . . . . .	65
8.2	sketch of the proof of Theorems 8.1 . . . . .	66
8.3	Hydrodynamic limit . . . . .	69
8.4	Small perturbation of equilibrium reservoirs . . . . .	71
8.5	Stronger boundary dynamics . . . . .	72
8.6	Weaker boundary dynamics . . . . .	73
<b>9</b>	<b>Static large deviations for SSEP with weak boundary interactions</b> . . . . .	<b>75</b>
9.1	Static large deviations functional for the non-equilibrium SSEP . .	75
9.2	Dynamical large deviations and weakly asymmetric dynamics . . .	76
9.3	DLS equation and static characterization . . . . .	77
9.4	Sketch of the proof of Theorem 9.1 . . . . .	78
<b>10</b>	<b>Destruction at the origin for the asymmetric ZRP</b> . . . . .	<b>79</b>
10.1	Asymmetric zero-range process with destruction at the origin . . .	80
10.2	Stationary states . . . . .	80
10.3	Hydrodynamic limit . . . . .	81
<b>11</b>	<b>Hydrodynamic behavior for the boundary-driven FEP</b> . . . . .	<b>83</b>
11.1	Kinetically constrained reservoirs and dynamics . . . . .	83
11.2	Hydrodynamic limit for weak and strong reservoir interactions . .	84
	<b>Conclusion and perspectives</b> . . . . .	<b>85</b>

---

In this chapter, I present results obtained on the macroscopic behavior of interacting lattice gases when particles can be created and deleted at the system's boundaries. Boundary-driven lattice gases have been under deep scrutiny in recent years, in parts because they provide simple examples of non-equilibrium systems, for which fluctuations and large deviations regimes cannot be described solely with the system's free energy, and non-equilibrium features need to be taken into account.

As laid out in the introduction, we consider throughout most of this chapter boundary-driven exclusion processes on  $\Lambda_N := \{1, \dots, N\}$ , characterized by their Markov generator

$$\mathcal{L}_N = N^\theta (\mathcal{L}_{\text{left}} + \mathcal{L}_{\text{right}}) + N^2 \mathcal{L}_{\text{bulk}}, \quad (\text{II.1})$$

where the SSEP's *bulk dynamics's* generator is simply given by

$$\mathcal{L}_{\text{bulk}} f(\eta) := \sum_{x=1}^{N-1} \{f(\eta^{x,x+1}) - f(\eta)\}. \quad (\text{II.2})$$

Let  $\eta^x$  denote the configuration where site  $x$  has been flipped (see (37)) and let  $p$  be a fixed integer. The *boundary dynamics* affect the boundary sets

$$\Lambda_{\text{left}} := \{1, \dots, p\} \quad \Lambda_{\text{right}} := \{N+1-p, \dots, N\} \quad (\text{II.3})$$

and is driven by the generators

$$\mathcal{L}_{\text{left}} f(\eta) := \sum_{x \in \Lambda_{\text{left}}} \gamma_x(\eta) \{f(\eta^x) - f(\eta)\} \quad \text{and} \quad \mathcal{L}_{\text{right}} f(\eta) := \sum_{x \in \Lambda_{\text{right}}} \gamma_x(\eta) \{f(\eta^x) - f(\eta)\}. \quad (\text{II.4})$$

Note that we ignore the dependency in  $N$  in our notation for  $\Lambda_{\text{right}}$  since it is just the rightmost box of size  $p$  in the system. In what follows, we assume that for  $x \in \Lambda_{\text{left}}$  (resp.  $x \in \Lambda_{\text{right}}$ ) the boundary rates  $\gamma_x(\eta)$  only depend on the configuration through  $\eta_{\Lambda_{\text{left}}}$  (resp.  $\eta_{\Lambda_{\text{right}}}$ ), meaning that the creation/annihilation rate at any site in the boundary sets only depends on the configuration in the same boundary set. A typical case is that of equilibrium reservoirs with density  $\alpha$  and  $\beta$  at each extremity, which correspond to the case  $p = 1$ , and the boundary rates are given by

$$\gamma_1(\eta) := \alpha(1 - \eta_1) + (1 - \alpha)\eta_1, \quad \gamma_N(\eta) = \beta(1 - \eta_N) + (1 - \beta)\eta_N \quad (\text{II.5})$$

as in (39).

At the macroscopic level, for  $\theta = 2$  (*strong* boundary interactions) we would expect fairly generally that boundary dynamics like (II.4) would impose on the hydrodynamic limit Dirichlet boundary conditions whose values depends on the boundary rates  $\gamma_x$  and in particular on the boundary dynamics equilibrium states. This is not always the case, however, and in the presence of boundary rates that create strong local correlations, at the hydrodynamic level, the boundary effect at the macroscopic level can remain random. We start by presenting the results we obtained on strong non-reversible boundary dynamics where Dirichlet boundary conditions are indeed enforced at the hydrostatic and hydrodynamic limit.

## 8 Hydrostatic and hydrodynamic limit for non-reversible boundary dynamics

## 8.1 Hydrostatics for a linear boundary dynamics

From the hydrodynamic limit perspective, the SSEP connected at each end to a reservoir of a given density with rates (II.5) is not very challenging : these reservoir dynamics also admit Bernoulli product measures as stationary states, so that entropy techniques can be applied at each boundary to derive the hydrodynamic limit, in the form of the heat equation with Dirichlet $(\alpha, \beta)$  boundary conditions. However, connecting additionally, for example, site  $x = 2$  to a reservoir with different density  $\alpha' \neq \alpha$ , entropy tools start to fail, because no common local product measure agrees with the dynamics at the boundary sites  $x = 1$  and  $x = 2$ , so that the left boundary would create entropy at a very fast rate w.r.t. any product measure. This emphasizes the need for different tools to approach boundary-driven models. The first boundary dynamics considered in [ELX18] is a generalization of the previous example, in which at each boundary set, three boundary mechanisms can coexist. More precisely, we consider for any  $x \in \Lambda_{\text{left}} \cup \Lambda_{\text{right}}$  non-negative rates  $r_x$ , and densities  $\alpha_x \in [0, 1]$  and for  $y$  in the same boundary set as  $x$  (either  $\Lambda_{\text{left}}$  or  $\Lambda_{\text{right}}$ ), two families of non-negative rates  $c_{x,y}, a_{x,y}$ . The left boundary dynamics is then defined, for  $x \in \Lambda_{\text{left}}$  for example, by the following.

- Site  $x$  is in contact at rate  $r_x$  with an equilibrium reservoir with density  $\alpha_x$ .
- Site  $x$  *copies* the value of site  $y$  at rate  $c_{x,y}$ : it becomes occupied if  $y$  is occupied, and empty otherwise.
- Site  $x$  *anti-copies* (becomes the opposite of) site  $y$  at rate  $a_{x,y}$ : it becomes occupied if  $y$  is empty, and empty otherwise.

It is not hard to check that these mechanisms correspond to the choice of boundary jump rates

$$\gamma_x := r_x \kappa_{\alpha_x}(\eta_x) + \sum_{y \in \Lambda_{\text{left}}} c_{x,y} \kappa_{\eta_y}(\eta_x) + a_{x,y} \kappa_{1-\eta_y}(\eta_x) \quad \text{for } x \in \Lambda_{\text{left}} \quad (\text{II.6})$$

in (II.4) and similarly for  $x \in \Lambda_{\text{right}}$ , where as in the introduction we defined

$$\kappa_r(\sigma) := r(1 - \sigma) + (1 - r)\sigma. \quad (\text{II.7})$$

We consider an analogous dynamics at the right boundary, so that these rates define a generator for the SSEP with strong boundary interactions,

$$\mathcal{L}_N = N^2(\mathcal{L}_{\text{left}} + \mathcal{L}_{\text{right}} + \mathcal{L}_{\text{bulk}}), \quad (\text{II.8})$$

and we denote by  $\bar{\mu}^N$  its (unique) stationary state. Note that obviously the scaling  $N^2$  above does not affect the stationary state, what matters is that we consider the boundary and bulk dynamics on the same timescales.

We now state the *hydrostatic limit*, showing that in the stationary state, a law of large numbers holds at the boundaries.

**Theorem 8.1 (Theorem 2.1 of [ELX18])** *Assume that*

$$\sum_{x \in \Lambda_{\text{left}}} r_x > 0 \quad \text{and} \quad \sum_{x \in \Lambda_{\text{right}}} r_x > 0. \quad (\text{II.9})$$

*Then, there exists two constants  $\alpha, \beta \in [0, 1]$ , such that the stationary state  $\bar{\mu}^N$  is associated in the sense of Definition 1.1 to the profile  $\bar{\rho}$  which is solution to the linear equation*

$$\begin{cases} \partial_u^2 \bar{\rho} = 0 \\ \bar{\rho}(0) = \alpha \quad \bar{\rho}(1) = \beta. \end{cases} \quad (\text{II.10})$$

Since the strategy will be similar for the other results obtained in [ELX18], [Eri18] and [EGN20b], we sketch the main arguments used to prove this result.

## 8.2 sketch of the proof of Theorems 8.1

As we have already mentioned, classical entropy-based techniques are not well suited to this boundary dynamics, whose stationary state is not a Bernoulli product measure. We instead exploit the SSEP's duality properties, which are preserved for our choice of boundary conditions. More precisely, define the stationary discrete density and two-points correlation fields, for  $x, y \in \Lambda_N$ , as

$$\bar{\rho}_x^N := \mathbb{E}_{\bar{\mu}^N}(\eta_x) \quad \text{and} \quad \bar{\varphi}_{x,y}^N := \mathbb{E}_{\bar{\mu}^N}(\eta_x \eta_y) - \bar{\rho}_x^N \bar{\rho}_y^N. \quad (\text{II.11})$$

Since  $\bar{\mu}^N$  is the stationary state for the process, for any  $x, y \in \Lambda_N$  we have

$$\mathbb{E}_{\bar{\mu}^N}(\mathcal{L}_N \eta_x) = \mathbb{E}_{\bar{\mu}^N}(\mathcal{L}_N \eta_x \eta_y) = 0. \quad (\text{II.12})$$

Applying this identity in the bulk yields after straightforward computations that for any  $x, y \notin \Lambda_{\text{left}}, \Lambda_{\text{right}}$  such that  $|y - x| \geq 2$

$$\Delta_N \bar{\rho}_x^N := \bar{\rho}_{x+1}^N + \bar{\rho}_{x-1}^N - 2\bar{\rho}_x^N = 0 \quad (\text{II.13})$$

and

$$\Delta_N^{(2)} \bar{\varphi}_{x,y}^N := \bar{\varphi}_{x+1,y}^N + \bar{\varphi}_{x-1,y}^N + \bar{\varphi}_{x,y+1}^N + \bar{\varphi}_{x,y-1}^N - 4\bar{\varphi}_{x,y}^N = 0.$$

In other words, both functions are harmonic in the bulk. When  $x$  and  $y$  are neighbors, however, the two-points correlation function picks up some contributions, and we have instead

$$\nabla_N \bar{\varphi}_{x,x+1}^N := \bar{\varphi}_{x-1,x}^N + \bar{\varphi}_{x,x+1}^N - 2\bar{\varphi}_{x,x+1}^N = (\bar{\rho}_{x+1}^N - \bar{\rho}_x^N)^2. \quad (\text{II.14})$$

The reason for our choice of boundary conditions is that they do not increase the degree of the equation, meaning that the boundary dynamics also yields a closed equation for the density field  $\bar{\rho}^N$ , as well as for the two-points correlation function  $\bar{\varphi}^N$ . This is a very simple instance of stochastic duality, a property that has been under deep scrutiny in recent years and has a number of applications [63, 16]. Because of this, we can write using (II.12), on two enlarged sets  $\widehat{\Lambda}_N$  and  $\widehat{\Lambda}_N^{(2)}$ , equipped with cemetery sets  $\Delta$  and  $\Delta_1, \Delta_2$ , that

$$\begin{cases} \mathcal{L}_1^\dagger \bar{\rho}^N = 0 & \text{on } \widehat{\Lambda}_N \\ \bar{\rho}^N = f & \text{on } \Delta. \end{cases} \quad \text{and} \quad \begin{cases} \mathcal{L}_2^\dagger \bar{\varphi}^N = m & \text{on } \widehat{\Lambda}_N^{(2)} \\ \bar{\varphi}^N = 0 & \text{on } \Delta_1 \\ \bar{\varphi}^N = g & \text{on } \Delta_2. \end{cases} \quad (\text{II.15})$$

In the second identity, the function  $m(x, y) := m_{x,y} := (\bar{\rho}_x^N - \bar{\rho}_y^N)^2 \mathbf{1}_{|x-y|=1}$  is the diagonal contribution identified in (II.14), and  $f, g$  are explicit functions on the boundaries depending on the reservoir densities  $(\alpha_x)$ . The cemetery states play the role of boundaries for the equations (II.15) above, but in order not to confuse with the boundary sets  $\Lambda_{\text{left}}$  and  $\Lambda_{\text{right}}$ , we call them cemetery states instead.

Crucially, these two dual operators  $\mathcal{L}_1^\dagger$  and  $\mathcal{L}_2^\dagger$  above can also be interpreted as Markov generators of random walks, as represented in Figure II.1 and II.2. We can therefore express  $\bar{\rho}^N$  and  $\bar{\varphi}^N$  with the help of two Markov processes  $X, Y$  on the enlarged sets  $\widehat{\Lambda}_N$  and  $\widehat{\Lambda}_N^{(2)}$ ,

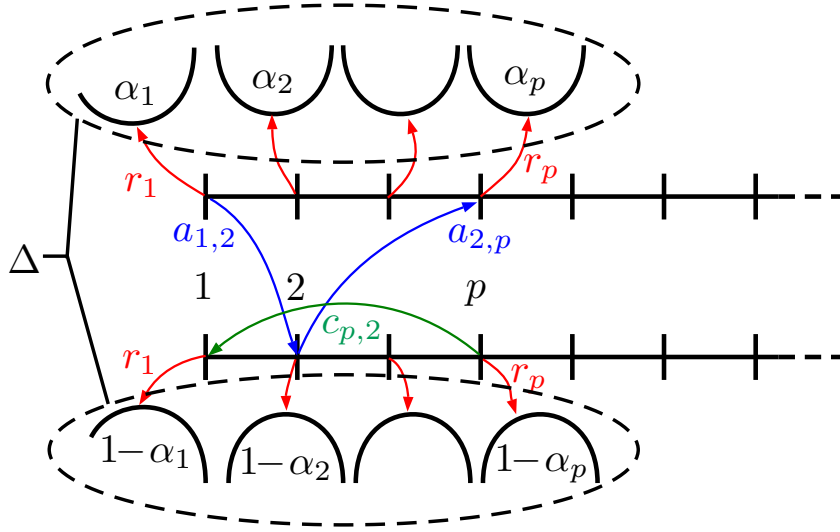


**Figure II. 1:** Representation of the enlarged set  $\hat{\Lambda}_N$  and the Markov process  $X$  in the neighborhood of the left boundary. The latter perform a random walk until a reservoir clock rings (red arrows) while it is on the corresponding boundary sites, at which point  $X$  reaches the cemetery set  $\Delta$  (dashed circles) and stays there. Two copies of the initial set  $\Lambda_N$  are made, and  $X$  passes from one to the other when an anticopy clock rings (blue arrows). Copy clocks (green arrows) makes  $X$  jump inside the boundary. On top of those clocks,  $X$  jump at rate 1 to any neighboring site (due to the SSEP dynamics).

stopped at the time  $\tau$  when they reach one of the cemetery states. More specifically, we obtain by Feynman-Kac's formula that for any  $x, y \in \Lambda_N$

$$\bar{\rho}_x^N = \mathbb{E}_x(f(X_\tau)) \quad \text{and} \quad \bar{\varphi}_{x,y}^N = \mathbb{E}_{x,y} \left( g(Y_\tau) \mathbf{1}_{\{Y_\tau \in \Delta_2\}} + \int_0^\tau m(Y_s) ds \right) \quad (\text{II.16})$$

where  $\mathbb{E}_x$  and  $\mathbb{E}_{x,y}$  represent the expectation w.r.t. the distributions of  $X, Y$  resp. started from  $x$  and  $(x, y)$ . Note that thanks to (II.13),  $\bar{\rho}^N$  is affine, and therefore the function  $m$  is of order  $1/N^2$

We now give a heuristic interpretation of the link between the fields  $\bar{\rho}^N$  and  $\bar{\varphi}^N$ . Recall that  $\bar{\rho}_x^N$  represents the probability that site  $x$  is occupied in the stationary state. To compute it, we consider a process in the stationary state, and we tag site  $x$ , whose value needs to be determined. Then, we explore the past of the process, by looking at all the Poisson clocks that have affected the tagged site; if a clock has rung between site  $x$  and site  $x+1$ , this means that the value we are looking for has moved to  $x+1$ , so that the tagged site moves as well. This process carries on, through SSEP jumps, copies and anticopies, until it reaches one of the reservoirs. Since the action of the reservoirs replace the site by a Bernoulli( $\alpha$ ), at that point the value of the tagged site is determined. The trajectory of the tagged site is exactly the Markov process  $X$ , and the final value is given by the function  $f$  in II.15.

The same strategy work for the two-points correlation field  $\bar{\varphi}^N$ , except that in this case we have a pair of tagged sites, and we can assume by symmetry that  $x < y$ . As for the density field, each of those tagged sites performs a random walk, so that we can see the corresponding dual process as a random walk on the triangle  $\{(x, y), x < y\}$ . In this case, if one of the tagged sites jumps to a reservoir, correlations are broken because the Bernoulli( $\alpha$ ) variable is centered and independent from the rest of the process, hence the boundary value

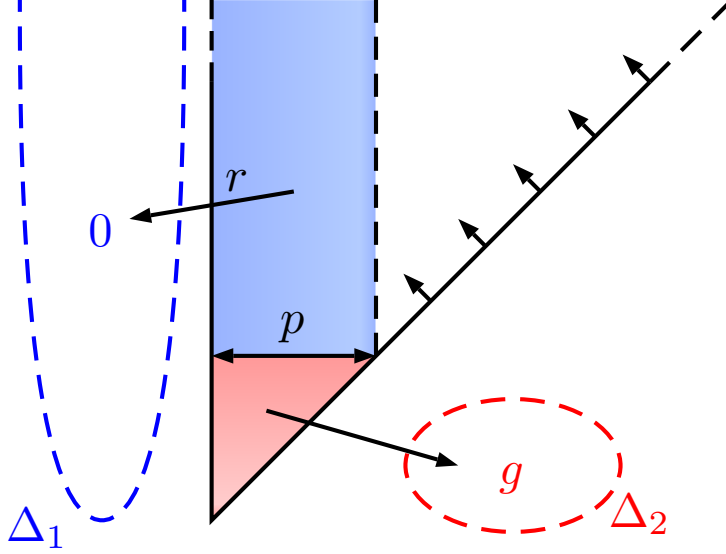


**Figure II.2:** A representation of the enlarged set  $\widehat{\Lambda}_N^{(2)}$  and the Markov process  $Y$  close to the left boundary. In the blue region, the  $x$  coordinate is in the left boundary set, and the other coordinate  $y$  is not, so that  $Y$  can jump at one of the rates  $r$  to the cemetery state. In the red region, the boundary function  $g$ 's value is not zero, but the red region is reached with very small probability for most values of  $Y_0 = (x, y)$ , so that the contribution of the red boundary to the second identity of (II.16) is small. Along the diagonal, we have  $(x, y) = (x, x + 1)$ , and  $Y$  can only be reflected.

0 at the cemetery set  $\Delta_1$ . As represented in Figure II.2, the second boundary set  $\Delta_2$  is in the corners of the triangle, and is reached with small probability. However, unlike for the density field, we have to estimate the diagonal contribution in (II.16) of the function  $m$ , which is proportional to the amount of time the two tagged sites have spent in neighboring sites before a cemetery state is reached. But since the system is of size  $N$ , this time is of order  $1/N$  and this contribution is negligible.

We now have all the tools to give the important ingredients of the hydrostatic limit given in Theorem 8.1. We will give the proof in some details, because the same type of arguments will be used to derive the hydrodynamic limit, and to treat the case of other boundary conditions. We want to show that for any test function  $H$ ,

$$\frac{1}{N} \sum_{x \in \Lambda_N} \eta_x H(x/N) - \int \bar{\rho}(u) H(u) du$$

vanishes in  $\bar{\mu}^N$ -probability. Adding and subtracting  $\frac{1}{N} \sum_{x \in \Lambda_N} \bar{\rho}_x^N H(x/N)$  in the difference above, one easily checks that the hydrostatic limit follows from two ingredients:

1. Showing that there exists  $\alpha, \beta$  in  $[0, 1]$  such that the discrete density field  $\bar{\rho}_x^N$  converges weakly (integrated against test functions) to the solution  $\bar{\rho}$  of (II.10).
2. showing that the correlation field  $\bar{\varphi}_{x,y}^N$  vanishes in  $L^1(\Lambda_N \times \Lambda_N)$

For the first point, according to (II.13)  $\bar{\rho}_x^N$  is affine in the bulk. In particular, we only need to show that the sequences  $p_N := \bar{\rho}_p^N$  and  $q_N := \bar{\rho}_{N+1-p}^N$  respectively converge to constants  $\alpha$  and  $\beta$  as  $N \rightarrow \infty$ . This is not too hard, thanks to the dual representation of those two

quantities given by the Feynman-Kac Formula (II.16): we start the process  $X$  at site  $p$  and wait for it to reach a cemetery state, at which point taking the expectation gives the value of  $\bar{\rho}_p^N$ . But the only way this quantity depends on the system size  $N$  is if the process  $X$  has reached the other boundary  $\Lambda_{\text{right}}$  before hitting a cemetery state. By Assumption (II.9), at each visit at one of the boundaries,  $X$  has a positive probability of reaching a cemetery state. Starting from site  $p$ , the process  $X$  therefore performs a geometric number of excursions away from the boundary (in the bulk) before time  $\tau$ , and since such an excursion has a probability  $O(1/N)$  of reaching the other boundary, we conclude that the influence of the system size is small, and that the limit  $\alpha$  we are looking for is simply

$$\alpha = \mathbb{E}_p(f(\tilde{X}_\tau)) \quad \text{and} \quad \beta = \mathbb{E}_{N+1-p}(f(\tilde{X}_\tau)) \quad (\text{II.17})$$

where  $\tilde{X}$  is the process  $X$  with all jumps to the bulk (i.e. to site  $p+1$  or  $N-p$ ) suppressed. This proves point 1. above.

For the second point, we consider a typical pair  $(x, y)$  at distance  $\delta N$  from the triangle's boundary (which is OK since we only need to show that  $\bar{\varphi}^N$  vanishes in  $L^1$ ). Once again, any visit to the boundary of one of the coordinates has a positive probability of leading to the cemetery state and killing the correlation function (except at boundary  $\delta_2$  which is only reached with small probability). The first term in the correlation identity in (II.16) therefore vanishes. To estimate the second term, since  $Y$  roughly behaves as a symmetric random walk reflected at the diagonal, it is not hard to check that  $\tau$  is w.h.p. of order  $O(N^2)$ , and therefore that the time spent at the diagonal before  $\tau$  is of order  $N$ . Furthermore, as we already pointed out,  $\bar{\rho}^N$  is affine, so that the contribution  $m$  is of order  $1/N^2$ . The last term in (II.16) is finally of order  $O(1/N)$ , which proves that the two points correlation field vanishes in  $L^1(\Lambda_N \times \Lambda_N)$ . Those two ingredients prove the hydrostatic limit.

### 8.3 Hydrodynamic limit

Building on the same techniques as in the hydrostatic limit allows to derive the hydrodynamic limit. We consider here a process  $\eta(\cdot)$  driven by the generator  $\mathcal{L}_N$  defined in (II.28) and started from an initial product distribution  $\mu^N$  fitting an initial smooth profile  $\rho_0 : [0, 1] \rightarrow [0, 1]$ . As before, the distribution of  $\{\eta(t), t \geq 0\}$  and the corresponding expectation are denoted by  $\mathbb{P}_{\mu^N}$  and  $\mathbb{E}_{\mu^N}$ , and we denote by  $\mu_t^N$  the process's distribution at time  $t$ .

**Theorem 8.2 (Hydrodynamic limit, Theorem 2.1 of [Eri18])** *Under the same assumption as in Theorem 8.1, the hydrodynamic limit of  $\{\eta(t), t \geq 0\}$  is the unique weak solution to the linear equation*

$$\begin{cases} \partial_t \rho = \partial_u^2 \rho \\ \rho(t, 0) = \alpha \quad \rho(t, 1) = \beta \\ \rho(0, \cdot) = \rho_0, \end{cases} \quad \text{for } t > 0 \quad (\text{II.18})$$

where  $\alpha$  and  $\beta$  are the same as in the hydrostatic limit and given by (II.17).

Let us now outline the proof for this results, that follows a similar strategy as the hydrostatic limit. This time, the density and correlation fields are time-dependent, and defined as

$$\rho_x^N(t) := \mathbb{E}_{\mu^N}(\eta_x(t)) \quad \text{and} \quad \varphi_{x,y}^N(t) := \mathbb{E}_{\mu^N}(\eta_x(t)\eta_y(t)) - \rho_x^N(t)\rho_y^N(t). \quad (\text{II.19})$$

Note that since the generator is accelerated by a factor  $N^2$ , time  $t$  here is a macroscopic quantity. As in the hydrostatic case, to prove the hydrodynamic limit, it is enough to show that for any time  $t$ , the discrete density field  $\rho^N(t)$  weakly converges as  $N \rightarrow \infty$  to the unique weak solution  $\rho(t, \cdot)$  to (II.29), whereas the correlation field  $\varphi^N(t)$  vanishes in  $L^1(\Lambda_N \times \Lambda_N)$  for any  $t > 0$ .

Dynkin's formula yields analogous identities to (II.15) on the same enlarged sets  $\widehat{\Lambda}_N$  and  $\widehat{\Lambda}_N^{(2)}$ , namely

$$\left\{ \begin{array}{ll} \partial_t \rho^N = N^2 \mathcal{L}_1^\dagger \rho^N & \text{on } \widehat{\Lambda}_N \\ \rho^N(t) = f & \text{on } \Delta \\ \rho^N(0) = \rho_0(\cdot/N) \end{array} \right. \quad \text{and} \quad \left\{ \begin{array}{ll} \partial_t \varphi^N = N^2 \mathcal{L}_2^\dagger \varphi^N - m_t & \text{on } \widehat{\Lambda}_N^{(2)} \\ \varphi^N(t) = 0 & \text{on } \Delta_1 \\ \varphi^N(t) = g_t & \text{on } \Delta_2 \\ \varphi^N(0) = 0. \end{array} \right. \quad (\text{II.20})$$

Note that the last boundary conditions comes from the fact that we started from a product distribution, with no correlations. The function  $m(t)$  can be defined, as in the stationary case, as

$$m_t(x, y) := (\rho_x^N(t) - \rho_y^N(t))^2 \mathbf{1}_{\{|x-y|=1\}}. \quad (\text{II.21})$$

In the time-dependent case, the initial time boundary must be taken into account when exploring the past of the process, so that the processes  $X$  and  $Y$  are now taken backwards in time, and we can rewrite (II.16) as

$$\rho_x^N(t) = \mathbb{E}_x \left( f(X_\tau) \mathbf{1}_{\{\tau \leq t\}} + \rho_0(X_t/N) \mathbf{1}_{\{\tau > t\}} \right) \quad (\text{II.22})$$

$$\varphi_{x,y}^N = \mathbb{E}_{x,y} \left( g_{t-\tau}(Y_\tau) \mathbf{1}_{\{Y_\tau \in \Delta_2, \tau \leq t\}} + \int_0^{\tau \wedge t} m_{t-\tau}(Y_s) ds \right), \quad (\text{II.23})$$

since the initial correlations vanish by assumption.

The strategy to derive the hydrodynamic limit then follows the same steps as the stationary case. First, we prove [Eri18, Proposition 3.1] that for any positive  $t$ ,

$$\lim_{N \rightarrow \infty} \rho_p^N(t) = \alpha, \quad \text{and} \quad \rho_{N+1-p}^N(t) = \beta, \quad (\text{II.24})$$

which yields that  $\rho^N$  given by (II.20) weakly converges as  $N \rightarrow \infty$  to the unique weak solution to (II.29). Second, that the correlation field vanishes in  $L^1$ . The first claim is proved using (II.22), for any macroscopic time  $t$ , by starting the dual process  $X$  at site  $p$ , and letting it performs excursions in the bulk until it reaches a cemetery state. Those excursions last on average a macroscopic time of order  $O(1/N)$  and the number of such excursions is distributed geometrically, so that w.h.p.  $\tau \leq t$  and the time boundary can be ignored for  $t > 0$ , thus recovering the boundary condition (II.17).

Estimating the correlations is more delicate because the function  $m$  in (II.21) is in general not of order  $O(1/N^2)$ . Indeed, the heat equation enforces Dirichlet Boundary condition instantaneously, so that if the initial profile  $\rho_0$  does not verify the same initial boundary conditions, the hydrodynamic limit  $\rho$  will exhibit very sharp gradients as  $t \rightarrow 0$  and  $u \rightarrow 0$  and 1. The same goes for the discrete derivative appearing in (II.21), so that as  $t \rightarrow 0$ ,  $m_t$  can be of order 1 rather than  $1/N^2$ . However, this is only an issue if the dual process  $Y$  hits the diagonal close to time  $t$ , which is unlikely, so that in general we have a sufficiently sharp bound on the gradients [Eri18, Corollary 3.6] to estimate the contribution of the function  $m_t$  and in turn obtain that the correlations vanish in  $L^1$  [Eri18, Proposition 4.1], which proves Theorem 8.2.

## 8.4 Small perturbation of equilibrium reservoirs

In the second general boundary dynamics we considered in [ELX18], the boundary dynamics did not depend too much on the boundary itself. For simplicity, we assume here that only the first and last sites can be flipped, meaning that  $\gamma_x = 0$  for  $x \neq 1, N$  in (II.4). For  $\sigma \in \{0, 1\}$ , define

$$\gamma_{\text{left}}^\sigma := \min_{\{0,1\}^{p-1}} \gamma_1(\sigma, \eta_2, \dots, \eta_p) \quad \text{and} \quad \gamma_{\text{right}}^\sigma := \min_{\{0,1\}^{p-1}} \gamma_N(\eta_{N+1-p}, \dots, \eta_{N-1}, \sigma) \quad (\text{II.25})$$

the minimal rate at which each boundary site is flipped when it is in a state  $\sigma$ . We then define for a boundary configuration  $\xi \in \{0, 1\}^{p-1}$ , we introduce

$$\lambda_{\text{left}}(\sigma, \xi) := \gamma_1(\sigma, \xi) - \gamma_{\text{left}}^\sigma \geq 0 \quad \text{and} \quad \lambda_{\text{right}}(\xi, \sigma) := \gamma_N(\xi, \sigma) - \gamma_{\text{right}}^\sigma \geq 0. \quad (\text{II.26})$$

By introducing these quantities, we can now interpret the boundary dynamics as follows. If the boundary site  $x = 1$  (resp.  $x = N$ ) is in a state  $\sigma$ , it is flipped to  $1 - \sigma$  at a constant rate  $\gamma_{\text{left}}^\sigma$  (resp.  $\gamma_{\text{right}}^\sigma$ ). On top of that, it is also flipped at an extra configuration-dependent rate  $\lambda_{\text{left}}(\sigma, \xi)$  if the boundary configuration is given by  $(\sigma, \xi)$ , and similarly at the other boundary. We can now state the hydrostatic limit for general boundary conditions, assuming that the boundary dynamics does not depend too much on the boundary state.

**Theorem 8.3 (Theorem 2.4 of [ELX18])** *We now assume that*

$$(p-1) \sum_{\eta \in \{0,1\}^p} \lambda_{\text{left}}(\eta) < \gamma_{\text{left}}^0 + \gamma_{\text{left}}^1 \quad \text{and} \quad (p-1) \sum_{\eta \in \{0,1\}^p} \lambda_{\text{right}}(\eta) < \gamma_{\text{right}}^0 + \gamma_{\text{right}}^1, \quad (\text{II.27})$$

*meaning that the configuration-dependent part of the flipping rates are small w.r.t. their constant counterparts. Then, there exists two constants  $\alpha, \beta \in [0, 1]$ , such that the stationary state  $\bar{\mu}^N$  is associated with the solution to the linear equation (II.10)*

We do not formally state the hydrodynamic limit, which would be Theorem 8.2's counterpart for this model. However, we emphasize that its hydrodynamic limit would only require incorporating straightforwardly elements of the proof of Theorem 8.3 into [Eri18]. We now briefly describe the proof of Theorem 8.3.

The basis for the proof is the same as the one presented in Section 8.2 for linear boundary conditions: the density profile is affine inside the bulk, so that to derive the hydrostatic limit it is enough to prove that  $\bar{\rho}_p^N$  and  $\bar{\rho}_{N+1-p}^N$  admit limits  $\alpha$  and  $\beta$  as  $N \rightarrow \infty$ . The main challenge in that respect is that the dual equations for  $\bar{\rho}^N$  and  $\bar{\varphi}^N$  are not closed because of the non-linear boundary condition. To try and see why this is the case, consider the dual process  $X$  which helped us derive the limiting density at the left boundary. The latter was interpreted as an exploration of the past of site  $p$ , which behaved as a random walk because of the linear boundary conditions, and was killed at the cemetery states. We make the following claim:

“The dynamics remains unchanged, if instead of flipping a site in state  $\sigma$  at constant rate  $\gamma_{\text{left}}^\sigma$ , we instead replace its content, regardless of what it previously was, at rate  $\gamma_{\text{left}}^0$  by an empty site, and at rate  $\gamma_{\text{left}}^1$  by a particle.” (C1)

This claim is trivial, because replacing an empty site by another empty site changes nothing to the dynamics, and removing a particle to place another particle in its place leaves the

system unchanged as well. The big upside of this new construction of the boundary dynamics comes through the graphical representation (see e.g. [39, Page 5]) with Poisson clocks of our Markov process. Fix for  $1 \leq x \leq N - 1$  rate 1 independent Poisson clocks  $\mathcal{N}_{x,x+1}$ . We can now choose at each boundary, and for  $\sigma \in \{0, 1\}$ ,  $\xi \in \{0, 1\}^p$ , a family of independent Poisson clocks  $\mathcal{N}_{\text{left}}^{\star,\sigma}, \mathcal{N}_{\text{left}}^\xi, \mathcal{N}_{\text{right}}^{\star,\sigma}, \mathcal{N}_{\text{right}}^\xi$ , with respective rates  $\gamma_{\text{left}}^\sigma, \lambda_{\text{left}}(\xi), \gamma_{\text{right}}^\sigma, \lambda_{\text{right}}(\xi)$ , and build the same process in the following way.

- When a clock  $\mathcal{N}_{x,x+1}$  rings, we exchange the content of sites  $x$  and  $x + 1$ .
- When a clock  $\mathcal{N}_{\text{left}}^{\star,\sigma}$  (resp.  $\mathcal{N}_{\text{right}}^{\star,\sigma}$ ), we replace the value of site  $x = 1$  (resp site  $x = N$ ) by  $\sigma$ .
- Finally, when a clock  $\mathcal{N}_{\text{right}}^\xi$  (resp.  $\mathcal{N}_{\text{left}}^\xi$ ) rings, we flip the value of site  $x = 1$  (resp site  $x = N$ ) if  $\eta_1, \dots, \eta_p = \xi$  (resp.  $\eta_{N+1-p}, \dots, \eta_N = \xi$ ).

It is not hard to check that this process follows our initial generator. Consider now the evolution of our dual process : we want to determine the value of an unknown site, and explore its past. it performs a symmetric random walk under the Poisson clocks  $\mathcal{N}_{x,x+1}$ , until it reaches one of the boundary sites and a boundary clock rings. Then, if the clock is one of the  $\mathcal{N}_{\text{left}}^{\star,\sigma}, \mathcal{N}_{\text{right}}^{\star,\sigma}$ , we know that at this point the site has taken the value  $\sigma$  and the exploration ends. If, instead, the clock is one of the  $\mathcal{N}_{\text{left}}^\xi, \mathcal{N}_{\text{right}}^\xi$ , in order to know whether something happened because of the clock, we need to know the state of all sites at the boundary at that moment. We therefore also tag all the  $p - 1$  other sites at the boundary, and keep on exploring all of their past with the same rules. The dual process is therefore a process that can branch or be killed at the boundary.

Assumption (II.27) ensures that this process is subcritical, so that with high probability the process dies after a finite number of branchings : on average, each time a boundary event occurs, the number of particles in the process decreases. In particular, since this process is roughly composed of random walks, if the process starts from the boundary, it will only explore w.h.p. a finite region (with size independent of  $N$ ) around the boundary, and not the rest of the system. As in the previous linear case, this shows that the branching process's exploration is not impacted by the size of the system and that  $\bar{\rho}_p^N$  and  $\bar{\rho}_{N+1-p}^N$  must converge as  $N \rightarrow \infty$ .

Regarding the correlations, the reasoning is roughly the same. Consider the correlations between sites  $x = p$  and  $y = \delta N$  (for a small  $\delta$ ) for example. The dual process starts with two tagged “particles”  $Y_t^1, Y_t^2$  at  $x$  and  $y$ , which perform random walks, branch out, and die as for the density. However, since  $Y_t^1$  is initially at the boundary, and  $Y_t^2$  has a macroscopic distance to travel before ever reaching it, w.h.p. the past of tagged site  $x$  is fully explored before it is ever influenced by the past of site  $y$ . This means that those two dual processes evolve close to independently, and therefore that for any positive  $\delta$ ,  $\bar{\varphi}_{p,\delta N} = o_N(1)$ . Letting then  $\delta \rightarrow 0$ , this shows that the boundary conditions in the second part of (II.15) vanish, and therefore that the static correlation field vanishes in  $L^1$  as wanted as  $N \rightarrow \infty$ , with the same estimate for the diagonal contribution  $m$ .

## 8.5 Stronger boundary dynamics

We now consider the case where the boundary dynamics is accelerated w.r.t. the bulk dynamics, meaning that the generator is given, for a sequence  $(\ell_N)_{N \in \mathbb{N}}$  going to  $\infty$  as  $N \rightarrow \infty$ , by

$$\mathcal{L}_N = \ell_N \mathcal{L}_{\text{left}} + \mathcal{L}_{\text{right}} + \mathcal{L}_{\text{bulk}}. \quad (\text{II.28})$$

We assume here for simplicity that

$$\mathcal{L}_{\text{right}}f = \{\beta(1 - \eta_N) + (1 - \beta)\eta_N\}(f(\eta^N) - f(\eta))$$

at the right boundary is given by a *non-accelerated* equilibrium reservoir dynamics with density  $\beta$ . We assume that the boundary generators are ergodic, meaning that  $\mathcal{L}_N$  has a unique stationary state. Note that since we will only state the hydrostatic limit, we did not accelerate the generator on a diffusive timescale, so that the  $N^2$  factor vanished. Because of the accelerated left boundary dynamics, the boundary relaxes very fast to equilibrium, and the hydrostatic limit holds in great generality.

**Theorem 8.4 (Theorem 2.9 of [ELX18])** *There exists a constant  $\alpha \in [0, 1]$ , such that the stationary state  $\bar{\mu}^N$  is associated with the solution to the linear equation (II.10)*

The proof of this result uses different tools than the duality approach of the previous results, and instead exploits the fast relaxation to equilibrium at the left boundary. We therefore consider the stationary state of the left boundary dynamics  $\mathcal{L}_{\text{left}}$  on its own, which is a distribution  $\nu$  on  $\{0, 1\}^p$ , and we define  $\alpha = \nu(\eta_p = 1)$ . Consider now the linear interpolation

$$f_x = \alpha + (\beta - \alpha)\frac{x - p}{N - p},$$

we approximate the stationary state  $\bar{\mu}$  of our process by

$$\nu_{N,p} := \nu \otimes \left[ \bigotimes_{x=p+1}^N \text{Bernoulli}(f_x) \right].$$

For any function  $g$  depending only on the boundary state  $\eta|_{\Lambda_{\text{left}}}$ ,  $g$  is only affected by the boundary dynamics and the stirring dynamics restricted to  $\{1, \dots, p+1\}$ , so that in particular we must have

$$\mathbb{E}_{\bar{\mu}}(\mathcal{L}_{\text{left}}g) = -\frac{1}{\ell_N}\mathbb{E}_{\bar{\mu}}(\mathcal{L}_{\text{bulk}}g) = O(1/\ell_N).$$

In particular, letting  $F_N$  be the boundary density between our two distributions,

$$F_N = \frac{d\bar{\mu}(\eta|_{\Lambda_{\text{left}}} = \cdot)}{d\nu},$$

we obtain after a short computation that

$$\|F_N - 1\|_{\infty} = O(1/\sqrt{\ell_N}).$$

This yields that the density  $\bar{\rho}_p^N$  at the left boundary does not depend too much on  $N$  and we obtain the wanted limit. The correlation field can be estimated exactly in the same way, thus proving the hydrostatic limit for accelerated boundary dynamics.

## 8.6 Weaker boundary dynamics

We now get back to our original definition (II.1) of the generator, and scale the boundary dynamics by a factor  $N^\theta$ , where the bulk dynamics is as before scaled diffusively in  $N^2$ . The duality tools were developed for strong boundary dynamics, meaning for  $\theta = 2$  (the boundary and bulk dynamics operate on the same timescales). Similar techniques were used for a specific set of non-linear boundary conditions, in the case of so called weak boundaries

( $\theta = 1$ ) in [20], where the cascading correlation field is carefully estimated by using dual branching processes. In subsequent work, we bridged the gap between these two regimes, and we use duality estimates for  $0 < \theta < 1$ , avoiding the delicate  $n$ -points correlation estimates necessary in [20]. The model we considered belongs to the class of perturbations of constant rates flipping described in Section 8.4, where sites  $x = 1$  and  $x = N$  are put in contact at rates  $r, r'$  with reservoirs with density  $\bar{\rho}$  and  $\bar{\rho}'$ , and sites  $x = 2, x = N$  can either copy sites 1 and  $N$  (at rates  $c, c'$ ), but also copy them *if they are occupied* at rates  $b, b'$ . The last mechanism breaks the linearity of the boundary conditions, resulting in cascading correlations at the boundary.

We consider for  $\theta < 2$  a SSEP  $\{\eta(t), t \geq 0\}$  with those boundary rates, and started from a product distribution fitting a profile  $\rho_0$ . We derive the following hydrodynamic limit for  $1 < \theta < 2$ , which holds under analogous assumptions to (II.27).

**Theorem 8.5 (Theorem 2.1 of [EGN20b])** *Assume that*

$$b < r \quad \text{and} \quad b' < r'$$

*the hydrodynamic limit of  $\{\eta(t), t \geq 0\}$  is the unique weak solution to the linear equation*

$$\begin{cases} \partial_t \rho = \partial_u^2 \rho \\ \rho(t, 0) = \alpha, \quad \rho(t, 1) = \beta \quad \text{for } t > 0 \\ \rho(0, \cdot) = \rho_0, \end{cases} \quad (\text{II.29})$$

*where  $\alpha$  and  $\beta$  are solution to*

$$r(\bar{\rho} - \alpha) + b\alpha(1 - \alpha) = 0 \quad \text{and} \quad r'(\bar{\rho}' - \beta) + b'\beta(1 - \beta) = 0. \quad (\text{II.30})$$

The proof of this result follows the same strategy as the one of Theorem 8.3. However, some refined duality estimates are required w.r.t. the latter, since the boundary dynamics, which was the one who broke correlations and allowed for explicit computation of the density, is now slower. We therefore need much sharper bounds, especially because our result encompasses all  $\theta$  going to 1, at which point a transition occurs and the boundary conditions are no longer of Dirichlet type, but rather of Robin type. Furthermore, we explore in much more details the behavior of the branching process at the boundary, and define with this branching process what we call a *determination tree*, which is stochastic labeled tree coupled with the process, whose distribution determines explicitly the boundary Dirichlet values (II.30) for weak boundary conditions [EGN20b, Lemma 5.4]. Although we did not state it in [EGN20b], the hydrostatic also holds for this model, since using our duality techniques, the hydrostatic limit is a simpler case of the hydrodynamic limit.

We then study the transition to Robin ( $\theta = 1$ ) and then Neumann ( $\theta > 1$ ) boundary conditions in the second part of our work, [EGN20a], in which a slightly more general model is considered. In these regimes, we prove both the hydrodynamic and hydrostatic limit.

**Theorem 8.6 (Hydrodynamic limit, Theorem 2.8 of [EGN20a])** *For  $\theta = 1$ , there exists two operators  $D_{\text{left}}, D_{\text{right}} : [0, 1] \rightarrow \mathbb{R}$  explicitly depending on the boundary rates, such that the hydrodynamic limit of  $\{\eta(t), t \geq 0\}$  is the unique weak solution to the linear equation with Robin boundary conditions*

$$\begin{cases} \partial_t \rho = \partial_u^2 \rho, \\ \partial_u \rho(t, 0) = D_{\text{left}}(\rho(t, 0)) \quad \text{for } t > 0, \\ \partial_u \rho(t, 1) = D_{\text{right}}(\rho(t, 1)) \quad \text{for } t > 0, \\ \rho(0, \cdot) = \rho_0. \end{cases} \quad (\text{II.31})$$

For  $\theta > 1$ , the same holds, but the boundary operators then vanish, meaning  $D_{left} = D_{right} = 0$ .

**Theorem 8.7 (Hydrostatic limit, Theorem 2.8 of [EGN20a])** *With the same notations as in Theorem (8.6), for  $\theta = 1$ , the stationary state  $\bar{\mu}$  of  $\{\eta(t), t \geq 0\}$  is associated with the linear profile*

$$\begin{cases} \partial_u^2 \rho = 0, \\ \partial_u \rho(0) = D_{left}(\rho(0)) \\ \partial_u \rho(1) = D_{right}(\rho(1)). \end{cases} \quad (\text{II.32})$$

For  $\theta < 1$ , there exists a unique constant  $m$  such that  $\bar{\mu}$  is associated with the constant profile  $\bar{\rho} \equiv m$ .

Because the boundary dynamics is very weak, to prove this result we can exploit once again entropy tools, because the entropy production at the boundaries is not strong enough to deeply perturb the SSEP's stationary states, whereas duality tools start to break down for very weak interactions with the reservoirs. For this reason, Theorem (8.6) follows from the same strategy as in [6], i.e. from replacement Lemmas, in the bulk and at the boundary, in the spirit of Lemma 1.2.

Using duality tools, the hydrostatic limit derived in [ELX18] is a simpler case of the hydrodynamic limit ([Eri18]), since it neglects the effect on the density and correlation field of the time boundary. With entropy techniques like the ones exploited in [EGN20a], however, this is in general not the case, and the hydrostatic limit can, on the contrary, require that the hydrodynamic limit be already established. This is the case here, and to establish Theorem 8.7, we exploit the long-time behavior of the hydrodynamic limit, where the hydrostatic profile arises, following the strategy developed in [54, 72].

## 9 Static large deviations for SSEP with weak boundary interactions

### 9.1 Static large deviations functional for the non-equilibrium SSEP

As clearly indicated by (II.15), even in the stationary state, the SSEP in contact with reservoirs at density  $\alpha$  and  $\beta$  exhibits, through the function  $m$ , non trivial correlations, which only disappear in the equilibrium case where  $\alpha = \beta$ , since in the latter, the dynamics is reversible w.r.t. *Bernoulli*( $\alpha$ ) product distributions. According to our previous work [ELX18, EGN20b], these correlations are small in the law of large numbers regime, so that the hydrostatic limit allows us to derive the stationary state's limiting profile (Theorems 8.1 and 8.7). At the level of large deviations, however, these correlations can no longer be neglected, and they have a deep impact on the SSEP's large deviations regime.

More precisely, consider in this section the SSEP in weak contact with equilibrium reservoirs with respective densities  $\alpha$  and  $\beta$ , with generator

$$\begin{aligned} \mathcal{L}_N f(\eta) := & N^\theta (\kappa_\alpha(\eta_1) \{f(\eta^1) - f(\eta)\} + \kappa_\alpha(\eta_1) \{f(\eta^N) - f(\eta)\}) \\ & + N^2 \sum_{x=1}^{N-1} \{f(\eta^{x,x+1}) - f(\eta)\}. \end{aligned} \quad (\text{II.33})$$

where the reservoir rates were defined in (II.7). Because of the different boundary densities, this model is maintained out-of-equilibrium by the constant flow of particles going from

the higher density reservoir to the lower density reservoir. For this reason, for any positive  $\theta$ , non-trivial correlations appear in the stationary state as soon as  $\alpha \neq \beta$ , meaning that although we are able to derive its macroscopic profile, the process's stationary state  $\bar{\mu}^\theta$  of  $\mathcal{L}_N$  is by not explicit, so that deriving for it a large deviations principle in the spirit of Theorem 1.4 is by no means trivial. To be more specific, we are interested in finding a functional  $S$  on the set of density profiles  $\gamma : [0, 1] \rightarrow [0, 1]$  such that the empirical measure  $\pi^N$  satisfies

$$\bar{\mu}(\pi^N \simeq \gamma du) \asymp \exp -NS[\gamma]. \quad (\text{II.34})$$

The identity above is to be taken in the large deviations sense, meaning that

$$\lim_{N \rightarrow \infty} \frac{1}{N} \log \bar{\mu}(\pi^N \simeq \gamma du) = -S[\gamma]$$

Since  $\bar{\mu}$  is non-explicit, one way to understand the static large deviations regime is to exploit the long-time convergence of the microscopic model to the stationary state. This is called the Onsager-Machlup principle, which roughly states the the *stationary* large deviations cost of creating a profile  $\gamma$ ,  $S[\gamma]$ , should be the minimal *dynamical* cost  $V[\gamma]$  of creating, over a long time  $T \rightarrow \infty$ , the same profile  $\gamma$  starting from the stationary profile  $\bar{\rho}$

$$V[\gamma] = \lim_{T \rightarrow \infty} \inf_{\rho} I_{[0,T]}[\rho], \quad (\text{II.35})$$

where  $\rho$  represent a time-dependent trajectory,  $I_{[0,T]}[\rho]$  represents the dynamical counterpart to  $S$  introduced in Theorem 1.4 and the infimum is taken over trajectories  $\rho$  satisfying  $\rho_0 = \bar{\rho}$ ,  $\rho_T = \gamma$ . Doing so, one has a reasonable strategy to characterize  $V$ , since the dynamical large deviations can in great generality be derived according to the Macroscopic Fluctuations Theory (MFT, [10]). However, It is not always clear that this *quasi-potential*  $V$  defined through (II.35) coincides up to a constant with the large deviations functional  $S$  associated with the stationary state, and has so far only be proved for Dirichlet boundary conditions, i.e. for strong boundary interactions, in [12].

## 9.2 Dynamical large deviations and weakly asymmetric dynamics

To understand the large deviations regime of the density profile for processes like the SSEP, rather than focusing on the density itself, one should rather focus on the particle current locally going through the system. Of course, with the exception of the boundary where particles can be created and deleted, the SSEP is conservative, so that regardless of the underlying stochasticity, at the macroscopic level the particle density and its current must be linked by the conservation relation

$$\partial_t \rho(t, u) = \partial_u j(t, u). \quad (\text{II.36})$$

For the SSEP at density  $\rho$ , one expects an average current  $J[\rho] = \nabla \rho$ . To produce a large deviations, the system creates a current that is far from its average, meaning at the microscopic level, at the edge  $(x, x + 1)$  that there has been an imbalance between the Poisson clocks for rightwards jumps  $\mathcal{N}_{x \rightarrow x+1}$  and that for the leftwards jumps  $\mathcal{N}_{x+1 \rightarrow x}$ . Particle jumps over the edge at a total rate  $(\eta_x - \eta_{x+1})^2$ , whose expectation under local equilibrium is given by  $2\rho_x(1 - \rho_x) + o_N(1)$ . In particular, assuming local equilibrium, the instantaneous current  $j_x^N$  over the edge  $(x, x + 1)$  has variance proportional to  $\sigma_x$ , and therefore its approximate distribution, by CLT for the local Poisson jump clocks

$$\mathbb{P}_N(j_x^N - J(\rho_x) \simeq \alpha) \asymp \exp \left( -\frac{\alpha^2}{\sigma(\rho_x)} \right), \quad (\text{II.37})$$

where we defined  $\sigma(r) = r(1-r)$ . In particular, since those currents rely on independent Poisson clocks, one finally obtains, at least formally, that the probability of observing a current  $j : [0, 1] \times [0, T]$ , and therefore the associated density field  $\rho$  defined by (II.36), is given by

$$\mathbb{P}_N(j) \asymp \exp(-NI_{[0,T]}[\rho]) := \exp\left(\frac{-N}{2} \int_0^T \int_{\mathbb{T}} \frac{(j - J(\rho))^2}{\sigma(\rho)} dudt\right).$$

Once this identity is established, one can wonder what a *typical* trajectory of the microscopic process creating a current large deviations  $j$  looks like. The answer to this question is obtained easily enough, and it is sufficient to submit the microscopic dynamics to a weak external field  $\partial_u H_t^{(j)}(t, u) = j(t, u) - J(\rho(t, u))$  proportional to the current deviation. In other words, assuming that sites  $x$  and  $x+1$  are exchanged at rate

$$1 - (\eta_{x+1} - \eta_x)\{H_t^{(j)}((x+1)/N) - H_t^{(j)}(x/N)\}. \quad (\text{II.38})$$

If  $j$  and  $\rho$  are smooth enough, the second term above is of order  $1/N$ , so that this new drifted process is a weakly asymmetric simple exclusion process, and this tilted weakly asymmetric dynamics defines the typical microscopic behavior of the SSEP in the presence of a large deviations producing a density/current profile  $(\rho, j)$ . Unfortunately, the conservation relation between current and density is not easily exploitable as is, and it can be useful to derive a self-contained definition for the large deviations functional only involving  $\rho$ . This can be done, but at the cost of a variational principle over the unknown weak field  $H$  that produces the large deviation, meaning that we can also define  $I$  as a function of the sole density as

$$I_{[0,T]}[\rho] = \sup_H J_{T,H}(\rho), \quad (\text{II.39})$$

where the supremum is taken over smooth functions  $H$ , and

$$J_{T,H}[\rho] := \langle \rho_T, H_T \rangle - \langle \rho_0, H_0 \rangle - \int_0^T dt \{ \langle \rho_t, \partial_t H_t \rangle + \langle \rho_t, \partial_u^2 H_t \rangle + \langle \sigma(\rho_t), (\partial_u H_t)^2 \rangle \} + \int_0^T dt B_t[\rho]. \quad (\text{II.40})$$

In this identity, the extra terms  $B_t[\rho] = B_t[\rho, \theta, \alpha, \beta]$  are boundary terms, and depend on the nature and scaling of the boundary dynamics.

### 9.3 DLS equation and static characterization

Recall that we are interested in estimating the quasi-potential  $V$ , meaning the dynamical cost of creating a profile  $\gamma$  starting from the stationary profile  $\bar{\rho}$  (see (II.35)). In this respect, inserting (II.39) into (II.35) yields a double variational principle, first over trajectories  $\rho$  linking  $\bar{\rho}$  and  $\gamma$ , first, and second on the weak field  $H$  that creates this deviation. Such variational principles are not easily exploitable, and it is therefore crucial to obtain other, more easily accessible formulations for the quasi-potential  $S$ . For strong boundary interactions ( $\theta = 1$  in (II.33)), Derrida et al. use in [23] the so-called *Matrix Ansatz* [21] to show that the quasi-potential  $S[\gamma] = S_{\text{bulk}}[\gamma]$  can be expressed as

$$S_{\text{bulk}}[\gamma] := \int_0^1 \gamma(u) \log \frac{\gamma(u)}{F(u)} + (1 - \gamma(u)) \log \frac{1 - \gamma(u)}{1 - F(u)} + \log \frac{F'}{\beta - \alpha} \quad (\text{II.41})$$

if  $\gamma(0) = \alpha$  and  $\gamma(1) = \beta$ , and  $\infty$  otherwise. The function  $F$  above does not have an explicit expression, but it is characterized as the  $\gamma$ -dependent solution of the non-linear so-called *DLS equation*

$$F'' = (\gamma - F) \frac{(F')^2}{F(1 - F)}. \quad (\text{II.42})$$

supplemented by the same Dirichlet boundary conditions as the density,  $F(0) = \alpha$  and  $F(1) = \beta$ .

In [BEL23], we tackle the case of the *weak boundary* regime  $\theta = 1$ , in which the hydrostatic and hydrodynamic limit are characterized by Robin boundary conditions

$$\partial_u \rho(0) = \rho(0) - \alpha, \quad \text{and} \quad \partial_u \rho(1) = \beta - \rho(1).$$

We rely on the characterization of the dynamical large deviations for the SSEP with weak boundary conditions derived in [28], and denote by  $I_{[0,T]}$  the corresponding large deviations functional given by (II.39). Not to burden further this paragraph, we do not explicitly describe the boundary terms  $B_t[\rho]$  in (II.40), they can be found in [BEL23, Equation (2.2)]. Our main result is the following, that expresses the quasi-potential depending on the solution to the DLS equation with Robin boundary conditions.

**Theorem 9.1 (Theorem 2.4 in [BEL23])** *For  $\theta = 1$ , the quasi-potential  $V$  defined by (II.35) can be written as  $V[\gamma] = S[\gamma] - S[\bar{\rho}]$ , where*

$$S[\gamma] := S_{\text{bulk}}[\gamma] + \log \frac{F(0) - \alpha}{\beta - \alpha} + \log \frac{\beta - F(1)}{\beta - \alpha}. \quad (\text{II.43})$$

*In the latter, as well as in the formula (II.41) for  $S_{\text{bulk}}$ , the function  $F = F[\gamma]$  is the unique solution to the DLS equation (II.42) with Robin boundary conditions*

$$F'(0) = F(0) - \alpha \quad \text{and} \quad F'(1) = \beta - F(1).$$

## 9.4 Sketch of the proof of Theorem 9.1

We now briefly sketch the salient points of the proof. Throughout, the profile  $\gamma$  is fixed, we do not indicate it in our notations, however all trajectories  $\rho$  considered here are assumed to be starting from the stationary profile  $\rho_0 = \bar{\rho}$  and ending at  $\rho_T = \gamma$ . We start by defining an (explicit) Hamiltonian  $\mathcal{H}$  depending on  $\rho$  and its conjugate  $F$ , with which we rewrite the dynamical large deviations functional  $I_{[0,T]}$  as the associated action functional

$$I_{[0,T]}[\rho] = \sup_H \int_0^T dt \{ \langle \partial_t \rho_t, H_t \rangle - \mathcal{H}(u_t, H_t) \}. \quad (\text{II.44})$$

First, we check that for any  $\gamma$ , a variational computation yields the Hamilton–Jacobi equation

$$\mathcal{H} \left( \gamma, \frac{\delta V}{\delta \gamma} \right) = 0, \quad (\text{II.45})$$

where  $\delta V / \delta \gamma$  stands for the functional derivative of  $V$  w.r.t.  $\gamma$ .

Then, we prove that given  $\gamma$ , if  $F[\gamma]$  solves the DLS equation with Robin boundary conditions, then  $\mathcal{H}(\gamma, \Gamma) = 0$ , where we defined

$$\Gamma[\gamma] = \log \frac{\gamma}{1 - \gamma} - \log \frac{F[\gamma]}{1 - F[\gamma]}, \quad (\text{II.46})$$

which together with (II.45), identifies  $\Gamma$  as  $\delta V/\delta\gamma$ . Given a trajectory  $\rho = \{\rho_t, 0 \leq t \leq T\}$ , we can then define  $\Gamma_t = \Gamma[\rho_t]$ , and use the Hamilton–Jacobi equation  $\mathcal{H}(\rho_t, \Gamma_t) = 0$  as well as (II.47) for  $H_t = \Gamma_t$ , to show that

$$I_{[0,T]}[\rho] \geq \int_0^T \langle \partial_t \rho_t, \Gamma_t \rangle dt. \quad (\text{II.47})$$

A straightforward computation shows that  $S$  was defined in such a way that

$$\frac{\delta S}{\delta \gamma}[\gamma] = \Gamma[\gamma], \quad (\text{II.48})$$

so that (II.47) yields, since  $\rho$  links  $\bar{\rho}$  and  $\gamma$ , that  $I_{[0,T]}[\rho] \geq S[\gamma] - S[\bar{\rho}]$ . Since the right-hand side does not depend on the chosen trajectory, only its endpoints, (II.35) yields the first inequality  $V[\gamma] \geq S[\gamma] - S[\bar{\rho}]$ .

We now turn to the proof of the second inequality, namely

$$V[\gamma] \leq S[\gamma] - S[\bar{\rho}]. \quad (\text{II.49})$$

To prove the latter, we need to identify the optimal trajectory for the variational problem (II.35). According to the general framework of the macroscopic fluctuations theory [10], this optimal trajectory is given by the time-reversal of the adjoint dynamics’s hydrodynamics, which is formally given by

$$\partial_t \tilde{\rho} = -\partial_u^2 \tilde{\rho} + 2\partial_u \left( \sigma(\tilde{\rho}) \partial_u \frac{\delta S}{\delta \tilde{\rho}} \right),$$

which, in light of (II.46) and (II.48), rewrites

$$\partial_t \tilde{\rho} = \partial_u^2 \tilde{\rho} - 2\partial_u \left( \sigma(\tilde{\rho}) \partial_u \log \frac{F[\tilde{\rho}]}{1 - F[\tilde{\rho}]} \right)$$

with suitable boundary conditions. The main difficulty in the proof of (II.49) is therefore to show that this trajectory  $\tilde{\rho}$  is indeed the optimal one, in the sense that its time reversal solves the variational principle (II.35). In [BEL23, Lemma 4.4], we show that this is the case, under the assumption that it converges to  $\bar{\rho}$ . However, because  $\tilde{\rho}$ ’s construction relies at each fixed time on the solution  $F[\tilde{\rho}]$  of the DLS equation, showing this assumption is by no means straightforward. However, thanks to the Hamiltonian formalism, we obtain an autonomous simple equation for the evolution of the function  $F_t := F[\tilde{\rho}_t]$ , which in turn allows us to show that  $\tilde{\rho} \xrightarrow[t \rightarrow \infty]{} \gamma$  and yields (II.49).

## 10 Destruction at the origin for the asymmetric ZRP

In keeping with our exploration of the effect on the macroscopic behavior of boundary-driven particle systems of the scaling of the boundary dynamics, we then turned to the asymmetric zero-range process on  $\mathbb{Z}$ , and studied in [ESZ23a] the effect of an empty reservoir linked to the origin.

## 10.1 Asymmetric zero-range process with destruction at the origin

The zero-range process we considered is characterized by its bulk generator

$$\mathcal{L}_{\text{bulk}}f(\omega) := \sum_{y \in \mathbb{Z}} g(\omega_y) \{pf(\omega^{y,y+1}) + (1-p)f(\omega^{y,y-1}) - f(\omega)\}, \quad (\text{II.50})$$

where  $p \in (1/2, 1]$ , so that the overall current throughout the system flows from left to right. The boundary dynamics intervenes at the origin, where particles are removed according to the same jump rates as in the bulk dynamics. In other words, the boundary dynamics is driven by the generator

$$\mathcal{L}_0f(\omega) := rg(\omega_0) \{f(\omega - \mathbf{1}_0) - f(\omega)\}, \quad (\text{II.51})$$

where  $\omega - \mathbf{1}_0$  represents the configuration obtained after removing a particle at the origin in  $\omega$ , and  $r > 0$  tunes the boundary dynamics. As explained for the FEP in Section 2.3, attractiveness is a crucial tool in order to derive the hydrodynamic limit of asymmetric models, so that we assume the rate function  $g$  to be non decreasing on the set of positive integers  $\{1, 2, \dots\}$ , making our zero-range process *attractive*. By convention, we assume  $g(0) = 0$ .

In [ESZ23a], we derive the hydrodynamic for the zero-range process  $\{\omega(t), t \geq 0\}$  with generator  $\mathcal{L}_N$  defined as

$$\mathcal{L}_N := N\mathcal{L}_{\text{bulk}} + N^\theta \mathcal{L}_0, \quad (\text{II.52})$$

depending on the value of  $\theta$ .

## 10.2 Stationary states

As emphasized in the introduction, understanding the process's local stationary states is crucial in order to be able to derive the hydrodynamic limit. For the zero-range process (with no boundary interaction), with generator (II.50), the stationary states are explicit. To introduce them, define for  $k \geq 1$ ,  $g!(k) := g(1)g(2) \dots g(k)$ , with the convention  $g!(0) = 1$ . We can then define  $\mathcal{L}_{\text{bulk}}$ 's stationary state as the product distribution on  $\mathbb{Z}^{\mathbb{N}}$  with site marginals

$$\tilde{\nu}_\zeta(\omega_y = k) = \frac{1}{Z(\zeta)} \frac{\zeta^k}{g!(k)}, \quad (\text{II.53})$$

where  $Z(\zeta) := \sum_{k \geq 0} \zeta^k / g!(k)$  is a suitable renormalizing partition function. However, this parametrization of the distribution is not very convenient, so that we define its marginal expectation  $R(\zeta) := \sum_k k \tilde{\nu}_\zeta(k)$ , which is a strictly increasing function, and by  $\Phi = R^{-1}$  its inverse. We now index the stationary states by their density, by defining  $\nu_\alpha = \tilde{\nu}_{\Phi(\alpha)}$ , for which straightforward computations yield the identity

$$\Phi(\alpha) = \sum_{k \geq 0} g(k) \nu_\alpha(\omega_0 = k), \quad (\text{II.54})$$

meaning that  $\Phi$  is the average jump rate at density  $\alpha$ . Whenever convenient, we denote by  $\mathbb{E}_\alpha$  the expectation w.r.t.  $\nu_\alpha$ . As explained in [ESZ23a, Lemma 3.1], stationary product distribution can also be found for the dynamics with destruction driven by the full generator  $\mathcal{L}_N$ . We do not give this construction here, and refer the interested reader to the article itself.

### 10.3 Hydrodynamic limit

We now state our main result from [ESZ23a]. Recall that we are dealing with an asymmetric zero-range process, whose hydrodynamic limit therefore takes the form of a hyperbolic PDE. As for the FEP, we therefore need to single out the unique entropy solution which is physically relevant, and is defined in a similar way as in Definition (7.1). Once again, not to burden excessively this section, we do not redefine completely each relevant hyperbolic solution, and instead refer to them simply as the entropy solution to the equation on a domain  $\Gamma \subset \mathbb{R}$

$$\begin{cases} \partial_t \alpha + (2p-1)\partial_u \Phi(\alpha) = 0 & \text{on } \Gamma \\ \alpha(0, \cdot) = \alpha_0. \end{cases} \quad (\text{II.55})$$

As we will see, because particles are destroyed at the origin, we need to distinguish three cases for this equation that will appear in the hydrodynamic limit. The first one, is the setting where the full macroscopic system  $\Gamma = \mathbb{R}$  is unaffected by the boundary condition, in which case we denote by  $\alpha^*$  the corresponding entropy solution on  $\mathbb{R}$ . The second one is the case

$$\begin{cases} \Gamma = (0, +\infty) \\ \alpha(t, 0) = a(t) \quad \text{for } t > 0, \end{cases} \quad (\text{II.56})$$

which corresponds to the right-hand side of the system, while the left-hand side acts through a source term  $a(t)$  at the origin operating as a Dirichlet Boundary condition. We denote by  $\alpha^{(a)}$  the unique entropy solution of (II.55) on  $(0, +\infty)$  with boundary condition (II.56). The third case we need to consider is the one where the boundary condition operates on the current  $j(t)$  going through the origin,

$$\begin{cases} \Gamma = (0, +\infty) \\ \partial_t \int_0^{+\infty} \alpha(t, v) dv = j(t) \quad \text{for } t > 0. \end{cases} \quad (\text{II.57})$$

We finally denote by  $\alpha^{(j)}$  the unique entropy solution of (II.55) on  $(0, +\infty)$  with boundary condition (II.57). Recall that  $r$  and  $\theta$  are respectively the strength and the scaling factor of the destruction dynamics (see (II.51) and (II.52)), and define

$$\nu_{\alpha_0} := \otimes_{y \in \mathbb{Z}} \nu_{\alpha_0(y/N)} \quad (\text{II.58})$$

the initial product state fitting a smooth initial profile  $\alpha_0$ . We are now ready to state our main result from [ESZ23a].

**Theorem 10.1 (Theorem 2.4 in [ESZ23a])** *The hydrodynamic limit of the process  $\{\omega(t), t \geq 0\}$  started from  $\nu_{\alpha_0}$  and driven by the generator  $\mathcal{L}_N$  defined in (II.52) is given by:*

- [Case  $\theta < 0$ ] by

$$\alpha := \alpha^*,$$

*meaning the boundary dynamics has no macroscopic effect.*

- [Case  $\theta = 0$ ] By  $\alpha := \alpha^* \mathbf{1}_{\{v < 0\}} + \alpha^{(a)} \mathbf{1}_{\{v \geq 0\}}$ , where the boundary condition  $a$  in (II.56) is given by

$$a(t) := R \left( \frac{2p-1}{2p-1+\alpha} \Phi(\alpha^*(t, 0)) \right). \quad (\text{II.59})$$

- [Case  $\theta > 0$ ] By  $\alpha := \alpha^* \mathbf{1}_{\{v < 0\}} + \alpha^{(j)} \mathbf{1}_{\{v \geq 0\}}$ , with current boundary condition  $j(t) \equiv 0$  in (II.57).

Let us now sketch the proof of this result. Once again, we exploit the fact that this process is attractive, as in the case of the Facilitated Zero-Range Process (see (I.17)), and create a process of second class particles in the following way. Consider our zero-range process  $\omega$ , we denote by  $\{\zeta(t), t \geq 0\}$  the process of second class particles, which is defined this way;

- initially, there are no second-class particles, so that  $\zeta_y(0) = 0, \forall y \in \mathbb{Z}$ .
- Whenever a particle is destroyed at the origin, we create a second class particle in  $\zeta$  at the origin.
- At site  $y$ , a second class particle jumps at rate  $g((\zeta + \omega)_y(t)) - g(\omega_y(t))$ , to the right with probability  $p$  and to the left with probability  $1 - p$ . It is not hard to check that the process  $\omega + \zeta$  behaves as a zero-range process without destruction, meaning with generator  $\mathcal{L}_{\text{bulk}}$  given by II.50.

Depending on  $\beta$ , we then obtain [ESZ23a, Lemma 3.3] a bound, depending on  $t, N$  and  $\beta$ , on the total number of second class particles created throughout the process.

Once this process is well defined, we are in a position to prove the hydrodynamic limit. Once again, since we are dealing with an asymmetric process, a big challenge to do so is to derive a microscopic equivalent of the entropy inequality, to show that as  $N \rightarrow \infty$ , the hydrodynamic limit converges to the unique physically relevant solution to the hyperbolic equation. This requires introducing local spatial averages, which can be done using attractiveness and by comparing with equilibrium zero-range processes: we can locally sandwich our original process between two equilibrium processes with slightly larger and slightly lower densities, and show that in a typical local box, these three processes will be ordered. This, in turn, allows us to introduce local averages, both to derive the microscopic entropy inequality and to prove the one block estimate. Once the entropy inequality is obtained, the last ingredient needed is the characterization of the macroscopic boundary dynamics.

In the case  $\theta < 0$ , particles are destroyed at a very low rate. In particular, we can show that the process of second-class particles has no macroscopic particle density, therefore the destruction at the origin as no macroscopic effect and hydrodynamic limit  $\alpha^*$  does not exhibit any boundary condition.

Furthermore, because of the asymmetry, particle cannot macroscopically move leftwards, so that regardless of the value of  $\theta$ , the process of second class particles has no macroscopic effect (see [ESZ23a, Lemma 3.4]) left of the origin. In particular, the hydrodynamic limit restricted to  $(-\infty, 0)$  coincides with  $\alpha^*$  for all values of  $\theta$ . In the case  $\theta = 0$ , we then couple with a stationary zero-range process to derive the macroscopic boundary condition (II.59). In the case  $\theta > 0$ , we further need to prove that no macroscopic current manages to cross the origin. To do so, we use once again attractiveness, and distinguish two cases. If  $\theta \geq 1$ , we can couple our zero range process with infinite-rate destruction of particles at the origin (meaning any particle at the origin is destroyed), and show with the process of second class particles that both processes have the same macroscopic behavior. Finally, in the intermediary regime  $0 < \theta < 1$ , this crude coupling does not work, and we instead adapt arguments from [52], once again coupling our process with a time-stationary copy, and then use attractiveness to compare their behavior around the origin and show that no current manages to go through the latter [ESZ23a, Lemma 4.5].

Finally, we present in this article an alternative proof in the particular case where  $g(k) = k$ , in which particles behave as independent random walkers. In the latter, we duality estimates like the ones from [ELX18, Eri18] (see Section 8), except in a simpler setting with no actual interaction between particles, which allows us to derive the hydrodynamic limit in the asymmetric setting.

## 11 Hydrodynamic behavior for the boundary-driven FEP

Most recently, we finally considered the effect of boundary dynamics on the facilitated exclusion process whose macroscopic behavior was studied in detail in the previous chapter. We study in [DCES24] the unique interaction the FEP has with reservoir dynamics, where the latter cannot impose their own density because they cannot enforce subcritical macroscopic densities at the FEP's boundaries. Once again, in this section we slightly modify our notations w.r.t. [DCES24] in order to keep coherent notations throughout the manuscript.

### 11.1 Kinetically constrained reservoirs and dynamics

For this boundary-driven FEP, we fix two parameters  $\alpha, \beta \in (0, 1)$  to represent the reservoir's densities. As in Chapter I, the bulk dynamics is driven by the FEP's generator

$$\mathcal{L}_{\text{bulk}} f(\eta) := \sum_{x=1}^{N-1} (\eta_{x-1} \eta_x (1 - \eta_{x+1}) + \eta_{x+2} \eta_{x+1} (1 - \eta_x)) \{f(\eta^{x,x+1}) - f(\eta)\}.$$

Note that the generator above requires the values  $\eta_0$  and  $\eta_N$ , which are set to  $\eta_0 := \alpha$  and  $\eta_N := \beta$  respectively. In other words, this convention entails that a boundary particle is active only with probability  $\alpha$  (resp.  $\beta$ ), in which case it can jump towards the inside of the bulk. The boundary dynamics is driven by the generators

$$\mathcal{L}_{\text{left}} f(\eta) := \gamma_1(\eta) \{f(\eta^1) - f(\eta)\} \quad \text{and} \quad \mathcal{L}_{\text{right}} f(\eta) := \gamma_N(\eta) \{f(\eta^N) - f(\eta)\},$$

where

$$\gamma_1(\eta) := (1 - \alpha) \eta_1 \eta_2 + \alpha (1 - \eta_1) \quad \text{and} \quad \gamma_N(\eta) := (1 - \alpha) \eta_N \eta_{N-1} + \alpha (1 - \eta_N).$$

In other words, a particle is created at one of the empty boundary sites at resp. rate  $\alpha, \beta$ , whereas an *active* particle at the boundary jumps out of the system at respective rate  $1 - \alpha, 1 - \beta$ . The boundary rates involved in  $\mathcal{L}_{\text{bulk}}, \mathcal{L}_{\text{left}}, \mathcal{L}_{\text{right}}$  are exactly the same as if the FEP was defined on the whole line  $\mathbb{Z}$ , but that the two boundary configurations on  $\{\dots, -2, -1, 0\}$  and  $\{N + 1, N + 2, \dots\}$  were permanently distributed as the equilibrium states  $\pi_{\rho(\alpha)}, \pi_{\rho(\beta)}$  defined in I.25 with respective *active* densities  $\alpha, \beta$ . Given these generators, we fix two positive parameters  $\theta, \kappa > 0$  that will allow us to tune the boundary dynamics, and define the complete generator

$$\mathcal{L}_N = \kappa N^\theta (\mathcal{L}_{\text{left}} + \mathcal{L}_{\text{right}}) + N^2 \mathcal{L}_{\text{bulk}}. \quad (\text{II.60})$$

For technical reasons, we want to start our process from the FEP's ergodic component (see Section 5.1), from a distribution fitting a given continuous macroscopic profile  $\rho_0$  :

$[0, 1] \rightarrow (1/2, 1]$ . This continuous density profile can be associated with an active density field

$$a_x^0 := \frac{\rho_0(x/N) + \rho_0((x+1)/N) - 1}{\rho_0(x/N)} \simeq a(\rho(x/N)),$$

where the function  $a$  was defined in [1.26](#). To build an initial state  $\mu^N$  fitting  $\rho_0$  and supported on the ergodic component, we exploit the Markovian construction of the FEP's equilibrium state (see [\(1.28\)](#)), and choose under  $\mu^N$  that  $\eta_1 \sim \text{Ber}(\rho_0(1/N))$ , and for any  $2 \leq x \leq N$ ,

$$\mu^N(\eta_x = 1 \mid \eta_{x-1} = 1) = a_{x-1}^0 \quad \text{and} \quad \mu^N(\eta_x = 1 \mid \eta_{x-1} = 0) = 1. \quad (\text{II.61})$$

It is not hard to check that for any  $x \in \Lambda_N$ ,  $\mu^N(\eta_x = 1) = \rho_0(x/N)$ , and by a simple decorrelation estimate on the initial state's Markov chain [[DCES24](#), Theorem A.3]

$$\frac{1}{N} \sum_{x=1}^{N-1} G\left(\frac{x}{N}\right) \eta_x \xrightarrow{N \rightarrow +\infty} \int_0^1 G(u) \rho_0(u) du$$

in  $\mu^N$  probability. Furthermore,  $\mu^N$  clearly only charges the ergodic component since under the Markovian construction, any empty site is always followed by a particle. We now consider a Markov process  $\{\eta(t), t \geq 0\}$  driven by the generator  $\mathcal{L}_N$  defined in [\(II.60\)](#) and started from  $\mu^N$ , whose distribution we denote as before by  $\mathbb{P}_{\mu^N}$ .

## 11.2 Hydrodynamic limit for weak and strong reservoir interactions

The main result of [[DCES24](#)] is the hydrodynamic limit for this boundary-driven FEP in the different regimes for  $\theta$ . For concision, we do not give the full description of the notion of solution in each case. Roughly speaking however, we consider solutions to the hydrodynamic equation which satisfy a weak form of the hydrodynamic equation, such that  $a(\rho) \in L^2([0, T], \mathcal{H}^1)$ . More precisely, we have the following result.

**Theorem 11.1 (Theorem 2.2 of [[DCES24](#)])** *The hydrodynamic limit for  $\{\eta(t), t \geq 0\}$  is given by the unique weak solution  $\rho(t, u) : [0, +\infty) \times \mathbb{T} \rightarrow [0, 1]$  to the diffusion equation*

$$\begin{cases} \partial_t \rho = \partial_u^2 a(\rho) \\ \rho(0, \cdot) = \rho_0, \end{cases} \quad (\text{II.62})$$

with boundary conditions respectively given by

$$\rho(t, 0) = \rho(\alpha) := \frac{1}{2 - \alpha}, \quad \text{and} \quad \rho(t, 0) = \rho(\beta) := \frac{1}{2 - \beta} \quad \text{for } \theta > 1$$

$$\partial_u \rho(t, 0) = \kappa(\rho(t, 0) - \rho(\alpha)), \quad \text{and} \quad \partial_u \rho(t, 1) = \kappa(\rho(\beta) - \rho(t, 1)) \quad \text{for } \theta = 1$$

and

$$\partial_u \rho(t, 0) = \partial_u \rho(t, 1) = 0 \quad \text{for } \theta < 1.$$

To prove this result, we rely on classical entropy tools. However, such tools are typically applied to SSEP-like processes with product equilibrium distribution [[13](#), [30](#)], so that a number of adaptations need to be made to account for locally correlated equilibrium states.

The first challenge, as for any entropy based argument, is to define a reference measure, i.e. an good enough approximation of the boundary-driven FEP's stationary state.

To do so, recall that the FEP is gradient, and that the quantity appearing in the hydrodynamic limit is the active density  $a(\rho)$ . We can therefore expect that in the stationary state, the boundary-driven FEP's *active density* interpolates between its boundary values. Furthermore, it is straightforward to check that our choice of boundary dynamics is reversible w.r.t. the equilibrium states  $\pi_\rho$  parametrized by the boundary densities  $\rho(\alpha), \rho(\beta)$  defined in Theorem 11.1, so that in particular the active density at the boundaries must be set at  $\alpha, \beta$ , at least for strong boundary interactions.

For this reason, we define the active stationary field interpolating between  $\alpha$  and  $\beta$

$$\bar{a}_x := \alpha + \frac{x-1}{N-1}(\beta - \alpha).$$

We then consider the distribution  $\bar{\mu}^N$  driven by the same Markov construction used for the initial profile, but this time started from  $\eta_1 \sim \text{Ber}(\rho(\alpha))$ , and with transition probabilities (II.61) built with  $\bar{a}_x$  instead of  $a_x^0$ . In the same way that the non-equilibrium SSEP's stationary state is not exactly a product one, the non equilibrium FEP stationary state is not  $\bar{\mu}^N$ . However, for the purpose of proving the hydrodynamic limit,  $\bar{\mu}^N$  provides a good enough approximation (see [DCES24, Lemma 4.4]) of the stationary state in order to apply the entropy method. Note that as for the SSEP, in the equilibrium case  $\alpha = \beta$ , the stationary state simply amounts to the grand canonical state  $\bar{\mu}^N = \pi_{\rho(\alpha)}$ . Locally around any site  $x$ , we can then show that  $\bar{\mu}^N \simeq \pi_{\rho(\bar{a}_x)}$ .

Once the stationary state is closely approximated, the main remaining challenges to adapt the entropy method is to prove the two-blocks estimate, and to estimate the density at the boundary. The quasi-reversible nature of our reference measure w.r.t. the boundary dynamics solves the latter. Regarding the former, some care needs to be taken to account for the non-product nature of the reference distribution, so that conditioning to the behavior of microscopic boxes is not straightforward.

As mentioned in the introduction, the kinetic constraint makes the FEP's interaction with boundary dynamics highly unusual: because of its two-phased nature, boundary dynamics are not able to impose their own equilibrium densities on the FEP, because they cannot dynamically impose subcritical densities. Instead, any reservoir interaction with the FEP (regardless of the reservoir's exact rates) imposes a supercritical boundary density  $\rho > 1/2$ , because it keeps pumping particles inside the system until the ergodic component is locally reached at the boundary.

## Conclusion and perspectives

Boundary-driven models have been under deep scrutiny in recent years. At the level of hydrodynamics, depending on the bulk and boundary dynamics considered, and whether the bulk dynamics is symmetric or not, a wide range of behavior can be obtained, see e.g. [77, 27], [Eri18]. At the level of large deviations, the presence of two boundaries enforcing different equilibrium densities maintains the system out of equilibrium, so that one cannot easily define a free energy to fully understand the large scale behavior of the process. One must therefore resort to the general framework of the Macroscopic Fluctuations Theory [10] to characterize the stationary and dynamical large deviation regime.

A natural question arising from our duality estimates from [ELX18, Eri18], which allow to characterize the large scale hydrodynamics of the SSEP with rather general boundary

conditions, is whether our central assumption (II.27) is purely technical, and if the hydrodynamic description we give actually holds outside of this assumption. As of writing this manuscript, I cannot give a definitive answer to this question, however one can define boundary dynamics which do not fulfill (II.27), and for which there is no *deterministic* hydrodynamic limit, meaning that our assumption are not only technical, but rather that they guarantee proper decorrelation at the boundary.

An example of a setting for which it can be shown the (deterministic) hydrodynamic limit does not hold is defined by “voting” boundary conditions, where for some integer  $p$ , a particle is created (resp. removed) at rate 1 if there are at least  $p$  particles (resp. empty sites) among the boundary set  $\{2, \dots, 2p\}$ . For  $p$  large enough (e.g.  $p \geq 4$ ), one can prove that starting for example from a  $\otimes Ber(1/2)$  product distribution, the hydrodynamic limit is not deterministic, in the sense that depending on a local fluctuation, the model macroscopically behaves as a reservoir with density 1 (resp. 0) with probability 1/2. It would be interesting to understand better the behavior of such a highly correlated boundary-driven model. On the one hand, its boundary behavior is very complex, in large parts because it does not preserve product distributions. On the other hands, it is paired with a simple SSEP bulk dynamics, which allows for rich duality estimates, so that many questions on its macroscopic behavior amount to random walks hitting time/probability estimates. In general, most of the work performed on boundary-driven models in recent years has centered around equilibrium reservoirs, which have the very nice property of breaking down correlations and introducing mixing in the system. To the contrary, the non-linear boundary dynamics described in Section 8 introduce strong correlation at the boundary, so that mixing relies strongly on the bulk dynamics. Such models are so far poorly understood in a general setting, and much remains to be done.

Duality properties like the ones exploited in Section 8 have been extensively used in recent years to derive the macroscopic behavior of various lattice gases with different boundary dynamics, e.g. the inclusion process [27], the KMP model [15], or even the SSEP in random environments [62]. This is particularly relevant given recent interest in non-equilibrium stationary states (NESS), as duality yields a potent tool to obtain fine estimates on non explicit stationary states for various processes. In this context, it would be of great interest to extend our results on general boundary dynamics [ELX18, Eri18] to more general dynamics than the SSEP. This would yield robust tools to derive the macroscopic behavior for fairly general pairings of boundary and bulk dynamics. Overall, duality can be exploited for a range of applications, and we strongly expect that e.g. non-equilibrium fluctuations and large deviations principles could be derived, at least in some regimes, for dual interacting particle systems interacting with non-linear boundary dynamics.

The FEP is an striking example of model which naturally adopts non-linear boundary interactions, and given its unusual interactions with reservoir dynamics, [DCES24] has only been a first step in understanding the interplay between kinetic constraints and boundary dynamics. In particular, technically speaking, a number of assumptions from [DCES24] need to be lifted. The first one is the assumption on the initial configuration, which we assumed fully supercritical and ergodic. We expect that none of these assumptions are necessary w.r.t. the existence and validity of the hydrodynamic limit, which should, under fairly general initial states fitting an initial profile  $\rho_0$ , be given by the Stefan problem (29) with appropriate boundary conditions. Proving this conjecture, however, requires overcoming very significant technical challenges, be it on the probability side or on the analysis side, where the existence and uniqueness of such solutions is not completely straightforward. In particu-

lar, the motion of the particle front, away from the boundary, starting e.g. from an empty configuration is not trivial, and would be very interesting to characterize.

Another strong restriction on our work [DCES24] relates to the boundary dynamics. Although our choice of boundary dynamics is the physically natural one, one naturally expect that the non-equilibrium FEP's hydrodynamic limit should hold for a much larger choice of boundary dynamics. For the set of boundary dynamics preserving the ergodic component (e.g. a particle at site 1 cannot be removed unless site 2 is occupied), our proofs should be adaptable to yield the wanted result. For boundary dynamics that do not preserve the ergodic component, entropy-based techniques might not be a fitting choice, and other approaches will be necessary.

Another natural question, in light of Chapter I, provided we are able to derive dynamical large deviations estimates and hydrodynamic limit for the boundary-driven FEP (see the concluding remarks at the end of chapter I), would be to understand the statical and dynamical large deviations regime and the effect of slowing down boundary dynamics on the FEP. I expect that its dynamical large deviations with boundary might be accessible, although this is by no means straightforward. However, assuming one is able to do so, it would be fascinating to know what would take the place of the DLS equation (43), which is very likely uniquely associated with the SSEP. Although some of these questions will likely be approachable mathematically, some of them may be too difficult given the intrinsic complexity of the FEP, so that a first step would be to concentrate on its ergodic phase, which is roughly SSEP-like. Formal computations and simulations might also considerably help in that respect.



## REFERENCES

- [1] N. Angelescu, S. Romano, and V.A. Zagrebnov. On long-range order in low-dimensional lattice-gas models of nematic liquid crystals. *Physics Letters A*, 200(6):433–437, 1995.
- [2] N. Angelescu and V.A. Zagrebnov. A lattice model of liquid crystals with matrix order parameter. *Journal of Physics A: Mathematical and General*, 15(11):L639, nov 1982.
- [3] J. Ayre and P. Chleboun. Mixing times for the facilitated exclusion process. *Preprint*, 2024.
- [4] A. Ayyer, S. Goldstein, J. L. Lebowitz, and E. R. Speer. Stationary states of the one-dimensional facilitated asymmetric exclusion process. *Annales de l'Institut Henri Poincaré, Probabilités et Statistiques*, 59(2), May 2023.
- [5] R. Baldasso, O. Menezes, A. Neumann, and R. Souza. Exclusion process with slow boundary. *Journal of Statistical Physics*, 167(5):1112–1142, 2017.
- [6] R. Baldasso, O. Menezes, A. Neumann, and R.R. Souza. Exclusion process with slow boundary. *Journal of Statistical Physics*, 167(5):1112–1142, mar 2017.
- [7] G. Barraquand, O. Blondel, and M. Simon. Weakly asymmetric facilitated exclusion process. *Preprint*, 2023.
- [8] U. Basu and P. K. Mohanty. Active–absorbing-state phase transition beyond directed percolation: A class of exactly solvable models. *Physical Review E*, 79:041143, Apr 2009.
- [9] L. Bertini, A. De Sole, D. Gabrielli, G. Jona-Lasinio, and C. Landim. *Mathematical Physics, Analysis and Geometry*, 6(3):231–267, 2003.
- [10] L. Bertini, A. De Sole, D. Gabrielli, G. Jona-Lasinio, and C. Landim. Macroscopic fluctuation theory. *Reviews of Modern Physics*, 87(2):593–636, jun 2015.
- [11] O. Blondel, C. Cancès, M. Sasada, and M. Simon. Convergence of a degenerate microscopic dynamics to the porous medium equation, 2020.
- [12] T. Bodineau and G. Giacomin. From dynamic to static large deviations in boundary driven exclusion particle systems. *Stochastic Processes and Applications*, 110:67–81, 2004.
- [13] L. Bonorino, R. de Paula, P. Gonçalves, and A. Neumann. Hydrodynamics of porous medium model with slow reservoirs. *Journal of Statistical Physics*, 179, 05 2020.

- [14] N. Cancrini, F. Martinelli, C. Roberto, and C. Toninelli. Kinetically constrained lattice gases. *Communications in Mathematical Physics*, 297:299–344, 07 2010.
- [15] M. Capanna, D. Gabrielli, and D. Tsagkarogiannis. On a class of solvable stationary non equilibrium states for mass exchange models. *Journal of Statistical Physics*, 191, 02 2024.
- [16] G. Carinci, S. Floreani, C. Giardinà, and F. Redig. Boundary driven markov gas: duality and scaling limits. *Ensaïos Matemáticos*, 2021.
- [17] M. E. Cates and J. Tailleur. When are active brownian particles and run-and-tumble particles equivalent? consequences for motility-induced phase separation. *EPL (Europhysics Letters)*, 101(2):20010, January 2013.
- [18] M. E. Cates and J. Tailleur. Motility-induced phase separation. *Annual Review of Condensed Matter Physics*, 6(1):219–244, 2015.
- [19] S. Chatterjee, A. Das, and P. Pradhan. Hydrodynamics, density fluctuations, and universality in conserved stochastic sandpiles. *Phys. Rev. E*, 97:062142, Jun 2018.
- [20] A. De Masi, E. Presutti, D. Tsagkarogiannis, and M. Vares. Truncated correlations in the stirring process with births and deaths. *Electronic Journal of Probability*, 17(none):1 – 35, 2012.
- [21] B. Derrida, M. R. Evans, V. Hakim, and V. Pasquier. Exact solution of a 1d asymmetric exclusion model using a matrix formulation. *Journal of Physics A: Mathematical and General*, 26(7):1493, apr 1993.
- [22] B. Derrida, O. Hirschberg, and T. Sadhu. Large deviations in the symmetric simple exclusion process with slow boundaries. *Journal of Statistical Physics*, 182(1), jan 2021.
- [23] B. Derrida, J. L. Lebowitz, and E. R. Speer. Large deviation of the density profile in the steady state of the open symmetric simple exclusion process,. *Journal of Statistical Physics*, 107(3/4):599–634, 2002.
- [24] M. D. Donsker and S. R. S. Varadhan. Large deviations from a hydrodynamic scaling limit. *Communications on Pure and Applied Mathematics*, 42(3):243–270, 1989.
- [25] C. Erignoux, A. Roget, A. Shapira, and M. Simon. Hydrodynamic behavior near dynamical criticality of a facilitated conservative lattice gas. *Phys. Rev. E*, 110:L032101, Sep 2024.
- [26] L. C. Evans. *Partial differential equations*. American Mathematical Society, Providence, R.I., 2010.
- [27] C. Franceschini, P. Gonçalves, and F. Sau. Symmetric inclusion process with slow boundary: Hydrodynamics and hydrostatics. *Bernoulli*, 28(2):1340 – 1381, 2022.
- [28] T. Franco, P. Gonçalves, C. Landim, and A. Neumann. Dynamical large deviations for the boundary driven symmetric exclusion process with robin boundary conditions. *ALEA*, 19:1497–1546, 2022.

- [29] J. Fritz. Entropy pairs and compensated compactness for weakly asymmetric systems. In *Stochastic Analysis on Large Scale Interacting Systems*. Mathematical Society of Japan, 2004.
- [30] S. Frómeta, R. Misturini, and A. Neumann. *The Boundary Driven Zero-Range Process*, page 253–281. Springer International Publishing, 2021.
- [31] T. Funaki. Free boundary problem from stochastic lattice gas model. *Annales de l’Institut Henri Poincaré, Probab. Stat.*, (35):573–603, 1999.
- [32] A. Gabel, P. L. Krapivsky, and S. Redner. Facilitated asymmetric exclusion. *Physical Review Letters*, 105:210603, Nov 2010.
- [33] J. Garrahan, P. Sollich, and C. Toninelli. Kinetically constrained models. *Dynamical Heterogeneities in Glasses, Colloids, and Granular Media*, 09 2010.
- [34] S. Ghosh and J. L. Lebowitz. Large deviations and rigidity in hyperuniform systems: A brief survey. *Indian J Pure Appl Math*, 48:609–631, 2017.
- [35] S. Goldstein, J. L. Lebowitz, and E. R. Speer. Stationary states of the one-dimensional discrete-time facilitated symmetric exclusion process. *Journal of Mathematical Physics*, 63(8):083301, 2022.
- [36] S. Goldstein, J.L. Lebowitz, and E.R. Speer. The discrete-time facilitated totally asymmetric simple exclusion process. *Pure and Applied Functional Analysis*, 6:177–203, 2021.
- [37] S. Goldstein, J.L. Lebowitz, and E.R. Speer. Approach to hyperuniformity of steady states of facilitated exclusion processes. *Journal of Physics: Condensed Matter*, 36(34):345402, may 2024.
- [38] P. Gonçalves. Equilibrium fluctuations for the totally asymmetric zero-range process. *Journal of Statistical Physics*, 138:645–661, 2010.
- [39] P. Gonçalves. Hydrodynamics for symmetric exclusion in contact with reservoirs. In Giambattista Giacomin, Stefano Olla, Ellen Saada, Herbert Spohn, and Gabriel Stoltz, editors, *Stochastic Dynamics Out of Equilibrium*, pages 137–205, Cham, 2019. Springer International Publishing.
- [40] P. Gonçalves, M. Jara, and S. Sethuraman. A stochastic Burgers equation from a class of microscopic interactions. *The Annals of Probability*, 43(1):286–338, 2015.
- [41] P. Gonçalves, C. Landim, and C. Toninelli. Hydrodynamic limit for a particle system with degenerate rates. *Annales de l’Institut Henri Poincaré, Probabilités et Statistiques*, 45(4):887 – 909, 2009.
- [42] M. Z. Guo, G. C. Papanicolaou, and S. R. S. Varadhan. Nonlinear diffusion limit for a system with nearest neighbor interactions. *Communications in Mathematical Physics*, 118(1):31–59, 1988.
- [43] J. Hermon and J. Salez. The interchange process on high-dimensional products. *The Annals of Applied Probability*, 31(1):84 – 98, 2021.

- [44] D. Hexner and D. Levine. Hyperuniformity of critical absorbing states. *Physical Review Letters*, 114:110602, Mar 2015.
- [45] M. Jara and O. Menezes. Non-equilibrium fluctuations for a reaction-diffusion model via relative entropy. *Preprint*, 2018.
- [46] M. Jara and O. Menezes. Non-equilibrium fluctuations of interacting particle systems. *Preprint*, 2018.
- [47] H. Kesten and V. Sidoravicius. A phase transition in a model for the spread of an infection. *Illinois Journal of Mathematics*, 50(1-4):547 – 634, 2006.
- [48] C. Kipnis and C. Landim. *Scaling Limits of Interacting Particle Systems*.
- [49] C. Kipnis, S. Olla, and S. R. S. Varadhan. Hydrodynamics and large deviation for simple exclusion processes. *Communications on Pure and Applied Mathematics*, 42(2):115–137, 1989.
- [50] W. Kob and H. C. Andersen. Kinetic lattice-gas model of cage effects in high-density liquids and a test of mode-coupling theory of the ideal-glass transition. *Physical Review E*, 48:4364–4377, Dec 1993.
- [51] H. Lacoin. The cutoff profile for the simple exclusion process on the circle. *The Annals of Probability*, 44(5), September 2016.
- [52] C. Landim. Hydrodynamical limit for space inhomogeneous one-dimensional totally asymmetric zero-range processes. *The Annals of Probability*, 24(2):599 – 638, 1996.
- [53] C. Landim, S. Olla, and S. R S Varadhan. Symmetric simple exclusion process: Regularity of the self-diffusion coefficient. *Communications In Mathematical Physics*, 224(1):307–321, 2001.
- [54] C. Landim and K. Tsunoda. Hydrostatics and dynamical large deviations for a reaction-diffusion model. *Annales de l’Institut Henri Poincaré, Probabilités et Statistiques*, 54(1):51 – 74, 2018.
- [55] J.L. Lebowitz and O. Penrose. Rigorous treatment of the van der waals-maxwell theory of the liquid-vapor transition. *Journal of Mathematical Physics*, 7:98–113, 1966.
- [56] F. Martinelli, R. Morris, and C. Toninelli. Universality results for kinetically constrained spin models in two dimensions. *Communications in Mathematical Physics*, 369(2):761–809, oct 2018.
- [57] J. Mason, R.L. Jack, and M. Bruna. Macroscopic behaviour in a two-species exclusion process via the method of matched asymptotics. *Journal of Statistical Physics*, 190(3), January 2023.
- [58] B. Massoulié. Cutoff for the mixing time of the facilitated exclusion process. *arXiv preprint 2412.04032*, 2024.
- [59] B. Morris. The mixing time for simple exclusion. *The Annals of Applied Probability*, 16(2):615–635, May 2006. Publisher: Institute of Mathematical Statistics.

- [60] L. Onsager. The effect of shape on the interaction of colloidal particles. *Annals of the New York Academy of Sciences*, 51(4):627–659, 1949.
- [61] J. Quastel. Diffusion of color in the simple exclusion process. *Communications on Pure and Applied Mathematics*, 45(6):623–679, 1992.
- [62] F. Redig, E. Saada, and F. Sau. Symmetric simple exclusion process in dynamic environment: hydrodynamics. *Electronic Journal of Probability*, 25, 01 2020.
- [63] F. Redig and F. Sau. *Stochastic Duality and Eigenfunctions*, page 621–649. Springer International Publishing, 2019.
- [64] F. Rezakhanlou. Hydrodynamic limit for attractive particle systems on  $\mathbb{Z}^d$ . *Communications in mathematical physics*, 140:417–448, 1991.
- [65] M. Rossi, R. Pastor-Satorras, and A. Vespignani. Universality class of absorbing phase transitions with a conserved field. *Physical Review Letters*, 85, 04 2000.
- [66] J. Salez. Universality of cutoff for exclusion with reservoirs. *The Annals of Probability*, 51(2):478 – 494, 2023.
- [67] V. Sidoravicius and A. Teixeira. Absorbing-state transition for Stochastic Sandpiles and Activated Random Walks. *Electronic Journal of Probability*, 22(none):1 – 35, 2017.
- [68] A.P. Solon, H. Chaté, and J. Tailleur. From phase to microphase separation in flocking models: The essential role of nonequilibrium fluctuations. *Physical Review Letters*, 114:068101, Feb 2015.
- [69] H. Spohn. Tracer diffusion in stochastic lattice gases. *Physica A: Statistical Mechanics and its Applications*, 163(1):134–139, 1990.
- [70] H. Spohn. Large scale dynamics of interacting particles. 1991.
- [71] H.Q. Tran. Cutoff for the non reversible SSEP with reservoirs. *Electronic Journal of Probability*, 28(none):1–24, January 2023.
- [72] K. Tsunoda. Hydrostatic limit for exclusion process with slow boundary revisited. *RIMS Kôkyûroku Bessatsu*, B79:149–162, 2020.
- [73] S. R. S. Varadhan. Nonlinear diffusion limit for a system with nearest neighbor interactions. II. In *Asymptotic problems in probability theory: stochastic models and diffusions on fractals*, volume 1 of *Pitman Research Notes in Mathematics*, pages 75–128. Longman Scientific & Technical, Harlow, 1993.
- [74] S. R. S. Varadhan. *Regularity of Self-Diffusion Coefficient*, pages 387–397. Birkhäuser Boston, Boston, MA, 1994.
- [75] T. Vicsek, A. Czirók, E. Ben-Jacob, I. Cohen, and O. Shochet. Novel type of phase transition in a system of self-driven particles. *Physical Review Letters*, 75:1226–1229, Aug 1995.
- [76] T. Vicsek and A. Zafeiris. Collective motion. *Physics Reports*, 517(3):71–140, 2012. Collective motion.

- [77] L. Xu and A. Zafeiris. Hydrodynamics for one-dimensional asep in contact with a class of reservoirs. *Journal of Statistical Physics*, 189(1):1572–9613, 2022. Collective motion.
- [78] H. T. Yau. Relative entropy and hydrodynamics of Ginzburg-Landau models. *Letters in Mathematical Physics*, 22(1):63–80, 1991.

# Séparation de phase et effets de bords pour des gaz sur réseau hors-équilibres

**Résumé:** l'un des défis majeurs de la physique statistique moderne est de construire des outils robustes pour l'étude des systèmes microscopiques hors-équilibre (e.g. sous l'action de thermostats, influence d'un champ extérieur, matière active), permettant de comprendre leur comportement à grande échelle. Parmi ces outils, la théorie des *limites d'échelles* des gaz sur réseau, qui a reçu ces dernières décennies beaucoup d'attention dans diverses communautés (Physiciens, Mathématiciens, Biologistes), permet de faire le lien entre un système stochastique de particules microscopique, et sa limite d'échelle typiquement caractérisée par une equation aux dérivées partielles.

Dans ce cadre général, mes travaux de recherche ont porté en grande partie sur l'étude du comportement macroscopique de trois grandes familles de modèles microscopiques :

- Les systèmes de *matière active*, qui présentent une phénoménologie extrêmement riche, en particulier des phénomènes d'auto-organisation et de condensation spontanée.
- Les *gaz sur réseau cinétiquement contraints*, en particulier le *processus d'exclusion facilitée (FEP)*, des modèles de séparation et de transitions de phase dans lesquels le mouvement des particules est soumis à une contrainte locale, perturbant leur équilibre.
- Les *modèles non-équilibre*, affectés par des dynamiques de bord, qui eux aussi peuvent avoir des comportements extrêmement variés selon le réseau, la dynamique de bord et la dynamique de bulk considérée.

L'introduction de ce manuscrit définit succinctement les objets mathématiques fondamentaux nécessaires à la construction des gaz sur réseaux et de leurs limites d'échelles, ainsi qu'à la présentation de ces trois thématiques et de leur état de l'art. Les deux chapitres du manuscrit sont ensuite respectivement dédiés à mes travaux sur l'effet macroscopique de contraintes cinétiques, et à celui de dynamiques de bords, qui ont représenté la majorité de mes travaux mathématiques post-thèse.

**Mots clés:** Mécanique statistique; Probabilités; Limites hydrodynamiques;

## *Phase separation and boundary effects in out-of-equilibrium lattice gases*

**Abstract:** One of the major challenges of modern statistical physics is to build robust tools to study out-of-equilibrium microscopic systems (e.g. submitted to thermostats or external fields, active matter) and understand their large-scale behavior. Among such tools, the theory of scaling limits of lattice gases, which has received in the last decades significant attention from various communities (physics, mathematics, biology) links microscopic stochastic particle systems with their macroscopic limit, typically characterized by a partial differential equation.

In this framework, my research work has focused on the the macroscopic behavior of three classes of microscopic models:

- *Active matter models*, whose phenomenology is very rich and exhibits both self organization patterns and spontaneous condensation phenomena.
- *Kinetically constrained lattice gases, with a specific focus on the Facilitated Exclusion Process (FEP)*, which are models for phase separation and transitions in which particle jumps are subject to a local constraint, which distorts their equilibrium states.
- *Non-equilibrium models*, affected by boundary dynamics, which can also exhibit varied behavior, depending on the microscopic lattice, as well as the microscopic details of both bulk and boundary dynamics considered.

This manuscript's introduction is dedicated to defining the fundamental mathematical objects on which lattice gases and their scaling limits are based, and to presenting these three statistical physics thematics in the context of their state of the art. The two chapters of the manuscript are then respectively dedicated to describing in more details my works on the macroscopic effect of boundary dynamics and kinetic constraints, on which most of my post-PhD work has focused.

**Keywords:** Statistical mechanics; Probability; Hydrodynamic limits;

Image en couverture : Stefan problem for the Facilitated Exclusion Process.

